Numerical Simulations of Detonation Re-Initiation Behind an Obstacle

by

Sébastien She-Ming Lau-Chapdelaine

Thesis submitted to the
Faculty of Graduate and Postdoctoral Studies
In partial fulfillment of the requirements
For the M.A.Sc. degree in
Mechanical Engineering

Ottawa-Carleton Institute for Mechanical and Aerospace Engineering
Faculty of Engineering
University of Ottawa

Abstract

This numerical study explored the mechanisms responsible for the re-initiation of a detonation, which quenched while diffracting over a half-cylinder obstacle. The purpose of the study was to make accurate predictions of when detonation re-initiation would occur, determine the role of various re-initiation mechanisms, and compare the effect of different chemical models.

The problem was modelled using the reactive Euler equations with either the one-step Arrhenius or two-step chain-branching chemical models, calibrated to post-shock conditions in order to properly reproduce the ignition delay. The simulations were validated using the stoichiometric methane-oxygen experiments of Bhattacharjee et al..

The numerical model was able to accurately predict detonation re-initiation conditions found in experiments. There was generally good qualitative and quantitative agreement between experiments and simulations. While the one-step model was sufficient in predicting re-initiation, the two-step model reproduced some of the finer details of the flow field and detonation re-initiation. The study found that Kelvin-Helmholtz and Richtmyer-Meshkov instabilities did not appear to influence detonation re-initiation of the Mach stem. Detonation re-initiation occurred due to adiabatic compression of the Mach stem, or transport of a flame along the wall jet. Transverse detonations were poorly reproduced, possibly because of the absence of proper resolution of Richtmyer-Meshkov instabilities.

Acknowledgements

I would like to thank my supervisor Matei I. Radulescu for his guidance, mentorship, patience and high expectations throughout my studies. Rohit Bhattacharjee's cooperation with the experimental side of this study was of great help.

The University of Ottawa's Admissions Scholarship and Excellence Scholarship, the provincial government's Ontario Graduate Scholarship, and the Natural Sciences and Research Council of Canada's Alexander Graham Bell Canadian Graduate Scholarship aided in funding this work.

Contents

List of Tables

List of Figures

Nomenclature

0	Initial condition (subscript)
Δ_i	Induction zone length
Δ_r	Reaction zone length
$\Delta_{\frac{1}{2}}$	Half-reaction length
γ	Isentropic exponent
λ_i	Induction progress variable
λ_r	Reaction progress variable
ν	Reaction order
ρ	Density
τ	Ignition time
CJ	Chapman-Jouget condition (subscript)
E	Total energy
E_a	Activation energy
k	Pre-exponential factor for reaction rate
k_i	Pre-exponential factor for induction zone
k_r	Pre-exponential factor for reaction zone
l_{throat}	Throat size
$lmax$	Maximum number of refinement levels
ls	Length scale factor
p	Pressure

Q	Heat release
r	Refinement ratio
R_s	Specific gas constant
T	Temperature
t	Time
u	x-component of velocity
v	y-component of velocity
vN	Post-shock state (subscript)
x	Location on horizontal axis
y	Location on vertical axis
$\tilde{}$	Non-dimensional variable (overscript)

Chapter 1

Introduction

1.1 Background and motivation

On December 11th, 2005, a 300-ton fuel leak from a storage tank at the Buncefield Oil Storage Depot in the U.K. caused a thick, reactive vapour cloud to form over a large area. The explosion which followed caused massive damage to the facility and its surroundings and measured 2.4 on the Richter scale. The subsequent investigation [2] raised many concerns, of which one was related to the lack of explanation for the magnitude of the blast. The investigation report recommended that research be conducted into this matter.

It is common practice in the chemical industry to avoid large clusters of pipes where there is the risk of reactive mixtures. A flame propagating through a series of obstacles, such as a pipe cluster, is accelerated by turbulence in the wake of the obstacles.

The Buncefield Oil Storage Depot, however, was free of such pipe clusters and the damage was inconsistent with pressures brought about by a rapid flame. Forensic evidence indicated a detonation may have occurred. Recent research into the matter [3] showed that dense brush in the area may have served as the obstacles which accelerated a subsonic flame (deflagration) into a detonation (a process known as the deflagration-detonation transition (DDT)). Detonations are supersonic combustion waves [4, 5] which typically travel at speeds on the order of kilometres per second and carry pressures tens of times larger than ambient.

The propagation of a detonation through such a porous medium is the subject of this thesis. Focus is placed on the so-called quasi-detonation regime, where detonations re-initiate periodically from interactions with obstructions. Previous studies have looked at this problem and found that detonations can be quenched if the pores (spacing between

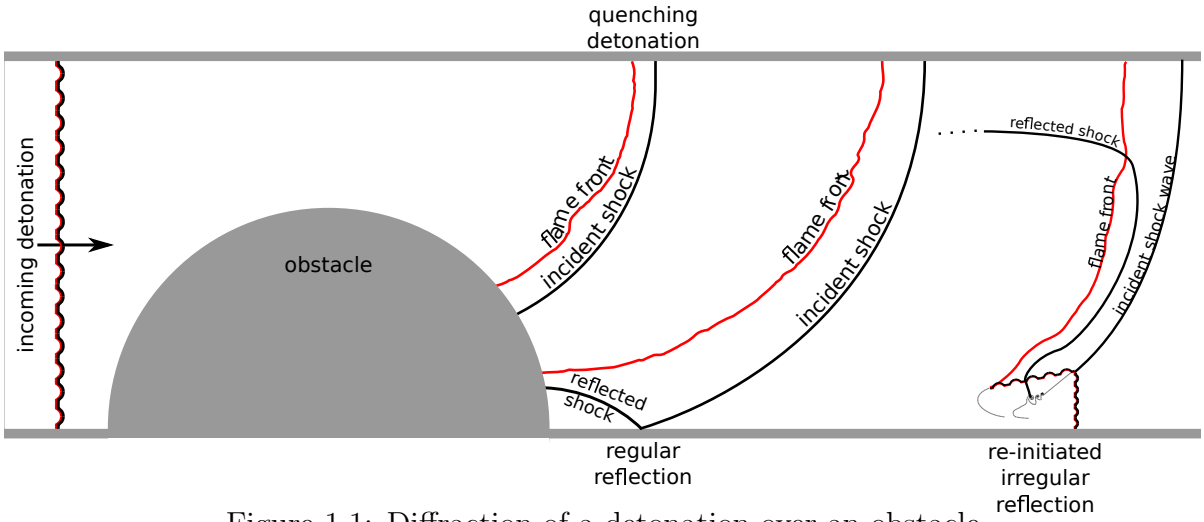

Figure 1.1: Diffraction of a detonation over an obstacle

obstacles) are small enough. Under certain conditions, however, quenched detonations have been found to re-initiate downstream of obstacles [6–14]. The purpose of this study is to clarify the mechanisms causing the re-initiation of quenched detonations following their diffraction past an obstacle, in order to be able to model and predict the conditions leading to local detonation re-initiation.

Consider a single obstacle, which partially obstructs a channel filled with reactive gas (e.g., gasoline and air), as illustrated by figure 1.1. The gas is ignited at an end of the channel, causing a detonation to diffract around the obstacle. As the front diffracts around, the gas driving the shock expands in the increasing cross-section and weakens the leading shock. The ensuing lower temperature may cause the shock wave and reaction zones to decouple, effectively quenching the detonation. The quenched detonation may re-initiate downstream of the obstacle following shock reflection.

The shock reflection process has been shown to be essential to the propagation of quasi-detonations. A shock reflection occurs when a shock wave impinges on a surface. The reflection generally adopts one of two configurations [15, 16]: a regular or a Mach reflection (irregular reflection), sketched in figure 1.2. The regular reflection occurs when the angle between the incident shock and the reflection surface is small and consists of the incident shock and a reflected (transverse) shock. When the angle grows too large, the reflected shock is unable to divert the reflecting flow so a third shock, the Mach stem (or Mach shock), is introduced, creating an irregular reflection. The Mach stem is joined to the incident and reflected shocks at the triple point. Another characteristic of the irregular reflection is the presence of a contact surface (often called a slip line) separating gases shocked by the Mach stem and those shocked by the incident and reflected waves.

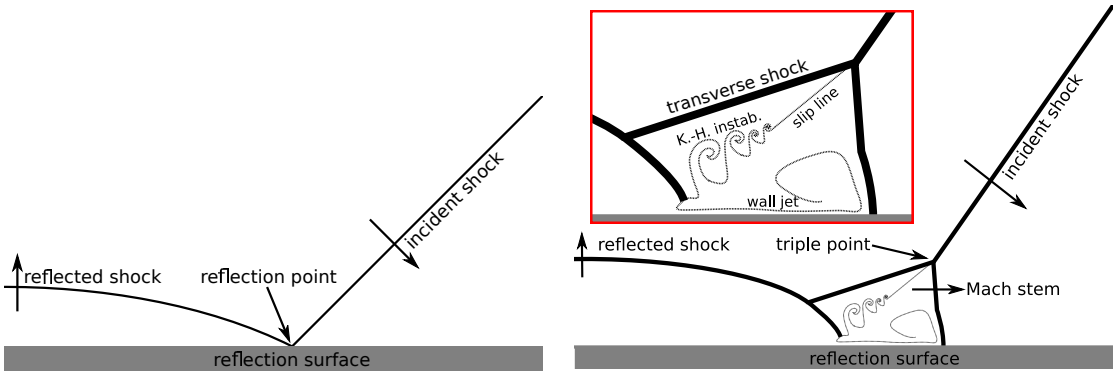

(a) Regular reflection

(b) Irregular reflection (Mach reflection; subtype: double Mach reflection)

Figure 1.2: Two types of shock reflections

The temperature increase across the incident and reflected shocks or the Mach stem, may be enough to cause auto-ignition and re-initiate the detonation. The shock compression across the Mach stem is generally believed to be the cause of detonation re-initiation.

Ohyagi et al. [10] diffracted detonations over a step while Obara et al. [9] diffracted detonations through slit plates. Both found detonation re-initiation along the Mach stem following reflection. Their soot foils provided evidence that transverse detonations (detonations along the reflected wave in vicinity of the triple point, sometimes called "super-detonations") accompany the Mach stem detonation re-initiation. Transverse detonations have been seen in the soot foils of Sorin et al. [17] and open-shutter photographs of Radulescu and Maxwell [11]. Transverse waves (although not necessarily transverse detonations) have been shown to be important to the propagation of detonations [11, 18, 19]. The transverse (or reflected) wave and Mach stem are both products of the shock reflection process.

Teodorczyk et al. [6, 7] passed detonations through channels with thin rectangular baffles. An example of their results is shown in Figure 1.3. Detonation re-initiation was witnessed following shock reflection off the bottom wall and was attributed to shock compression along the Mach stem with mixing along the slip line possibly also providing significant influence.

Mixing hot, burnt gas with cool, unburnt gas can cause the latter to react much faster by virtue of increased heat diffusion, or the presence of chemical radicals from the products. Kelvin-Helmholtz instabilities grow across slip lines and have the potential to increase contact surface area between burnt and unburnt gases, and thus increase

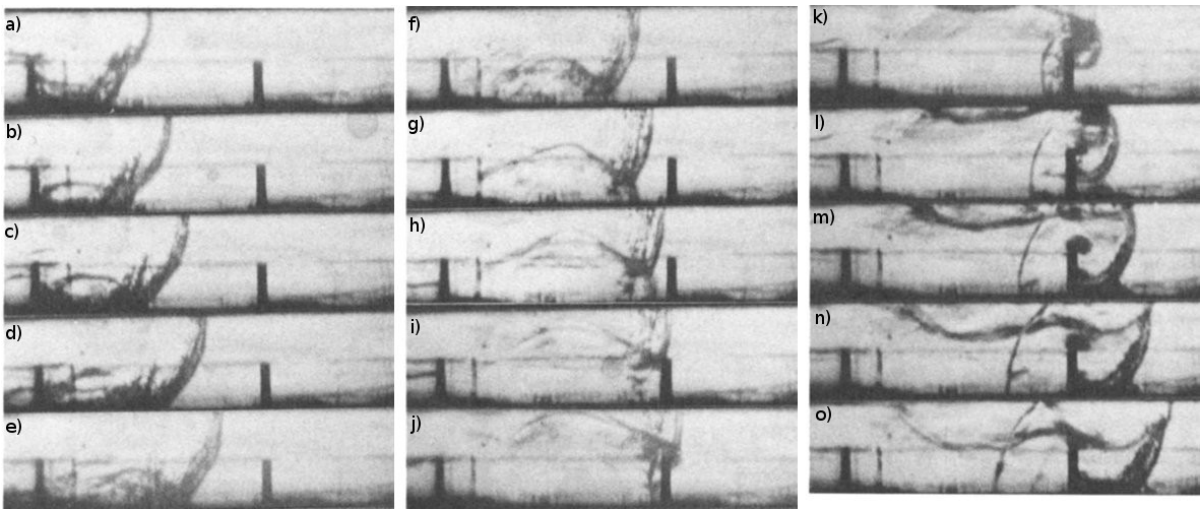

Figure 1.3: Schlieren photographs of periodic quenching and re-initiation of a detonation passing through an obstacle-filled channel [6]

reaction rates.

Kelvin-Helmholtz instabilities [20] are an expected by-product of the irregular shock reflection process described in figure 1.2(b). Gas shocked by the Mach stem is separated from gas shocked by the incident and reflected shocks by a contact discontinuity. While the pressure and flow direction across the contact discontinuity are equal, the temperature and flow velocity are not. Kelvin-Helmholtz instabilities are prone to form along the contact discontinuity due to velocity disturbances (which cause variations in pressure) on either side. Kelvin-Helmholtz instabilities create whirls, which grow along the slip-line as sketched in the figure 1.2(b) inset.

The Kelvin-Helmholtz instabilities allow for mixing between gas shocked by the Mach stem and gas shocked by the incident and reflected shocks. If gas on either side is burnt, diffusion of heat and chemical radicals through the surface, increased by the instabilities, may accelerate reactions on the other side. The rapid chemical reaction and expansion of products may re-initiate a detonation.

Another mechanism with the potential to increase mixing is the wall-jetting effect. This phenomenon appears as a by-product of the irregular shock reflection process [21]. The wall jet is a stream, travelling along the reflection surface, in which gas shocked by the Mach stem can recirculate towards the shock front, as shown in the figure 1.2(b) inset.

In the irregular reflection, flow along the contact discontinuity must eventually inter-

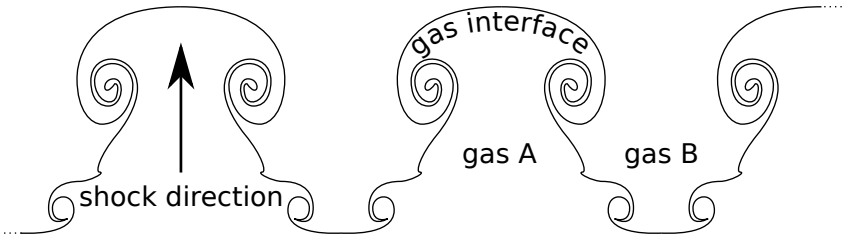

Figure 1.4: Richtmyer-Meshkov instability occurring after a shock has passed from gas A to gas B of different densities

sect the reflecting surface. If the pressure at this point is strong enough, it will force the flow back towards the Mach stem. Gas from the rear, also possibly burnt or burning, can be entrained with the wall jet as well, together forming a large, rolled-up vortex behind the Mach stem. The wall jet strength depends on the reflection angle [21].

Wall jetting was suggested by Sorin et al. [17] to be a vehicle for injecting combustion products behind the Mach stem, accelerating reaction rates and creating a detonation. Mahmoudi and Mazaheri [22] have shown numerically that wall jetting plays an important role in the consumption of gas behind the Mach stem.

The long residence time of gas in the wall jet or vortex, compared to newly shocked gas, may cause the gas to react in vicinity of the Mach stem. The vortex behind the Mach stem increases the mixing surface area between the two gases. If the flame front or burnt gas from the rear is entrained in the wall-jet, it can ignite the gas behind the Mach stem as it mixes, re-initiating an over-driven detonation.

Experiments by Bhattacharjee et al. [23] have diffracted a detonation over a half-cylinder and produced high resolution images indicating the importance of shock compression across the Mach stem and the wall jetting effect. In some of their recent work [24], they have also shown the potential role Richtmyer-Meshkov and Kelvin-Helmholtz instabilities may play in re-initiating a transverse detonation.

Richtmyer-Meshkov instabilities [25] occur when a shock wave passes through a sharp density gradient, due to wave-shape perturbations. Gas from either side of the density gradient protrude into the other as mushroom-like structures, sketched in Figure 1.4. Density gradients exist within the detonation structure in a few forms: along the slip line, along burnt/unburnt gas interfaces, and flame fronts. Richtmyer-Meshkov instabilities are expected whenever a shock wave pass through these interfaces.

The increased surface area caused by the instability will allow for increased mixing between burnt and unburnt gas on either side of the density gradient. Accelerated reaction rates and energy release generated by rapid combustion of unburnt pockets may

lead to detonation re-initiation.

The existing body of literature thus point to various mechanisms whereby a detonation can be reformed following shock reflection, namely

a. auto-ignition following shock compression,

b. jet entrainment of reaction products and subsequent mixing,

c. mixing via Richtmyer-Meshkov instability, and

d. mixing via Kelvin-Helmholtz instability.

At present, it is not clear which mechanism primes. More importantly, however, it is not clear which mechanism is required to be incorporated in a numerical model for predictive purposes. For example, the first mechanism requires the correct gas dynamic and chemical kinetic modelling behind shocks, while the last three require either Direct Numerical Simulation, or alternatively, turbulence models to be incorporated in order to make predictions. The present thesis attempts to answer this important question:
What type of model is required to make accurate predictions about the detonation re-initiation behind an obstacle?

1.2 Current study

Recently, a comprehensive experimental study has been conducted by Bhattacharjee, another student in the author's research group currently completing his Masters' degree, on the detonation interaction with an obstacle. Although significant insights have been achieved in that study, the questions raised above remain. In order to complement that investigation and attempt to answer the questions raised above, the present study has implemented a predictive numerical model.

The present study does not attempt to model the turbulent effects intrinsic in the last three mechanisms. Instead, the computational model uses the reactive Euler equations for compressible fluid flow, which neglect diffusive effects. Ideally, realistic chemical mechanisms could be used to accurately reproduce the time history of energy release in such highly compressible flow, and monitor hot spot activity and re-initiation transients. Nevertheless, since the chemical kinetics are usually very stiff (characterized by very small characteristic time and spatial scales), such computations are currently prohibitive. Instead, the current thesis focuses on two chemical models, which are both calibrated

against complex kinetic schemes. Specifically, a one-step Arrhenius chemical model [4] is used, which has already been used by Radulescu and Maxwell [11] with some success in modelling such flow fields, and a two-step chain-branching chemistry model [26], which can more accurately capture the correct exothermicity evolution behind shocks.

The present thesis is organized as follows. Chapter 2 presents a brief summary for the experiments conducted by Bhattacharjee [23], which this thesis aims to model. Chapter 3 presents the calibration of the single and two-step chemical models used for the modelling, along with the details of the numerical solver used to integrate the unsteady reactive Euler equations for the detonation interaction with a cylinder. Chapters 4 and 5 follow with the results obtained numerically, comparison with the experimental flow-fields, and discussion of the fidelity of the numerical model to predict detonation re-initiation behind an obstacle.

Chapter 2

Target experiment

The results of Bhattacharjee et al. [23] were used to validate the numerical model and simulations. In their experiments, a detonation propagating at approximately Chapman-Jouget (CJ) velocity (velocity of a steady-state detonation) impinged on a half-cylinder obstacle with a radius of 152 mm, in a manner similar to that illustrated by figure 1.1. Their experiments were conducted in stoichiometric methane-oxygen mixtures (the test gas) confined within a shock tube whose rectangular cross-section measured 203 mm in height by 19 mm in width. A side view of the shock tube is shown in figure 2.1.

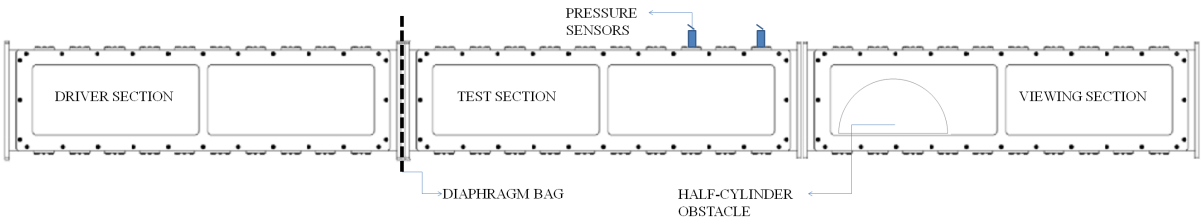

Figure 2.1: Experimental apparatus [23]

The shock tube measured 3.4 m in length and was composed of three sections: the driver, test, and viewing sections. The first section contained the driver gas. A spark plug initiated a detonation which burst a diaphragm separating the driver and test gases. Use of a driver gas and diaphragm was in some cases unnecessary, and the driver section would be filled with the test gas. The diaphragm burst initiated a detonation in the second section. Pressure sensors at the end of the this section allowed for the detonation arrival time to be measured at two consecutive locations, thus allowing for detonation speed measurements. The detonation then passed over the obstacle into the viewing section (also filled with the test gas) where high resolution schlieren photographs or

videos were used to capture the detonation diffraction and re-initiation process.

A Z-configuration schlieren setup was used to take two photographs, 11 μs apart. Several experiments were used to create the flow fields which are, in part, shown in the results, chapter 4. The recent acquisition of a high speed camera has also allowed schlieren videos to be taken. Frames from two example videos are shown in figures 2.2 and 2.3.

The experimental schlieren photographs show density gradients. A dark feature indicates decrease of density from left to right while a bright feature indicates the contrary. For example, a dark line could be interpreted as a shock wave travelling from left to right. Vertical gradients (i.e. changes between the top and bottom) do not always appear due to the experimental set-up. Furthermore, methane-oxygen reactions are self-luminescent (i.e. they emit visible light) so it is possible for a reaction to obscure dark features.

The initial gas pressure in the shock tube was varied from 5.5 kPa to 17.6 kPa while the temperature was kept constant at approximately 300 K. Varying the initial pressure changed the gas's sensitivity to re-initiation and allowed for the exploration of different regimes.

The first regime encountered was that of *detonation quenching*. It occurred consistently at low pressures (e.g. 5.5 kPa). The shock front and reaction zone would decouple as the detonation diffracted over the obstacle. No detonation re-initiation occurred and the detonation remained quenched.

The *critical* regime occurred at pressures around 10.3 kPa. This regime sits on the verge of detonation re-initiation and two different outcomes are possible: ignition behind the Mach stem ("ignition" will refer to subsonic combustion (deflagration) in this thesis), and detonation re-initiation along the Mach stem.

An example of ignition behind the Mach stem is shown in figure 2.2. The field of view is located downstream, to the right, of the obstacle and first captures the detonation after it has transitioned to irregular reflection as shown in figure 2.2(a). A large induction zone can be seen between the incident shock and reaction front. A small Mach stem can be seen near the bottom wall. This Mach stem grows in the following frames. Gas behind the Mach stem remains unburnt until figure 2.2(d) where burnt gas fills the wall jet and vortex. A reaction wave can be spotted closely trailing the Mach stem in the remaining frames (seen as a rough, bright feature to the left of the Mach stem, and denoted in figure 2.2(h)). The wall jet's influence on the slip line can be seen in figure 2.2(f), curling it towards the Mach stem. A long tongue of unburnt gas, composed of gas shocked by the incident and reflected waves, trails from the triple point towards the bottom left. It

lies to the left of the slip line, shows textured bright features, and can be seen in figure 2.2(h), for example.

In the case of detonation re-initiation along the Mach stem, the flame couples with the Mach stem and a detonation is initiated, in a similar fashion to what is seen in figure 2.3(e).

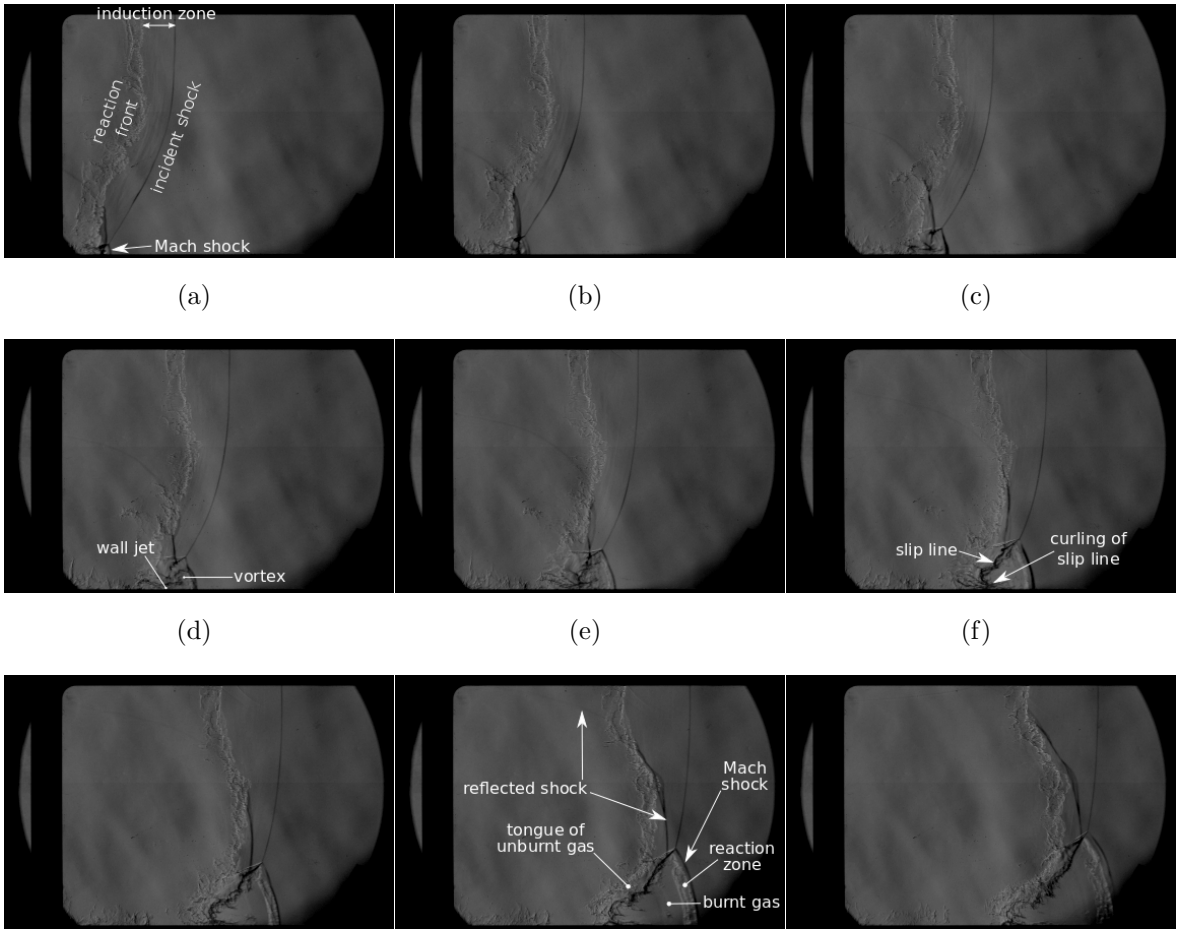

Figure 2.2: Experimental schlieren photographs of an ignition behind the Mach stem (10.1 kPa, 11 μs inter-frame delay) [24]

The regime of *detonation re-initiation along the Mach stem and transverse wave* occurs at pressures slightly above the critical regime. An example is shown in figure 2.3. As in the critical case discussed above, an irregular reflection is seen in the first frame, figure 2.3(a). The irregular reflection grows, as before, and gas behind the Mach stem is consumed. In this case, a detonation is re-initiated at the Mach stem foot, as

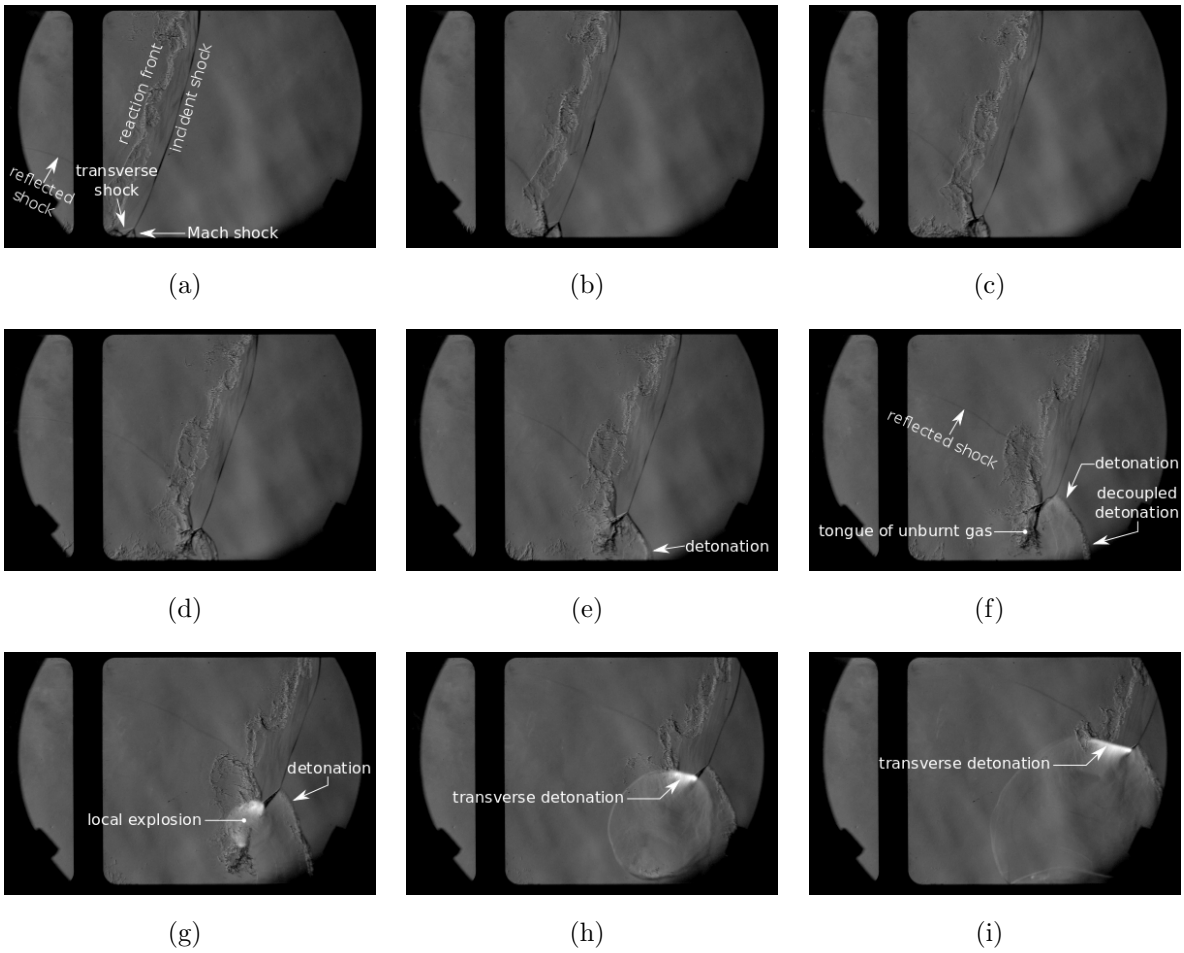

Figure 2.3: Experimental schlieren photographs of a detonation re-initiation (12.1 kPa, 11 μs inter-frame delay) [24]

shown in figure 2.3(e) by light emission, fine whisker-like features (local transverse shocks) and inter-frame velocity measurements. Figure 2.3(f), shows the top of the Mach stem detonates while the bottom has quenched due to expansion. An explosion has occurred in the tongue of unburnt gas by the next frame, figure 2.3(g), shown by luminosity and the presence of a circular shock behind which textured features of unburnt gas quickly disappear. The explosion initiates a detonation along the transverse wave in the following frames which have similar features to the Mach stem detonation.

Further increase of pressure leads to the *detonation transmission* regime where the detonation never quenches while diffracting over the obstacle.

A model should be capable of replicating the various regimes presented in experiments, with a particular emphasis on the detonation re-initiation regime. This is the goal of the present thesis.

Chapter 3

Model

3.1 Gas dynamic model

The problem was addressed through numerical experiments. The dissipation terms in the Navier-Stokes equation were neglected. The hydrodynamics of the problem were modelled using the reactive Euler equations for a calorically perfect gas in two dimensions

$$\frac{\partial W}{\partial t} + \frac{\partial F}{\partial x} + \frac{\partial G}{\partial y} = 0 \tag{3.1}$$

where

$$W = \begin{bmatrix} \rho \\ \rho u \\ \rho v \\ E + Q\lambda_r \end{bmatrix}, F = \begin{bmatrix} \rho u \\ \rho u^2 + p \\ \rho uv \\ (E + p + Q\lambda_r)u \end{bmatrix}, G = \begin{bmatrix} \rho v \\ \rho vu \\ \rho v^2 + p \\ (E + p + Q\lambda_r)v \end{bmatrix} \tag{3.2}$$

and ρ is the density, u is the x-component of velocity, v is the y-component of velocity, Q is the heat release, λ_r is the reaction progress variable, E is the total energy given by

$$E = \frac{R_s T}{\gamma - 1} + \frac{1}{2}\rho u^2 + \frac{1}{2}\rho v^2,$$

where R_s is the specific gas constant, γ is the isentropic exponent, T is the temperature, and p is the pressure found from the ideal gas law

$$p = \rho R_s T. \tag{3.3}$$

3.1.1 Zel'dovich-von-Neumann-Döring (ZND) Detonations

The reactive Euler equations admit a travelling wave solution comprised of a shock followed by a reaction zone. This one-dimensional structure is the so-called Zel'dovich-von-Neumann-Döring (ZND) structure [4] for a detonation travelling at constant speed. Profiles of the solution are shown in figure 3.1 where the realistic chemistry detonation is compared with the profiles computed using calibrated, simplified chemistry models as detailed below.

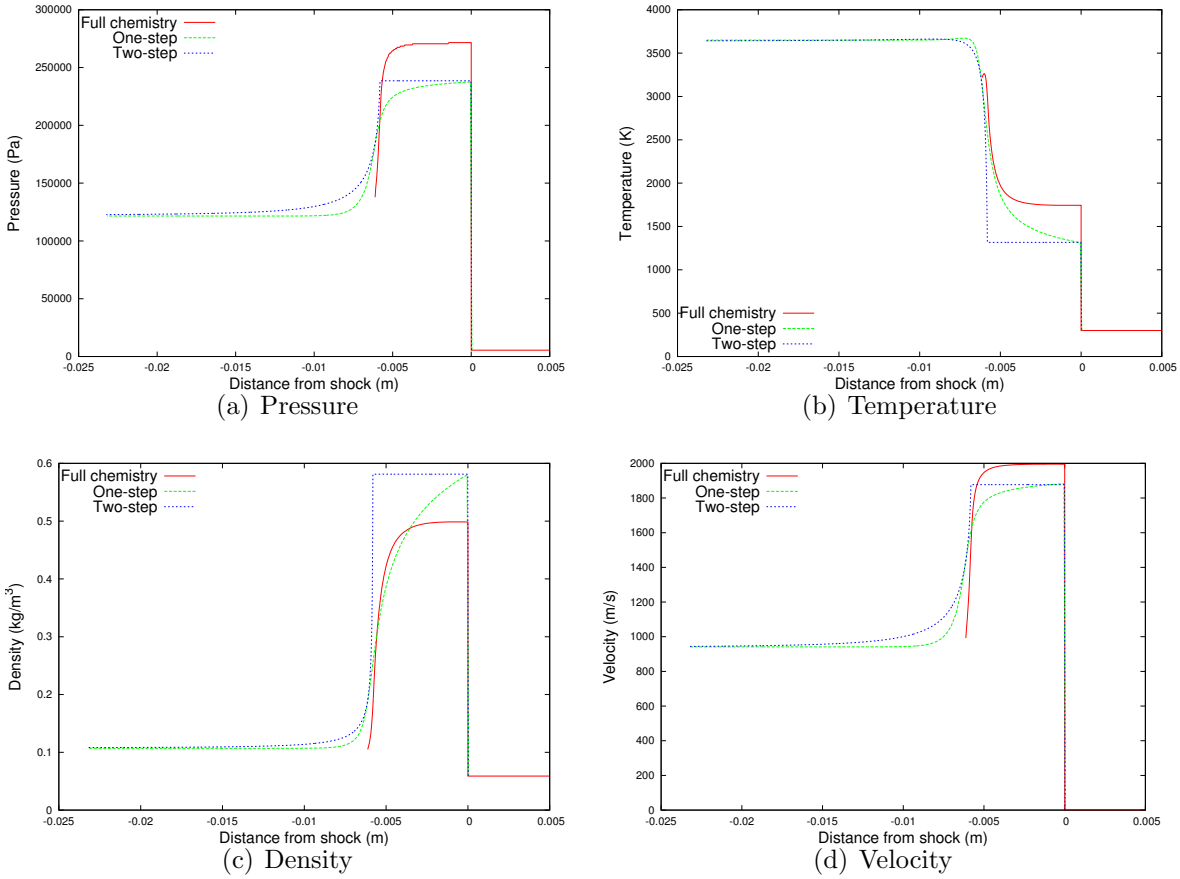

(a) Pressure (b) Temperature

(c) Density (d) Velocity

Figure 3.1: ZND profiles of a detonation through stoichiometric methane-oxygen at 5.5 kPa (full chemistry computed with GRI 3.0 mechanism [1])

The ZND profiles shown in figure 3.1 illustrate the two characteristic steps in the reaction zone. This is shown schematically in figure 3.2. Following the shock compression,

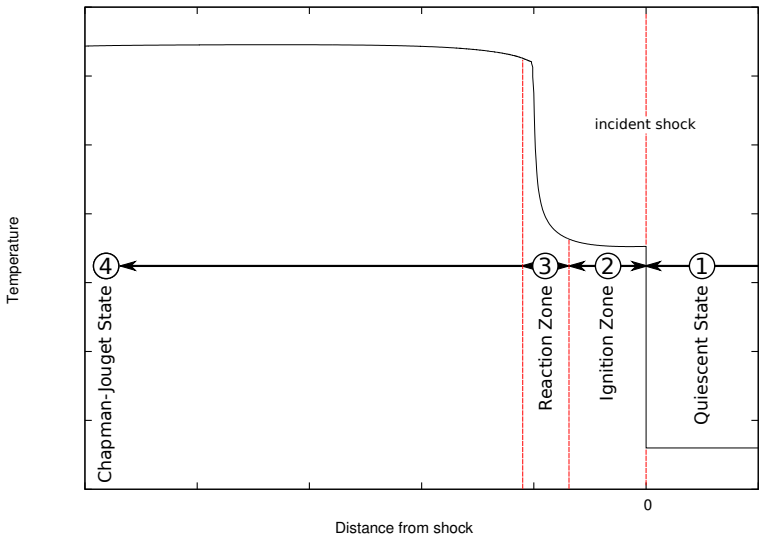

Figure 3.2: ZND detonation profile

the first zone consists of the induction (ignition) layer. The induction zone is characterized by very weak exothermicity. At the end of the induction period, energy is liberated at a fast rate in a much thinner reaction layer. Usually, the ignition delay depends exponentially on the local temperature and more weakly on pressure. For example, figure 3.3 illustrates a compilation of experimental measurements of the induction time delay obtained using the reflected shock technique over the temperature range relevant to detonation waves, namely 1000K to 2500K [1, 27–36]. As can be seen, the ignition delays recover the well known Arrhenius dependence, whereby the ignition delay is proportional to the exponential of the inverse temperature.

The isentropic exponent, heat release, and activation energy were assumed to be constant throughout the simulations. This was done to simplify the model as much as possible. Figure 3.3 shows that activation energy remains constant. The constant isentropic exponent assumption has previously been made in numerical detonation studies [11, 37–41]. Selection of a proper value for the isentropic exponent is important as it usually is a function of temperature and composition in reality, both of which change during combustion. This is discussed in the following sections and in more detail in appendix A. The correct post-shock state must be reproduced in order to accurately choose and produce these parameters and ignition time, which is crucial to reproducing the correct ZND structure.

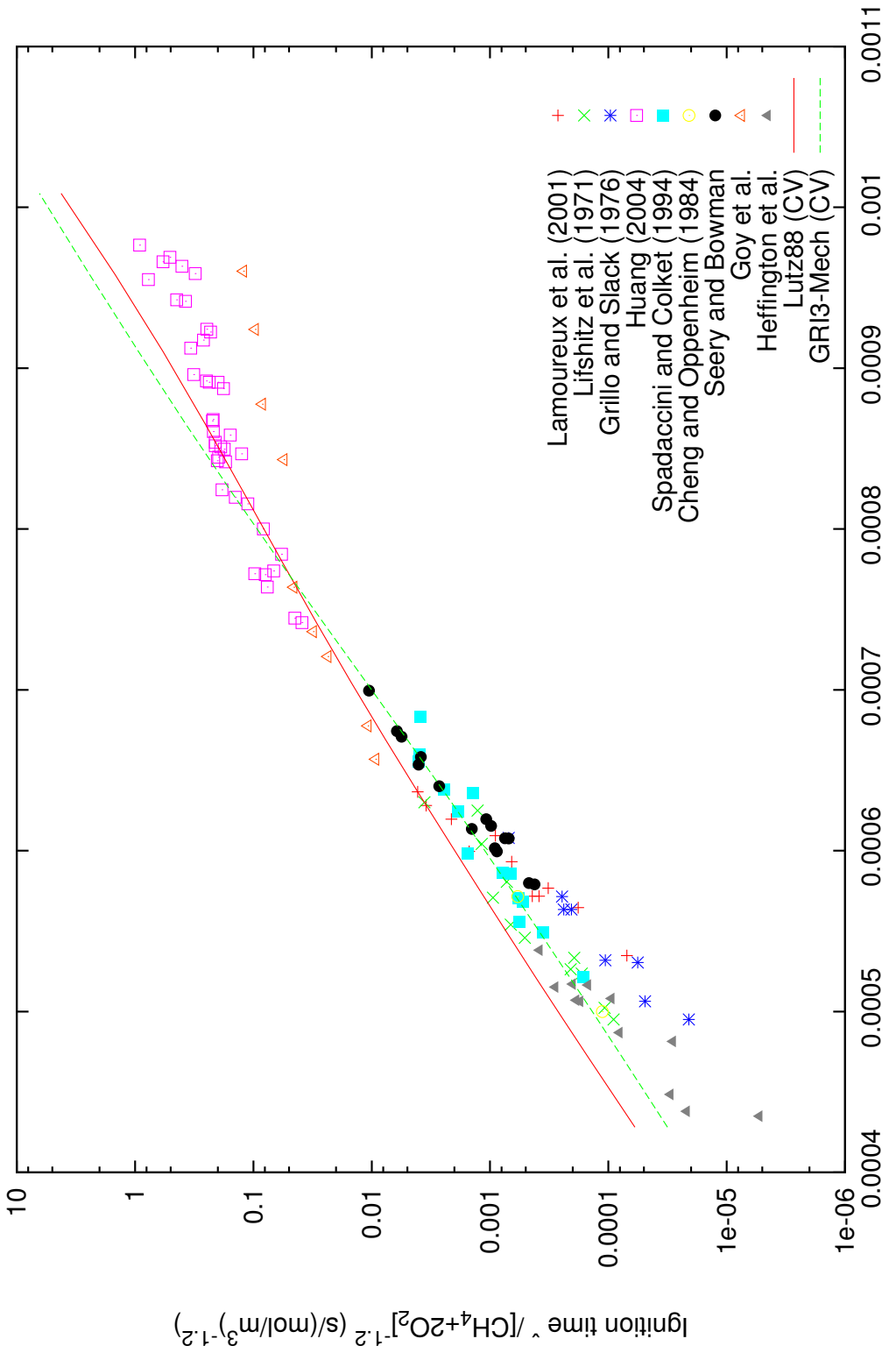

Figure 3.3: Ignition delay of stoichiometric methane-oxygen [1, 27–36]

3.2 Chemical model

3.2.1 Realistic chemical models

Constant-volume combustions can be used to approximate the rapid combustion occurring behind shocks and detonations [42]. The constant-volume ignition delays of two hydrocarbon mechanisms valid for methane combustion, the GRI 3.0 [1] and Lutz88 [36] chemical mechanisms, at quiescent post-shock conditions are plotted in figure 3.3 for comparison. The GRI 3.0 mechanism has been developed for natural gas and methane combustion. It also provides a better fit to the experimental data at high temperatures, while the Lutz88 mechanism provides a slightly improved fit at low temperatures. The ignition delay for stoichiometric methane-oxygen increases at a constant exponential rate as temperature decreases until a certain point (about 1100 K), where this rate slows. Neither mechanism is able to model this change and it remains an open problem in methane combustion [28, 34]. Note that this regime also corresponds to anomalous ignition in the shock tube experiments, and is usually characterized by hot spot ignition [43].

While full-chemistry models arguably simulate real chemistry accurately, they are computationally expensive. Every intermediate reaction and species must be accounted for, and both of these realistic chemical models contain tens to hundreds of equations. The computational mesh required to resolve the scale at which these reactions occur would also be incompatible with the scale of the apparatus, given the available computing resources. Simplified chemical models were used as an alternative way to approximate the reactions. The simplified models used in this study were the one-step Arrhenius chemistry model [4] and the two-step chain-branching chemistry model [26]. They reduce the global chemical reaction rate to one and two equations, respectively. They must be calibrated to correctly approximate the desired chemistry due to their simplicity. In this study they were calibrated to match the ignition delay and post-shock conditions (behind the detonation's incident shock wave) using the GRI 3.0 mechanism in order to reproduce conditions where the chemical reactions occur in the detonation and detonation re-initiation processes.

3.2.2 One-step Arrhenius chemistry

The one-step Arrhenius chemistry model [4] lumps the entire reaction into a single reaction progress variable. The rate at which the reaction progresses is expressed in a simple Arrhenius form, hence the model's name. The model has the disadvantage that induc-

tion and reaction zones are poorly defined, seen in figure 3.1, and are both governed by the same activation energy. The induction zone cannot be changed without the reaction zone changing, and vice-versa. Gases with different ratios of induction to reaction times are therefore poorly modelled, which is the case for methane.

The one-step Arrhenius chemistry model's reaction rate is written as

$$\frac{D\lambda_r}{Dt} = -k\lambda_r e^{\frac{-E_a}{R_s T}}. \tag{3.4}$$

where λ_r is the reaction progress variable such that

$$\lambda_r = \begin{cases} 1 & \text{in reactants} \\ 0 & \text{in products} \end{cases},$$

the activation energy is E_a and k is a pre-exponential factor used for scale.

The solution was reported in non-dimensional form. Initial density, pressure and temperature were chosen for their respective scales. Velocity was scaled by $\sqrt{p_0/\rho_0}$ in order for the equations to remain invariant. Lengths in both the horizontal and vertical directions were scaled by the half-reaction length $\Delta_{\frac{1}{2}}$ (the distance by which half the heat of reaction has been released and when the reaction progress variable reaches a value of one-half) for the problem. The non-dimensional variables, denoted by tildes, are

$$\tilde{p} = \frac{p}{p_0}, \quad \tilde{\rho} = \frac{\rho}{\rho_0}, \quad \tilde{T} = \frac{T}{T_0}, \quad \tilde{u} = \frac{u}{\sqrt{\frac{p_0}{\rho_0}}}, \quad \tilde{v} = \frac{v}{\sqrt{\frac{p_0}{\rho_0}}}, \quad \tilde{x} = \frac{x}{\Delta_{1/2}}, \quad \tilde{y} = \frac{y}{\Delta_{1/2}}.$$

The heat release and activation energy were scaled by $R_s T_0$

$$\tilde{Q} = \frac{Q}{R_s T_0}, \quad \tilde{E_a} = \frac{E_a}{R_s T_0}. \tag{3.5}$$

Sensitivity of the gas was adjusted by changing the initial pressure in the experiments. For the numerical simulations, this required changing the length scale $\Delta_{\frac{1}{2}}$ at the desired initial pressure P_0 in order to account for the change in reaction time. The half-reaction length was used to compute the pre-exponential factor k in the chemical rate equation 3.4. The half-reaction length was determined in the same manner as by Radulescu and Maxwell [11]: the velocity for a stoichiometric methane-oxygen detonation initially at 300 K and 5.5 kPa was calculated using the NASA Chemical Equilibrium with Applications (CEA) code [44] and thermodynamic data. This detonation velocity and each desired initial condition were then used to compute ZND profiles using Shepherd's ZND code [45] and the GRI 3.0 chemical mechanism [1]. The half-reaction length was approximated to

Table 3.1: Simulation parameters for use with one-step Arrhenius chemistry reaction

P_0	5.5 kPa	10.3 kPa	11.9 kPa	12.5 kPa	17.6 kPa
$\Delta_{\frac{1}{2}}$	5.81 mm	2.77 mm	2.34 mm	2.21 mm	1.48 mm

T_0	γ	$\tilde{Q}$	$\tilde{E}_a$
300 K	1.17	60.5	48.3

be equal to the induction length which was measured as the distance between the shock and the maximum temperature derivative in the ZND profile.

The parameters were calibrated to match post-shock conditions, the area of interest concerning the detonation re-initiation mechanisms. The post-shock conditions were calculated using frozen chemistry and the NASA CEA code [44]. The post-shock state (denoted with the subscript vN) was used as the initial conditions for a constant-volume combustion calculation performed with Shepherd's CV code [46] and the GRI 3.0 mechanism [1]. The ignition delay was measured as the time necessary to reach the maximum temperature derivative. The calculation was performed again for $T_{vn} \pm 5\%$ and the slope of the $\left(\frac{1}{T}, \ln(\tau_{ig})\right)$ points was used to find activation energy.

The heat release Q, required by the conservation of energy equation 3.2, was calculated using CJ Theory [5] for steady-state detonations

$$\frac{Q}{R_s T_0} = \frac{\gamma}{2(\gamma^2 - 1)} \left(M_{CJ} - \frac{1}{M_{CJ}} \right)^2 .$$

The parameter values used in the simulations appear in table 3.1.

3.2.3 Two-step chain-branching chemistry

The two-step chain-branching chemistry model [26] was developed to model reactions with an important chain-branching period [47, 48]. This model is another simple alternative to simulating real chemistry. It begins with a thermally neutral induction zone, whose duration has the appropriate exponential dependence on temperature. This models the temperature-sensitive chain-branching step of a reaction where reactants form chemical radicals. At the end of the induction zone begins the reaction layer, where the energy is released with a controllable rate independent of the induction duration. This models the temperature-insensitive chain-termination step. The two-step chain-branching model is composed of two equations, one describing the induction zone

$$\frac{D\lambda_i}{Dt} = -k_i e^{\frac{-E_a}{R_s T}} \tag{3.6}$$

and the other describing the reaction zone

$$\frac{D\lambda_r}{Dt} = -k_r\lambda_r^{\nu}. \tag{3.7}$$

Each has its own progress variable; the induction progress variable λ_i is

$$\lambda_i = \begin{cases} 1 & \text{in reactants} \\ 0 & \text{in reaction zone and products} \end{cases},$$

and the reaction progress variable λ_r is

$$\lambda_r = \begin{cases} 1 & \text{in reactants and induction zone} \\ 0 & \text{in products} \end{cases}.$$

When the induction zone begins, the induction progress variable decreases towards zero at which point the induction zone rate equation 3.6 is turned off and the reaction zone rate equation 3.7 is turned on.

The half-reaction length, activation energy and heat release were measured the same way as for the one-step chemistry section 3.2.2. The half-reaction length was used to calculate the pre-exponential factor k_i in the rate equation 3.6. The reaction zone length was measured as the thermicity's half-height width described by Kao and Shepherd [49] resulting in the ratio $\frac{\Delta_i}{\Delta_r} = 19.1$ used to scale the reaction zone factor k_r. Thermicity is the normalized chemical energy release rate [50] and is defined for a full-chemistry reaction as

$$\dot{\sigma} = \sum_{i=1}^{N_s} \left(\frac{W}{W_i} - \frac{h_i}{c_p T} \right) \frac{dY_i}{dt} \tag{3.8}$$

where N_s is the total number of species, W is the molecular weight, h is the enthalpy, c_p is the specific heat at constant pressure, and Y is the mass fraction of the species.

The reaction order was selected $\nu = 0.8$ to approximate the full chemistry ZND profile. The parameters used are summarized in table 3.2.

The solution was again reported in non-dimensional form, however values in the post-shock state were used to scale the results, meaning that for the two-step model

$$\tilde{p} = \frac{p}{p_{vN}}, \quad \tilde{\rho} = \frac{\rho}{\rho_{vN}}, \quad \tilde{T} = \frac{T}{T_{vN}}, \quad \tilde{u} = \frac{u}{\sqrt{\frac{p_{vN}}{\rho_{vN}}}}, \quad \tilde{v} = \frac{v}{\sqrt{\frac{p_{vN}}{\rho_{vN}}}},$$

$$\tilde{x} = \frac{x}{\Delta_i}, \quad \tilde{y} = \frac{y}{\Delta_i}, \quad \tilde{Q} = \frac{Q}{R_s T_{vN}}, \quad \tilde{E_a} = \frac{E_a}{R_s T_{vN}}.$$

Table 3.2: Simulation parameters for use with two-step chain-branching chemistry

P_0	5.5 kPa	10.3 kPa	11.9 kPa	12.5 kPa	17.6 kPa
Δ_i	5.81 mm	2.77 mm	2.34 mm	2.21 mm	1.48 mm

T_0	γ	$\tilde{Q}$	$\tilde{E}_a$	$\frac{\Delta_i}{\Delta_r}$	ν
300 K	1.17	13.7	11.0	19.1	0.8

3.3 Numerical environment

The reactive Euler equations coupled with the one step or two step model were solved in two dimensions using the AMRITA CFD program developed by Quirk [51]. The hydrodynamic solver for the convective terms in the governing equations was based on the Roe's linearized Riemann finite-volume solver [52, 53], with Harten's entropy fix [54] and the minmod flux limiter [55] resulting in second-order spacial accuracy. Mach [56] compared different solvers (Advection Upstream Splitting Method (AUSM) [57], Equilibrium Flux Method (EFM) [58], Godunov's method [59], Einfeldt's Harten-Lax-van-Leer method (HLLE) [60], and Roe's method [52, 53]) and found little qualitative, but some quantitative, differences regarding Mach stem bifurcation during inert shock reflections at detonation-like conditions. Sharpe and Quirk [61], comparing a Lax-Friedrichs based solver with WENO reconstruction to Roe's solver, found that cellular dynamics were insensitive to the numerical scheme used. They also found little difference between the use of minmod and superbee [55] flux limiters. Roe's solver was selected, from many viable options, so the results would be comparable to similar simulations done by Radulescu and Maxwell [11]. A solver study was not conducted.

The obstacle was implemented using the embedded boundary technique described by Xu and Aslam [62], permitting the use of a Cartesian computational grid.

An example of the computational domain is shown in figure 3.4. The base grid consisted of 200 points along the horizontal and 24 points along the vertical axes. The throat (minimum distance between the cylinder and top wall), spanning 0.057 m in experiments, was covered by 6 base grid points. The top, bottom and internal (obstacle) boundaries were reflective. The left boundary was set to the CJ state while the right boundary condition was a linear extrapolation of the right-most cells. The simulation was initiated with a planar ZND detonation, whose shock discontinuity was located at $\tilde{x} = 5.5$, upstream of the obstacle centred at $\tilde{x} = 9$.

An adaptive mesh refinement technique was used to improve the accuracy of the solution near areas of interest while reducing computational effort. This came included as

(a) Density plot

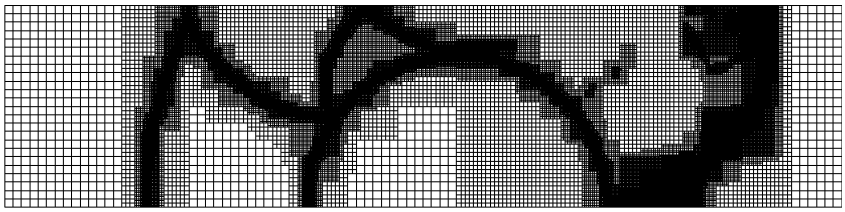

(b) Adapted mesh

Figure 3.4: Density plot and corresponding grid focused on areas with density gradients, the obstacle, and zones of chemical change (12.5 kPa, one-step model, portion of entire domain shown)

part of the AMRITA package, adapted by Quirk [63,64] from work by Berger et al. [65,66]. Rectangular patches of refined mesh were positioned at areas of interest, using the coarser grid as boundary conditions. Each level of refinement increased the mesh density by a factor of two, in each direction. The refined mesh flux terms, followed by source terms, were integrated, and the process repeated recursively until the desired resolution was reached. The refined meshes were then projected back onto their coarser meshes. Smaller time steps were taken on refined meshes in order to maintain stability. The explicit time stepping size was determined using the Courant-Friedrichs-Lewy condition [67] with a Courant number of 0.5 [68]. The mesh was refined around regions of density gradients, the obstacle, reaction and induction zones as shown in figure 3.4. A minimum of 32 grid points per half-reaction length of the ZND detonation was used to resolve in areas of interest [11]. For reference, the most resolved grid, if it were to cover the entire domain, would correspond to a grid 3072 by 25,600 points covering the domain. Information on the effect of resolution can be found in the discussion section 5.3. Such resolved simulations require the adaptive mesh refinement capability in order to become computationally feasible.

3.4 State of the art

Many previous numerical studies have focused on the deflagration-to-detonation transition of subsonic flames travelling over obstacles [14, 69–71]. These studies have used the Navier-Stokes equations for ideal gases and one-step chemistry. They have mostly looked at the problems in two-dimensions with simplified diffusion terms. Previous numerical simulations of detonation diffraction and detonation re-initiation [11, 17, 40, 41, 72, 73] have neglected diffusion terms, using the two-dimensional Euler equations instead of the Navier-Stokes equations. A variety of solvers are used. The chemical mechanisms are reduced and consist of one- or two-step models. As a consequence, isentropic exponents have been either held constant or varied with temperature, however, details of model calibration vary between studies.

The use of the Euler equations for a perfect gas with one-step or two-step chemical models in this study conforms with the state of the art. The code for the one-step model was based of the work done by Radulesu and Maxwell [11]. The code used for the two-step model was adapted from the work of Leung [74], where the two-step model [26] was adapted from the work of Short and Quirk [75]. Computations each took approximately one month on single cores of an Intel Core2 Duo E8400 and AMD Phenom II X6 1090T processor. The scripts are available in appendix B.

Chapter 4

Results

4.1 Overview

The present chapter shows the results obtained from the numerical simulations and comparison with the experimental results of Bhattacharjee et al. [76]. Simulations of stoichiometric methane-oxygen detonations interacting with a cylindrical obstacle are presented for the five different conditions studied experimentally. In the experiments, the initial pressure was varied from 5.5 kPa, to 10.3 kPa, 11.9 kPa, 12.5 kPa, and finally 17.6 kPa. Experimental schlieren photographs from Bhattacharjee et al. [76] are shown for comparison. The locations in the channel where the photographs were taken are not necessarily the same as those shown in the numerical results due to the somewhat stochastic nature of methane detonations.

The numerical figures show linear density plots where dark regions (black: $\tilde{\rho} \geq 20$) are more dense than light ones (white: $\tilde{\rho} = 0$). Reaction progress plots show unreacted gas as white and fully reacted gas as black. Results are shown at various times, in position (with the exception of enlarged plots), and are separated by dashed lines. The time elapsed between frames is not constant. Other plots (i.e. temperature, pressure, reaction progress, velocity) are not shown unless necessary to clarify the detonation re-initiation mechanisms or flow field.

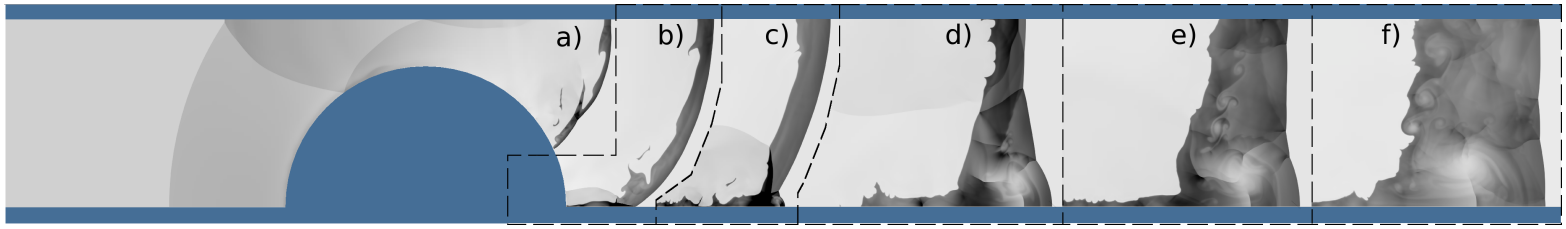

(a) Density plot (simulation, one-step chemistry)

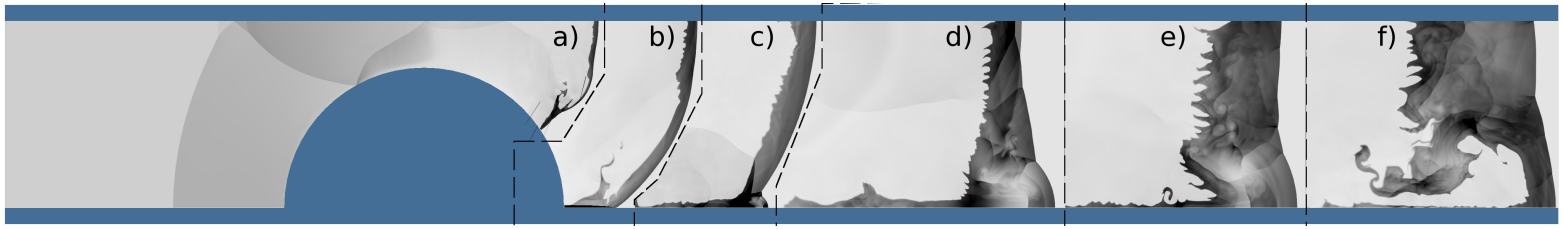

(b) Density plot (simulation, two-step chemistry)

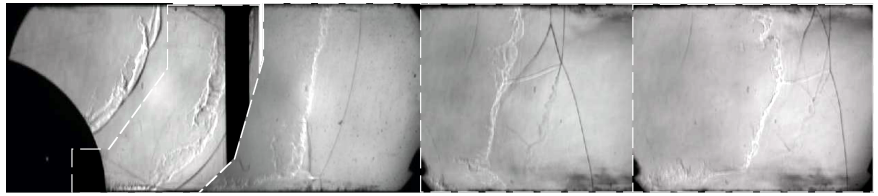

(c) Schlieren photographs (experiments [76])

Figure 4.1: Detonation through stoichiometric methane-oxygen at 5.5 kPa

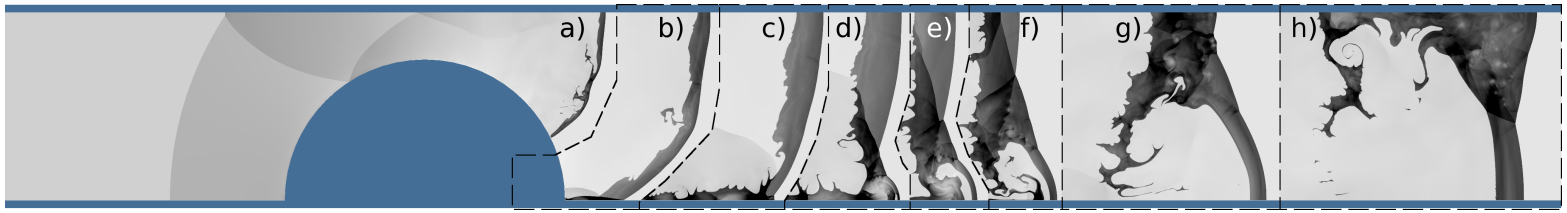

(a) Density plot (simulation with one-step chemistry)

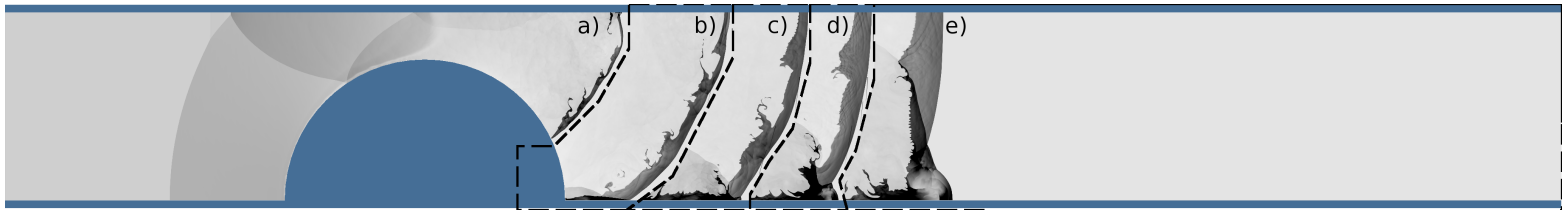

(b) Density plot (simulation with two-step chemistry)

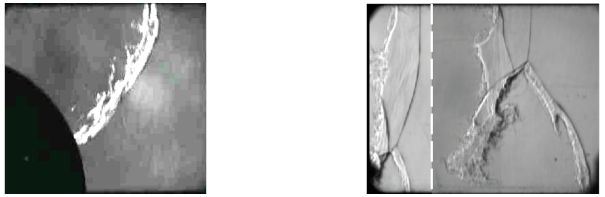

(c) Schlieren photographs (experiments [76])

Figure 4.2: Detonation through stoichiometric methane-oxygen at 10.3 kPa

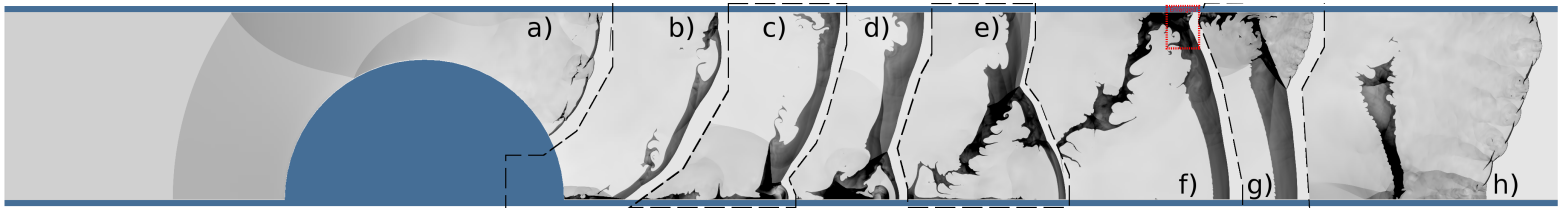

(a) Density plot (simulation, one-step chemistry)

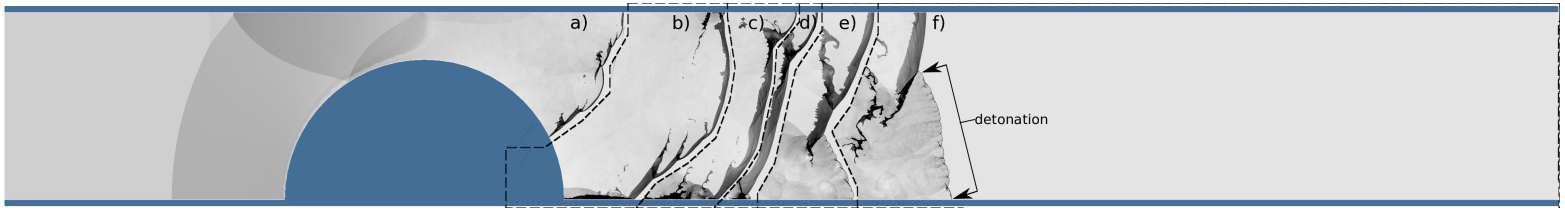

(b) Density plot (simulation, two-step chemistry)

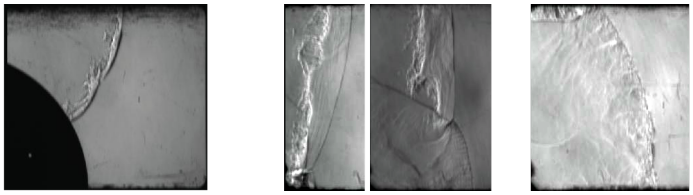

(c) Schlieren photographs (experiments [76])

Figure 4.3: Detonation through stoichiometric methane-oxygen at 11.9 kPa

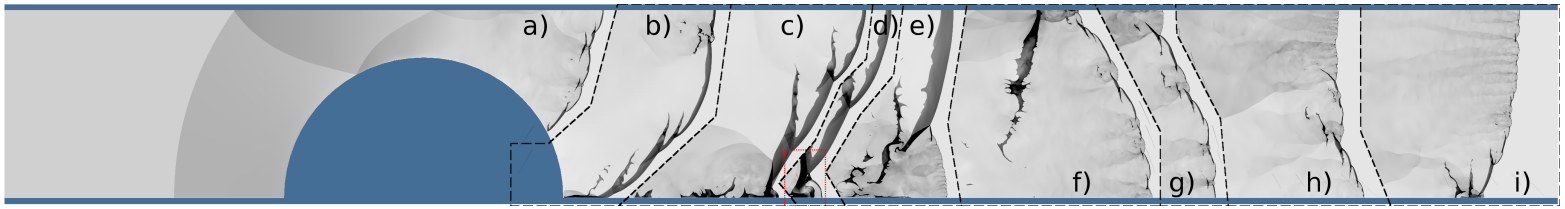

(a) Density plot (simulation, one-step chemistry)

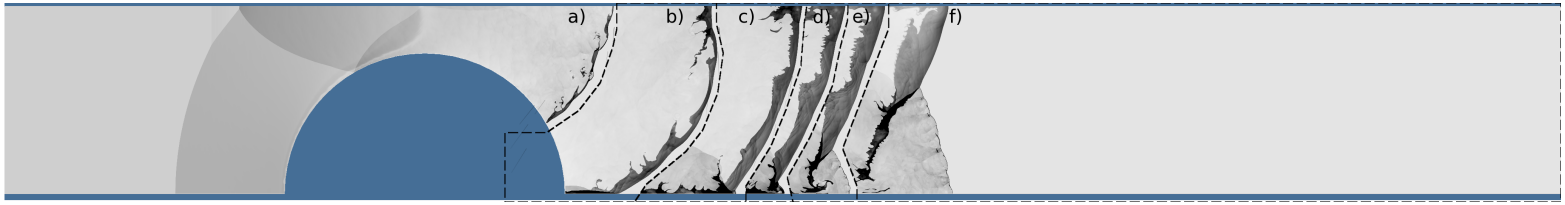

(b) Density plot (simulation, two-step chemistry)

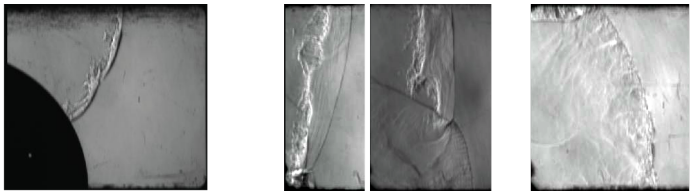

(c) Schlieren photographs (experiments [76], 11.9kPa)

Figure 4.4: Detonation through stoichiometric methane-oxygen at 12.5 kPa

4.2 Detonation quenching (5.5 kPa)

Simulation results for a detonation through stoichiometric methane-oxygen at 5.5 kPa are shown in figure 4.1. The first row corresponds to the one-step chemistry model, while the second corresponds to the 2 step model. The bottom row shows select experimental frames obtained at similar conditions.

4.2.1 One-step Arrhenius chemistry

Frame a) of figure 4.1(a) shows that the detonation is quenched as it travels over the obstacle; the shock front is separated from the reaction zone. A regular reflection occurs in frame b) as the incident wave reflects off the bottom wall. The induction zone behind the incident wave can be seen to lengthen. The angle between reflection surface and incident wave increases due to the incident wave's curvature, which causes a transition to an irregular reflection, seen in frame c). The reflected wave in the burned products has now travelled almost halfway to the top of the channel. It diffracts into the induction zone (towards the incident shock) due to the lower speed of sound in the unburnt gas. Details are shown in figure 4.5(a). By frame d), the reflected wave in the burnt products has reflected off the top wall and is travelling downwards. The triple point on the incident wave has travelled more than halfway up and the Mach stem is clearly bifurcated with a large vortex-like structure growing from the bottom wall. The slip-line is clearly visible and Kelvin-Helmholtz instabilities are beginning to form along it. Details are shown in figure 4.5(b). The flow field has become complicated by frame e). The shock front has flattened and large Kelvin-Helmholtz instabilities are visible but their origin is now obscured. Structures resembling Richtmyer-Meshkov instabilities appear in the bottom-most Kelvin-Helmholtz instabilities; however, their actual cause is unclear. The reaction zone has separated itself far from the shock front and the detonation remains quenched through frame f).

4.2.2 Two-step chain-branching chemistry

Figure 4.1(b) shows simulation results using the two-step chemistry model. Frames a) through c) are quite similar to those of the one-step model; however, the induction zone is slightly thinner. Frames d) and e) differ from the one-step model with largely increased corrugation of the reaction front. Finer and more detailed structures appear in the two-step model results. Frame e) contains structures resembling Richtmyer-Meshkov

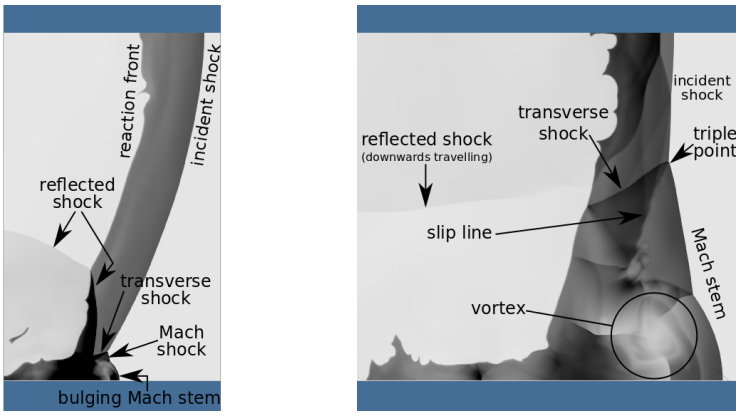

(a) Figure 4.1(a) frame c) (b) Figure 4.1(a) frame d)

Figure 4.5: Density plot details from figure 4.1(a) (5.5 kPa, one-step chemistry)

instabilities. Combustion along the wall jet is more pronounced than in the one-step model, consuming and growing into the region behind the Mach stem by frame f).

4.2.3 Experiments

Experimental results are shown in figure 4.1(c) for comparison. The same series of events occur and are qualitatively similar to the simulations. Experiments at this pressure were very reproducible. In-depth analysis and description has been done by Bhattacharjee et al. [76].

4.2.4 Shock velocity

A quantitative comparison can also be made between experiments and numerical simulations in terms of the shock strength. In the experiments, measurements of shock speed were performed along the top and bottom walls of the channel [24]. Experimental shock speeds are compared here with the distance measured from the throat in units of obstacle diameters, as reported by Bhattacharjee [24].

The velocity profiles of the incident shock, along the top wall, and the Mach stem, along the bottom wall, appear in figure 4.6. Transition from regular to Mach reflection occurs along the bottom wall at about one diameter from the throat. The Mach stem velocity increases to a maximum then begins to decay and does so for the remainder of the simulation. The incident shock along the top wall travels with the detonation at first, but its velocity decays as the detonation quenches, until a distance of about 2.2

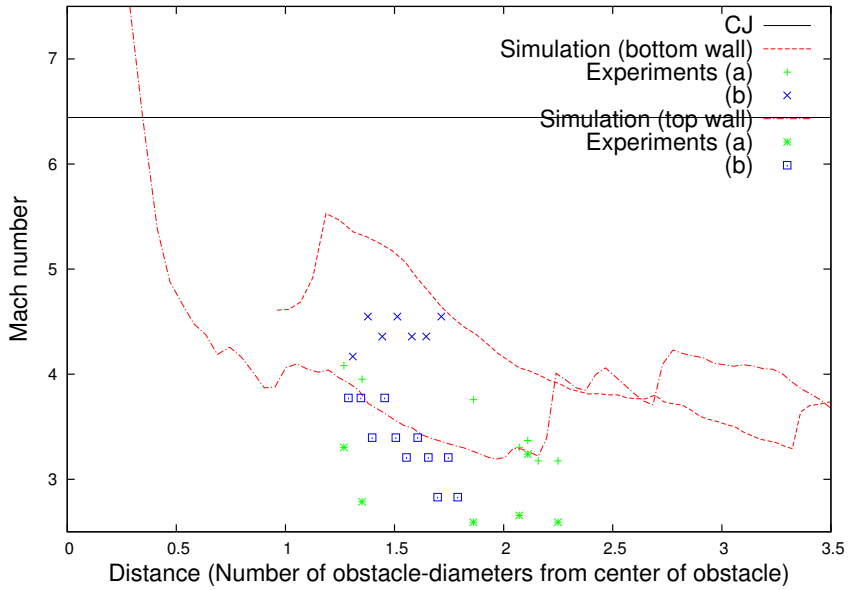

Figure 4.6: Comparison of shock velocities between simulations (5.5 kPa, one-step chemistry) and experiments [24]

diameters from the throat where the reflected wave reaches the shock front along the top wall, slightly after frame d) of figure 4.1(a).

4.3 Ignition behind Mach stem (10.3kPa)

Simulation results for a detonation through stoichiometric methane-oxygen at a higher pressure of 10.3kPa are shown in figure 4.2. The first row corresponds to the one-step chemistry model, while the second corresponds to the 2 step model. The bottom row shows select experimental frames obtained at similar conditions.

4.3.1 One-step Arrhenius chemistry

Frame a) of figure 4.2(a) shows the detonation quenching over the obstacle. A regular reflection occurs in frame b) which transits to an irregular reflection in frame c) much as in the previous case. A hotspot of burnt gas appears at the foot of the Mach stem in frame d), with details shown in figure 4.7(a). This pocket consumes gas behind the Mach stem but remains contained to the area shocked by the lower half of the bifurcated Mach stem. Kelvin-Helmoltz instabilities are easily seen in frames e) and f) and act as an interface between burnt and unburnt gas in frame f), shown in detail in figure 4.7(b).

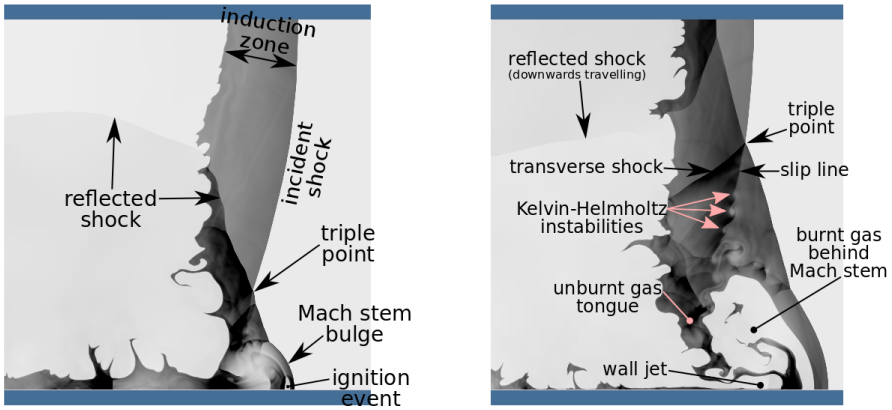

(a) Figure 4.2(a) frame d) (b) Figure 4.2(a) frame f)

Figure 4.7: Density plot details from figure 4.2(a) (10.3 kPa, one-step chemistry)

A reaction wave propagates along the wall jet between frames e) and f). The reflected shock travelling through the burnt products diffracts through the flame front, behind the incident shock from frames c) through e). This reaction front becomes slightly more corrugated. Gas behind the lower half of the bifurcated Mach stem has been completely consumed by frame g). A long tail of unburnt gas shocked by the incident and transverse waves remains. The detonation remains quenched in frame h) and a significant separation exists between the shock front and the reaction zone.

4.3.2 Two-step chain-branching chemistry

Figure 4.2(b) shows simulation results using the two-step chemistry model. The detonation diffracts over the obstacle in frame a) and reflects off the bottom wall as a regular reflection in frame b), and quenches. The regular reflection has transitioned to an irregular reflection by frame c). The irregular reflection grows and the Mach stem bulges in frames d) and e). No auto-ignition event occurs by frame e), the limit of simulations.

4.3.3 Experiments

Experiments at 10.3 kPa were less reliable than those performed at 5.5 kPa. This is due to the fact that the transition from detonation quenching to re-initiation occurs around this pressure and temperature (figure 4.8(a)). The majority of experiments saw ignition of gas behind the Mach stem but not re-initiation. At other times, the Mach stem alone (figure 4.8(b)) or the Mach stem and transverse wave (figure 4.8(c)) would re-initiate.

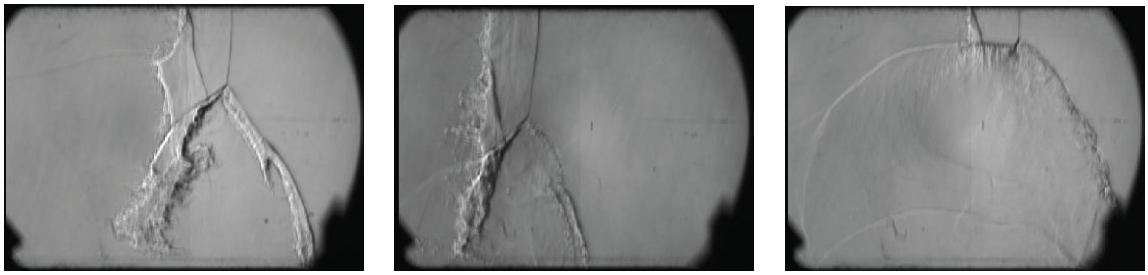

(a) Ignition behind Mach stem (b) Detonation re-initiation along the Mach stem (upper portion) (c) Detonation re-initiation along the Mach stem and transverse wave

Figure 4.8: Potential experimental outcomes following detonation diffraction through stoichiometric methane-oxygen at 10.3 kPa [76]

The detonations can be identified by the small whisker-like transverse waves (along the detonation itself), their thin, rough features, and quantitatively through velocity measurements.

4.3.4 Shock velocity

The velocity profiles of the incident shock, along the top wall, and the Mach stem, along the bottom wall, appear in figure 4.9.

Along the bottom wall, transition from regular to Mach reflection occurs at about one diameter from the throat. The Mach stem velocity increases to a maximum then begins to decay. The small spike in velocity following this decay (seen at about 1.7 diameters from the throat) occurs at the same time as the auto-ignition behind the Mach stem seen in frame d) of figure 4.2(a). A more significant increase in velocity follows (before 2.5 diameters). This corresponds to the arrival of the wall-jet flame near the Mach stem, seen in frame f) of figure 4.2(a). This wall-jet flame at 10.3kPa originates from products behind the incident and reflected shock.

The velocity profile along the top wall decreases from slightly above CJ to approximately $M = 3.5$. The sudden jump in velocity seen at about 2.3 diameters occurs when the reflected wave from below arrives at the incident wave along the top wall.

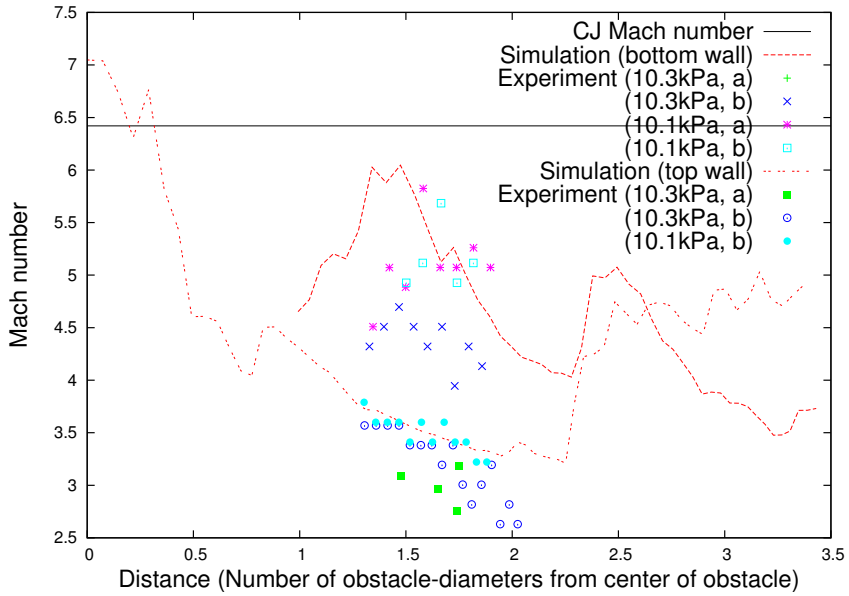

Figure 4.9: Comparison of shock velocities between simulations (10.3 kPa, one-step chemistry) and experiments [24]

4.4 Detonation re-initiation (11.9kPa)

Simulation results for a detonation through stoichiometric methane-oxygen at 11.9 kPa are shown in figure 4.3.

4.4.1 One-step Arrhenius chemistry

Frame a) of figure 4.3(a) shows the detonation diffracting over the obstacle. The detonation begins to quench near the bottom; however, the beginning of two thin cells can be seen, one along the top wall and one near the center. The shock front and the reaction zone have fully decoupled by frame b) where a regular reflection occurs. Transition to an irregular reflection has occurred by frame c) with the same features as previously seen. The bifurcation in the Mach stem almost disappears by frame d). Gas behind the Mach stem is consumed up to the Kelvin-Helmholtz instabilities on the main slip line and now also spans to the main triple point. The flame pocket appears along the bottom wall near the rear of the frame; however, it seems unable to catch up to the front by frame e). By then most of the gas behind the Mach stem is consumed, leaving a long tongue of unburnt gas which has been shocked by the incident and transverse shock waves. The Mach stem has reflected off the top wall by frame f) and is now considered the incident

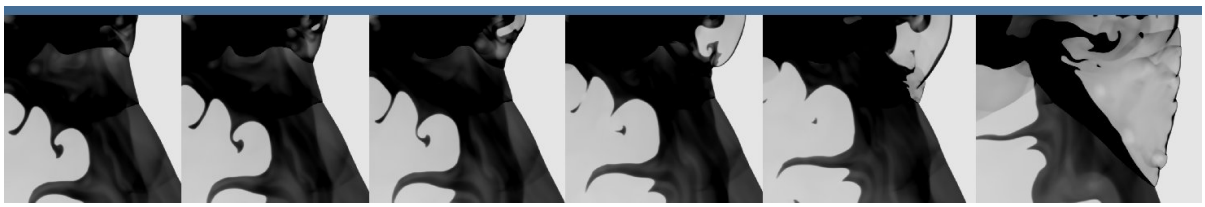

(a) Density plot detail (simulation, one-step chemistry)

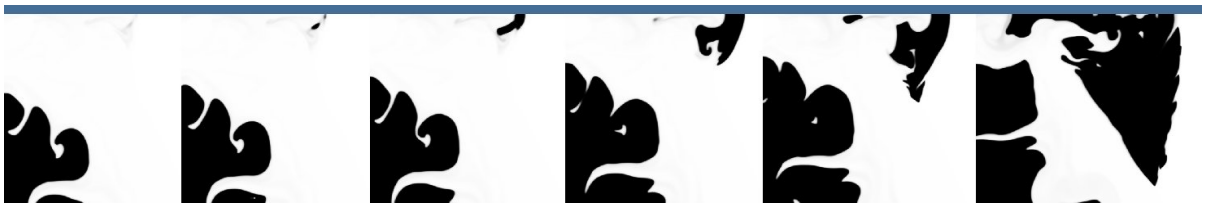

(b) Reaction progress variable (simulation, one-step chemistry)

Figure 4.10: Detail of detonation re-initiation around frame f) of figure 4.3(a) (11.9 kPa, one-step chemistry)

wave. An irregular reflection is formed and gas at the foot of the Mach stem (along the top wall) has begun to burn. It reacts very rapidly and re-initiates a detonation along the Mach stem by frame g). The detonation front spans the entire channel by frame h).

The events behind the Mach stem in frame 6 before and during the detonation re-initiation are shown in more detail in figure 4.10(a). Gas shocked by the bifurcated Mach stem auto-ignites and consumes the gas behind it, causing it to bulge ahead. A pocket of gas in the wall jet simultaneously auto-ignites and is carried forward. The detonation re-initiates near the triple point and overtakes the bulge. The reaction progress figure 4.10(b) confirms these sudden drops in density are indeed a result of combustion.

4.4.2 Two-step chain-branching chemistry

Figure 4.3(b) shows simulation results using the two-step chemistry model. The detonation diffracts past the obstacle in frame a) then reflects off the bottom wall in frame b). The last localized over-driven detonation is seen in frame c) as the rest of the detonation quenches. Meanwhile, rapid reactions occur behind the reflection point. The gas behind the Mach stem in frame d) is burnt, with a tail leading to the burnt gas behind the reflection point in frame c).

Magnification of frames c) and d) are shown in figures 4.11(a) and 4.11(b) with the reaction progress screened in colour. Gas behind the very small Mach stem in figure

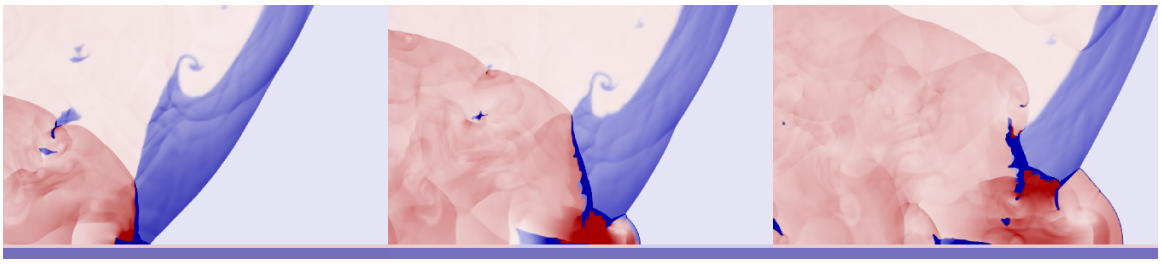

(a) (b) (c)

Figure 4.11: Detail of detonation re-initiation of figure 4.3(b) around frame d) showing reaction progress (blue=unreacted; red=reacted) and density (light-dark) (11.9 kPa, two-step chemistry)

4.11(a) is consumed by the next frame and what appears to be a transverse detonation appears, as shown by figure 4.11(c). It is short-lived, disappearing by figure 4.3(b) frame f). The detonation, re-initiated along the Mach stem, is maintained as seen in figure 4.3(b) frames e) and f).

4.4.3 Experiments

The experiments shown in figure 4.3(c) consistently re-initiated detonations along the Mach stem and transverse waves upon reflection off the bottom wall.

4.4.4 Shock velocity

The velocity profiles of the incident shock, along the top wall, and the Mach stem, along the bottom wall, appear in figure 4.12.

Transition from regular to Mach reflection occurs along the bottom wall at about one diameter from the throat. The Mach stem velocity increases to a maximum then begins to decay as in the previous case. A small increase in velocity following this decay is again due to auto-ignition behind the Mach stem; however, it occurs slightly earlier, at about 1.4 diameters from the throat. The Mach stem velocity continues to decay. A more significant increase follows (at 1.85 diameters). This corresponds to the arrival of the wall-jet flame near the Mach stem, seen between frames d) and e) of figure 4.3(a). The wall-jet flame comes from the auto-ignited flame behind the Mach stem which has wrapped around the vortex and comes back towards the shock front. A subsequent velocity jump occurs at 2.1 diameters from the throat, caused by the rapid combustion

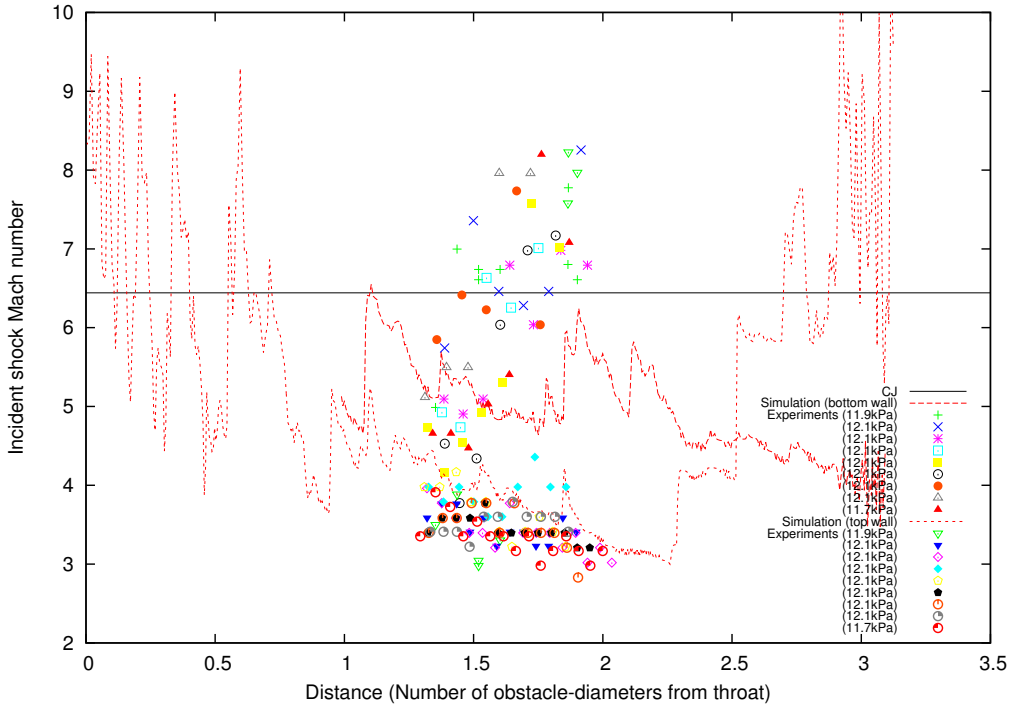

Figure 4.12: Comparison of shock velocities between simulations (11.9kPa, one-step chemistry) and experiments [24]

of gas immediately behind the Mach stem (not shown in figure 4.3(a)). The consequences of this rapid combustion can be seen in frame e) of figure 4.3(a) as an area of higher pressure and thinner induction zone behind the re-bifurcated Mach stem.

The first instance of detonation re-initiation seen in these simulations occurs along the top wall. The detonation along the top wall fails slightly past the downstream edge of the obstacle. The incident shock velocity decreases until the reflected shock reaches the shock front along the top wall about 2.3 diameters from the throat. The shock velocity once again increases when the main triple point reaches the top wall. The gas behind the new Mach stem along the top wall reacts and re-initiates the detonation which travels at around CJ velocity.

4.5 Detonation re-initiation (12.5kPa)

Simulation results for a detonation through stoichiometric methane-oxygen at 12.5 kPa are shown in figure 4.4.

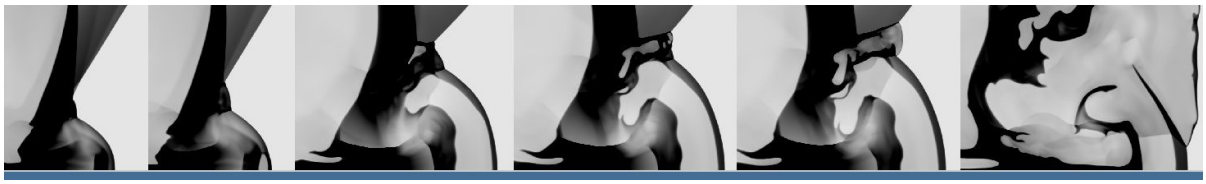

Figure 4.13: Detail of detonation re-initiation around frame d) of figure 4.4(a) (12.5kPa, one-step chemistry)

4.5.1 One-step Arrhenius chemistry

The detonation diffracts over the obstacle in frame a) but has not quite quenched. A regular reflection then takes place on the bottom wall in frame b). The detonation is quenched but for one cell near the top wall. A transition to irregular reflection occurs by frame c) where the Mach stem has bifurcated with its bottom portion already bulging out. A portion of gas behind this section has quickly been burnt by frame d). Gas behind the Mach stem near the triple point has also burnt and can be seen in detail in the third frame of figure 4.13. Several more hotspots are ignited near the (main) triple point and detonation re-initiation occurs along the Mach stem in a similar manner as in the 11.9 kPa case. Frame e) of figure 4.4(a) shows the detonation is re-initiated along only the Mach stem, and frames f) through i) show the detonation is maintained.

4.5.2 Two-step chain-branching chemistry

Figure 4.4(b) shows simulation results using the two-step chemistry model. The detonation diffracts over the obstacle in frame a) and has quenched by frame b) where it reflects off the bottom wall. It transitions to an irregular reflection in frame c). A flame travels along the wall jet in frame d) and reaches near the Mach stem. The detonation is re-initiated along the Mach stem as shown in frames e) and f).

Details of the Mach stem just before and after frame d) are shown in figure 4.14. A flame from the rear travels along the wall jet and reaches the area behind the Mach stem. The foot of the Mach stem is over-driven by figure 4.14(c) and followed immediately by a pocket of burnt gas, separated from the wall-jet flame by a strip of unburnt gas. A left-travelling pressure wave appears on the other side of this strip. The Mach stem near the triple point has become a a self-supported detonation wave by the last frame.

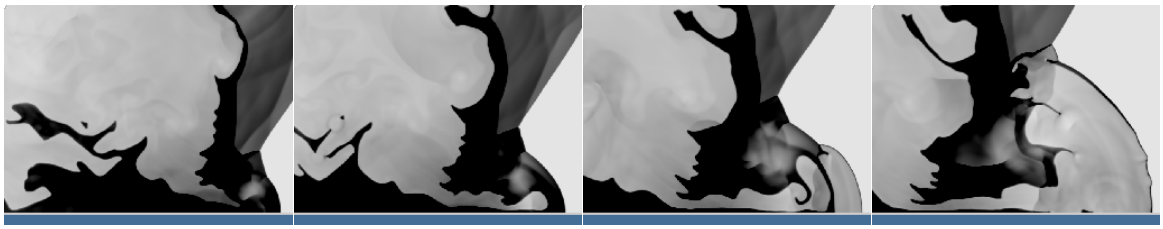

(a) (b) (c) (d)

Figure 4.14: Detail of detonation re-initiation around frame d) of figure 4.4(b) (12.5kPa, two-step)

4.5.3 Experiments

No experiments were performed at 12.5 kPa so figure 4.4 compares the simulations at this pressure to experiments at 11.9 kPa, where detonation re-initiation also occurred along the bottom wall.

4.5.4 Shock velocity

The velocity profile of the Mach stem, along the bottom wall, appears in figure 4.15. The transition from regular to irregular reflection occurs slightly after a distance of one diameter from the throat. Although the Mach stem is quenched at this point, triple-points from recently quenched detonation cells arrive at the bottom wall, causing several sudden jumps in velocity. The quenched state of the Mach stem is then seen for a brief period of time until detonation re-initiation occurs, seen in frame d) of figure 4.4(a). It travels around CJ velocity, suddenly slows locally, and is quickly re-accelerated.

4.6 Detonation transmission (17.6kPa)

Simulation results for a detonation through stoichiometric methane-oxygen at 17.6 kPa are shown in figure 4.16.

4.6.1 One-step Arrhenius chemistry

Frame a) of figure 4.16(a) shows the detonation as it diffracts over the obstacle. The reaction front closely follows the shock front and distinction between the two is impossible at some points. The detonation appears to begin quenching in frame b), but re-initiates

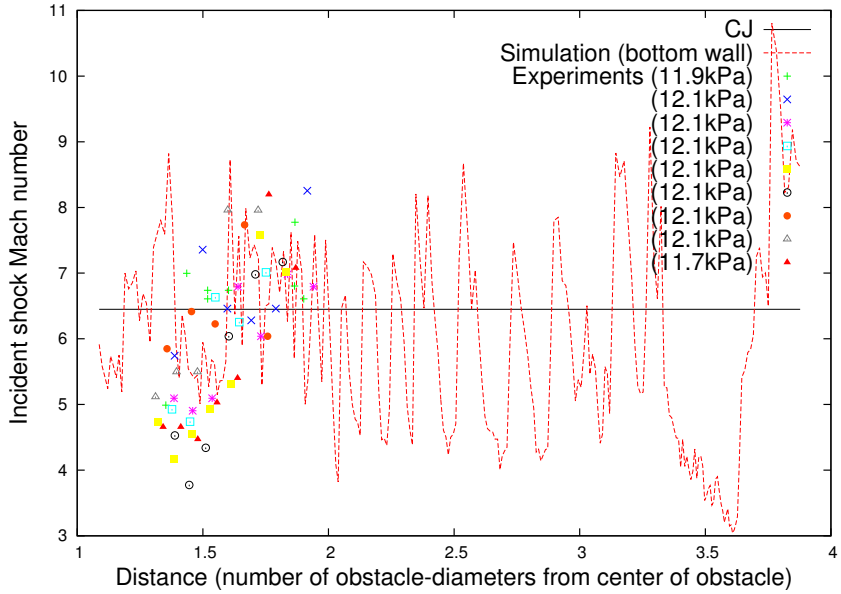

Figure 4.15: Comparison of shock velocities between simulations (12.5 kPa, one-step chemistry) and experiments [24]

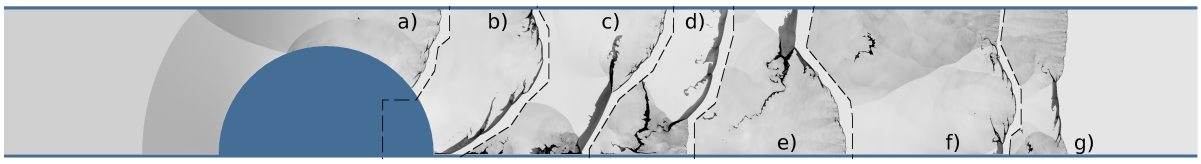

(a) Density plot (simulation, one-step chemistry)

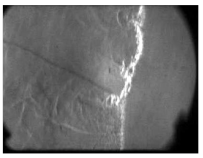

(b) Schlieren photograph (experiment [76], resembling frame d) of simulations

Figure 4.16: Composite density plot of a detonation through stoichiometric methane-oxygen at 17.6 kPa computed with one-step Arrhenius chemistry (simulation, one-step chemistry)

before frame c) following a shock reflection off the top wall. The detonation proceeds in this manner, quenching locally but never globally. The detonation is almost completely recovered by frame g). Transverse detonations are not observed.

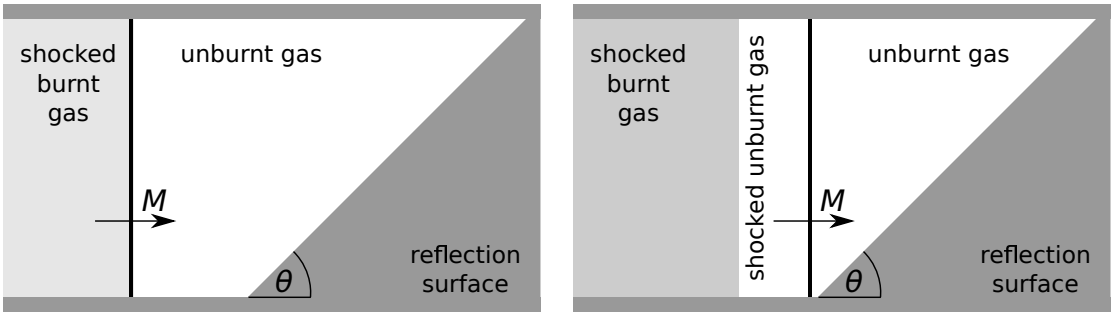

(a) Initial state (b) State after initial state

Figure 4.17: Sketch of the artificial wedge simulation at initial state (a) and slightly after (b)

4.6.2 Two-step chain-branching chemistry

The two-step model was not used at 17.6 kPa due to the high computational demand.

4.6.3 Experiments

The experiment at this pressure in figure 4.16(b) also show a detonation transmitted past the obstacle without quenching.

4.7 Reflection off a wedge

A second series of numerical experiments were conducted to further study the initiation transient following the Mach reflection with higher spatial resolution. The simulations only focused on the immediate vicinity of the reflection. It considered the reflection of an incident shock at a constant angle wedge, in order to approximate the reflection of the incident shock at the bottom wall in the experiments. A sketch of the problem set-up is shown in 4.17. The incident Mach number was set to $M = 4$, in order to match the experimental condition of the incident shock immediately before the Mach reflection process. The wedge angle was set to $\theta = 40°$ to simulate the process occurring just prior to detonation re-initiation. The simulation was initiated with the shock positioned upstream of the compressive corner. The gas behind the shock was set to reacted. The initial conditions are sketched in figure 4.17.

Simulations were run at three different resolutions: 8, 16 and 32 grid points per induction length, using the one-step chemical model. The results shown in these figures

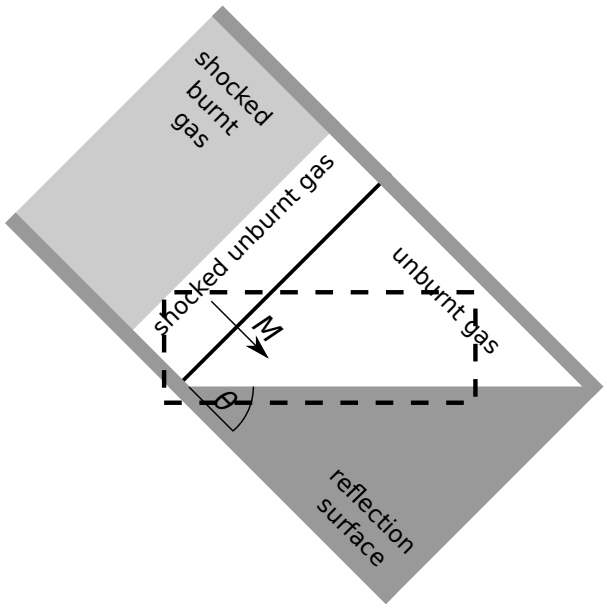

Figure 4.18: Artificial wedge simulation results have been rotated such that the reflecting surface appears horizontal, and has been cropped by the dashed line

have been rotated clockwise by the wedge angle θ and cropped as shown in figure 4.18.

The wall-jet vortex and Mach stem bulge are most apparent at high resolutions. Gas shocked by the Mach stem auto-ignites. The auto-ignition center is located furthest back in the gas shocked by the Mach stem (figure 4.19(a)). At a resolution of 32 grid points per induction length (figure 4.19), the reaction wave travels fastest, with respect to the Mach stem, along the wall jet (figure 4.19(b)) and causes detonation initiation near the foot of the Mach stem (figure 4.19(c)). A strip of unburnt gas separates the wall-jet flame from the pocket of burnt gas immediately behind the Mach stem (figure 4.19(d)). The transverse wave does not become a self-sustained detonation wave.

At a resolution of 16 grid points per induction length (figure 4.20), the auto-ignition happens slightly closer to the Mach stem (figure 4.20(a)). The flame again travels along the wall jet (figure 4.20(b)) and initiates a detonation at the Mach stem foot (figure 4.20(c)). However, the portion of the reaction wave travelling above the vortex is able to detonate the portion of the Mach stem unaffected by the vortex before the detonation from the Mach stem foot is able to disturb that area (figure 4.20(d)), effectively resulting in two detonation initiation events along the Mach stem.

At a resolution of 8 grid points per induction length (figure 4.21), auto-ignition occurs even closer to the Mach stem (figure 4.21(a)), between the vortex and the slip line. The

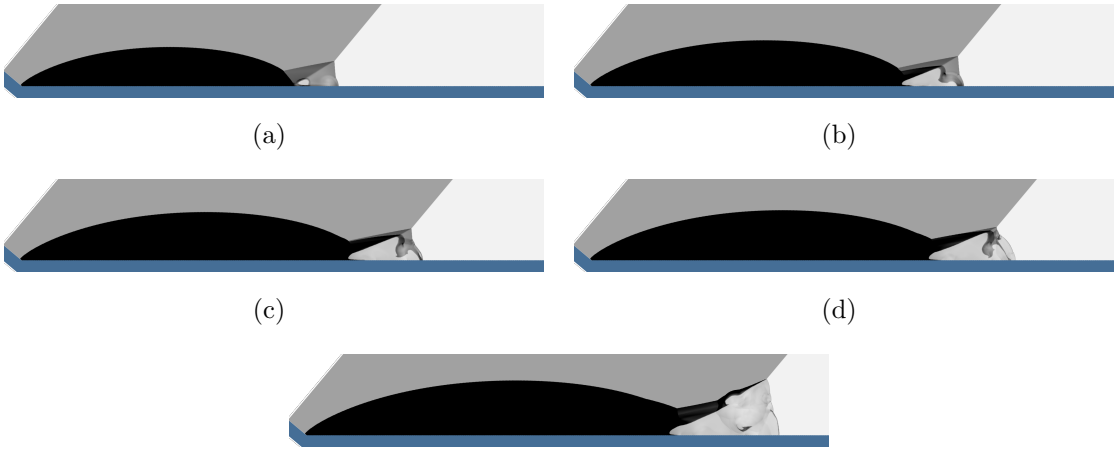

(a) (b) (c) (d) (e)

Figure 4.19: Artificial wedge simulation at a resolution of 32 points per induction length

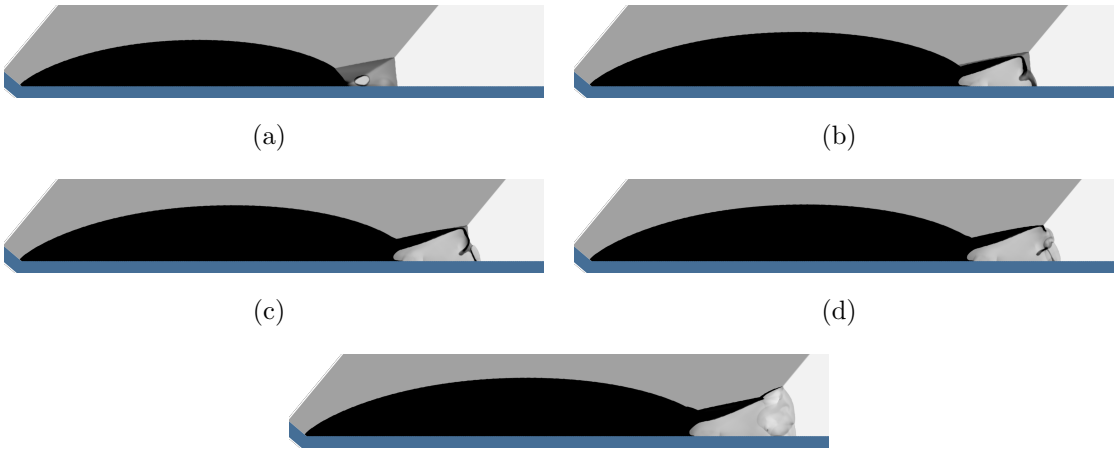

(a) (b) (c) (d) (e)

Figure 4.20: Artificial wedge simulation at a resolution of 16 points per induction length

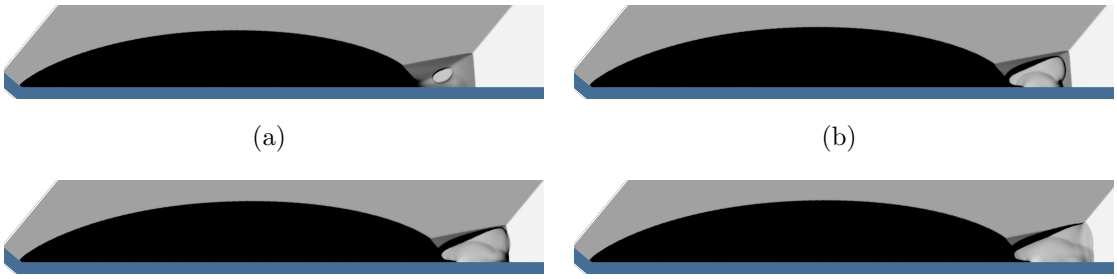

(a) (b)

(c) (d)

Figure 4.21: Artificial wedge simulation at a resolution of 8 points per induction length

flame travels slightly faster outside of the vortex (figure 4.21(b)) and reaches the Mach stem above the vortex, shortly before it can reach the foot of the Mach stem (figure 4.21(c)), but again resulting in two detonation initiation events (figure 4.21(d)).

The Mach stem detonations seen in figure 4.19(e), 4.20(e), and 4.21(d) eventually adopt a small cellular structure and do not quench. Auto-ignition occurs earlier at high resolutions.

Chapter 5

Discussion

5.1 Comparison of models and experiments

The experiments and numerical simulations were found to agree very well in terms of conditions for re-initiation of the detonation. The flow field details were also in generally good agreement. A summary of the results is shown in table 5.1

When the detonation wave quenched and no re-initiation was observed, the agreement was very good. The reflected wave, its diffraction into the unburnt gas behind the incident shock, and its speed relative to the incident wave and Mach stem were well matched between simulations and experiments. The regular reflection to irregular reflection transition occurred at the same location in simulation and experiments. Kelvin-Helmholtz instabilities appeared in both with similar length scales. These phenomena are attributed mostly to the gas-dynamic model and indicate that the Euler equations are a good choice for modelling this process.

One exception to this is the Mach stem bulging and bifurcation, which is more prominent in simulations. Mach stem bifurcations have been shown to be a source of new detonation cells by Mach and Radulescu [21]. This numerical phenomenon is not well understood and bulging has been attributed to the effect of the wall-jet on the Mach stem. Euler equations ignore dissipative effects such as viscosity. The inviscid bottom wall in simulations represents a plane of symmetry in the detonation structure. More recent experiments by Bhattacharjee et al. [24] have used a full cylinder as an obstacle. The use of a plane of symmetry in substitution of a wall eliminates wall friction but the slight bulging along the plane of symmetry in these new experiments remains nowhere as prominent as in simulations. Quirk [59] suggested the lack of dissipation of the Roe

Table 5.1: Summary of results

P_0	Experimental	1-step	2-step
5.5kPa	Quenched	Quenched	Quenched
10.3kPa	Ignition behind Mach stem	Ignition behind Mach stem	Quenched
11.9kPa	Re-initiation behind Mach stem and transverse wave	Re-initiation behind Mach stem	Re-initiation behind Mach stem and transverse wave
12.5kPa		Re-initiation behind Mach stem	Re-initiation behind Mach stem
17.6kPa	Direct transmission	Direct transmission	

numerical solver is to blame for this phenomenon, however, Mach's solver study [56] showed that Mach stem bifurcations remained when other solvers were used. This issue requires further investigation.

The induction delay behind the incident shock was found comparable between both models and experiments. The one-step model creates a smoother reaction front than the two-step model. The experimental reaction fronts are more similar to those of the two-step model. A comparison of the ZND profiles for the one-step, two-step, and real chemistry models appears in figure 3.1.

The induction-to-reaction length ratio is a controlling parameter in detonation stability [77]; the larger this ratio, the more unstable the detonation. The real chemistry model falls between the one-step and two-step models in this respect. Figure 3.1 shows this ratio is smaller when using the one-step model, and larger when using the two-step model. It is possible that this ratio also affects the reaction front in quenched detonations.

The detonation re-initiation limits are the same for the one- and two-step models but the re-initiation cause differs. The detonation re-initiation at 11.9 kPa occurs along the top wall following auto-ignition using the one-step model, but occurs along the bottom wall when the two-step model is used. The cause of the re-initiation in the latter case is unclear, requiring additional time resolution. It is suspected to be caused by an explosion behind the reflection point along the bottom wall either initiating the detonation directly, allowing for a flame to be convected along the wall jet, or causing auto-ignition behind the Mach stem. At 12.5 kPa, re-initiation occurs along the bottom wall in both models; however, the cause is different. Local auto-ignition behind the Mach stem re-initiates

the detonation when using the one-step model, while a reaction front travelling along the wall jet re-initiates the detonation when using the two-step model. Further analysis of this phenomenon is required.

While the one-step model is able to adequately predict detonation re-initiation, the additional control given by using the two-step model allows the details surrounding detonation re-initiation to be better replicated. For example, the tongues of unburnt gas, shocked by the incident and reflected waves (e.g figure 4.3(a) frame f)), are more reactive in experiments, where they can cause detonation initiation along the transverse wave. Transverse detonations are not seen using the one-step model but do appear briefly when the two-step model is employed (figure 4.11). A finer calibration may allow this phenomenon to be better replicated. The wall jetting effect with respect to re-initiation is as prominent in the two-step model as in experiments. When using the one-step model, auto-ignition appears more important at first glance. The two-step model predicts detonation re-initiation slightly better than the one-step model. At 11.9 kPa, it correctly predicts that re-initiation will occur along the bottom wall, while the one-step model fails to do so.

5.2 Limitations

The Euler equations used to model gas dynamics neglect dissipative effects such as species, momentum and energy diffusion. Mixing between burnt and unburnt gas, or hot and cold gas, was not modelled. Any diffusion was due to numerical diffusion, a consequence of discretization, which is difficult to measure. Unfortunately, the small scales of turbulence, and the rapid transients of chemical reactions, particularly at re-initiation events and ignition phenomena, may occur on scales smaller than the grid could resolve. This modifies the solution structure, which is expected to behave more mildly (smaller pressure pulses) in the simulations than in the experiments. This can account for small scale discrepancies in the simulations.

Full chemistry models, basis of the one-step and two-step model calibrations, are themselves only models of the true chemical processes and are generally validated using experimental ignition times, not pressure, temperature, density, or species profiles, as these are experimentally difficult or impossible to obtain with adequate temporal and spatial resolution. Full-chemistry models also differ from each other at extremities of the range shown in figure 3.3. Furthermore, full-chemistry models for methane are only able to accurately predict ignition times at higher temperatures (> 1100 K) [28,34], as shown

in figure 3.3. The activation energy, which was assumed constant, may be inaccurate at shock speeds below $M \approx 5.5$.

The one- and two-step chemical models approach the full chemistry models, as shown by the ZND profiles in figure 3.1, but are still different. The differences could be important factors in certain cases. Use of the one- and two-step models is justified by profile similarity and their reduction of the number of chemical equations (thus computation time) from hundreds to one or two, respectively. The two-step model calibration requires further adjustment: changing the induction time to the period between the shock and thermicity half-height as well as tuning refinement criteria could help better replicate the experiments in a shorter time.

The isentropic exponent γ typically varies slightly with temperature and significantly with chemistry in real gases. The use of a constant γ over the large temperature range and for both burnt and unburnt gas may affect aspects of the simulation. The post-shock γ (used in these simulations) is lower than the quiescent γ which leads to a lower temperature jump across the incident shock as illustrated by figure 3.1. The burnt gas γ also differs from the post-shock γ and may change the effect of burnt gas in wall-jet and behind the Mach stem.

The use of a cylinder as an obstacle is interesting as it allows a large range of reflection angles between the shock front and bottom wall. However, this does not represent the same range of angles present between two reflecting shocks within the real detonation structure. The current obstacle causes reflection angles which are much smaller than those present in the actual detonation structure. Reflection angles and their initial conditions [78] play a very important role in Mach shock, reflected shock and wall-jet strengths. The initial reflection angle within the detonation structure differs for every mixture, so this technique still offers valuable insight into the general phenomenon of detonation re-initiation within the detonation structure.

5.3 Effect of resolution

The effect of resolution was studied for the case detonation re-initiation along the top wall (11.9 kPa). The results presented in the study are for a resolution of 35.36 grid points per induction length. Halving the resolution resulted in a detonation similar to the detonation transmission case but slightly more reactive. The detonation never completely quenched, with local over-driven detonations being reformed in the center and top of the channel. The cell size of the detonation as it diffracted over the obstacle

was smaller than that of the presented results. The quenched bottom re-initiated upon reflection off the bottom wall and propagated to the end.

Doubling the studied resolution to 70.72 grid points per induction length resulted in a quenched detonation that did not re-initiate. It should be noted that the simulation was only run to a distance between to frames d) and e) of figure 4.3. Bulging of the Mach stem was more prominent near the foot at this resolution, but no auto-ignition event was observed.

The case with ignition behind the Mach stem but no detonation re-initiation (10.3 kPa) used a resolution of 41.97 grid points per induction length. No auto-ignition event occurred behind the Mach stem when the resolution was halved. Instead, a flame travelling along the wall jet consumed the gas behind the Mach stem following the reflected wave's return to the bottom wall. This took place much further downstream than the auto-ignition event seen in figure 4.2.

The detonation transmission case (17.6 kPa) used a resolution of 44.76 grid points per induction length. Reducing it by three quarters saw a stronger detonation transmission with less quenching.

Shock reflections off a straight wedge showed similar trends. Increasing the resolution generally increased the gas' tendency to auto-ignite, increased the wall jet's affect on the Mach stem, but made the detonation more prone to decoupling.

5.4 Detonation re-initiation mechanisms

In view of the results obtained and comparison with experiments, the mechanisms of re-initiation identified in the introduction can now be addressed.

5.4.1 Mach stem shock compression

Auto-ignition behind the Mach stem is believed to be the main mechanism of re-ignition and detonation establishment. Indeed, these simulations fully support this premise. With an appropriate model for the induction zone duration and sensitivity to shock compression (through the activation energy of the induction zone), the numerical results reproduced the experimental trends. Nevertheless, small discrepancies were observed. The Mach stem in the simulations bulges out more than in the experiments, through the action of the wall jet. This causes the Mach stem to travel faster than otherwise and a stronger shock and temperature increase (although it is unclear if this causes auto-

ignition, as discussed in the previous section) is expected. Auto-ignition is seen at the foot of the bulged Mach stem in one-step model simulations. While this event increases the shock velocity, it does not cause re-initiation; the flame instead wraps around the vortex burning gas behind the Mach stem. The curved Mach stem bulge grows and this expansion prevents re-initiation. It is possible that given a straighter Mach stem, a detonation would be re-initiated.

Gas ignited behind the flattened portion of the Mach stem, nearer to the main triple-point, later re-initiates the detonation instead. Adiabatic shock compression by the Mach stem appears to play an important role in re-initiating detonations, especially following strong shocks.

5.4.2 Incident and transverse shock compression

Gas shocked by the incident and transverse shocks does not cause detonation re-initiation in simulations. Rapid combustion of the tongue of unburnt gas, shocked by the incident and transverse shocks, is responsible for the transverse detonations seen in experiments. This detonation wave was never observed in simulations, where they burn much slower. This is not a matter of increasing gas sensitivity; simulations at 17.6 kPa yield detonation transmission past the obstacle yet transverse detonations remain absent.

Using the one-step model at 11.9 kPa, when the detonation re-initiates along the top wall, the arrival of the reflected wave at the top wall increases the velocity of the incident shock. However, the auto-ignition causing re-initiation occurs only following reflection of the Mach stem, which brings about a greater velocity increase.

Recent experiments have shown that the transverse detonation is re-initiated when a shock from combustion behind the Mach stem is transmitted through the slip line into the tongue of unburnt gas. Explosions in the tongue of unburnt gas then drive the transverse wave to detonating. However, Mach stem detonations are already present when this phenomenon takes place. In simulations, combustion of gas behind the Mach stem seems to have little impact on the tongue of unburnt gas.

5.4.3 Kelvin-Helmholtz instabilities

Kelvin-Helmholtz instabilities do not appear to play a role in detonation re-initiation on the whole. The slip-line on which these instabilities grow serves as a division between burnt gas behind the Mach stem and the unburnt gas shocked by the incident and transverse waves. As previously discussed, combustion of this tongue of unburnt gas

does not lead to detonation re-initiation in simulations. The suspected mixing due to these instabilities cannot be properly modelled with the techniques used in this study. The instabilities' role in detonation re-initiation from experiments so far remains unsure. It is quite clear however that these instabilities do not cause re-initiation of the Mach stem, which has always appeared prior to transverse detonation.

5.4.4 Wall-jetting effect

The wall-jetting effect causes detonation re-initiation in simulations using the two-step model (section 4.5). Experiments using a full-cylinder obstacle [24] have shown flames travelling along the wall jet rapidly igniting gas behind the Mach stem, re-initiating a detonation around the vortex, shocking the tongue of unburnt gas, and initiating a transverse detonation.

When a flame travelling along the wall jet reaches the Mach stem, the Mach stem speed is greatly increased, revealed in shock velocity figures 4.9 and 4.12. Auto-ignition behind the bulged Mach stem has occurred in both cases prior to the flame's arrival but this auto-ignition may be prematurely caused by the unrealistic Mach stem bulging, discussed in section 5.4.1. The important velocity increase associated with a flame from the burnt products, travelling along the wall-jet as seen in figure 4.2(a), indicates the wall-jetting effect may responsible for detonation re-initiation, without the exaggerated Mach stem bulge and the auto-ignition it brings.

We can thus conclude that the wall-jetting effect plays an important role in detonation re-initiation.

5.4.5 Richtmyer-Meshkov instabilities

The effect of Richtmyer-Meshkov instabilities on detonation re-initiation remains uncertain. Any mixing caused by these instabilities cannot be modelled with the Euler equations, one- or two-step models. While it is expected Richtmyer-Meshkov instabilities should appear at burnt-unburnt interfaces, they likely occur on a scale that is currently unresolved.

A mild ignition is seen in experiments where a shock is transmitted through the tongue of unburnt gas from combustion behind the Mach stem. The mild ignition, characterized by combustion starting at several distinct points, may be accelerated by Richtmyer-Meshkov instabilities; however, this is uncertain. This ignition leads to initiation of the

transverse detonation. Richtmyer-Meshkov instabilities are not responsible for a Mach stem detonation as no shocks pass through density gradients in the Mach stem's vicinity.

Chapter 6

Conclusion

Numerical simulations of a detonation diffracting over a cylindrical obstacle and the following reflections were carried out using the Euler equations and one-step or two-step chemical models. The numerical simulations were compared with experiments carried out by Bhattacharjee et al. [76] in stoichiometric methane-oxygen in order to identify the main mechanism controlling the re-initiation phenomenon.

Good agreement was found both qualitatively and quantitatively. The numerical model accurately predicted detonation re-initiation conditions. The one-step chemical model was found to be sufficient in predicting re-initiation; however, the two-step chemical model better reproduced finer details. The models used contained no diffusive and mixing terms; mixing (or rather a lack thereof) at Kelvin-Helmholtz and Richtmyer-Meshkov instabilities did not seem to influence detonation re-initiation which first occurred at 11.9 kPa in both simulations and experiments.

Detonation re-initiation, especially at high pressures, appeared to occur due to adiabatic compression of the Mach stem shock wave or arrival of a flame travelling along the wall jet at the Mach stem. Autoignition caused by adiabatic shock compression led to detonation re-initiation in some simulations while the wall-jet, found to significantly increase velocity of the Mach shock, led to detonation re-initiation in others.

Unrealistic bulging of the Mach stem foot was likely an impediment of detonation re-initiation along the Mach stem in simulations. Numerical simulations were unable to replicate transverse detonations found in experiments and the reason remains unknown. Future study should thus investigate this transient, which appears to be dependent on the rapid burning rates of the gases trapped in the non-reacted pockets, possibly through turbulent interactions.

Bibliography

[1] G. P. Smith, D. M. Golden, M. Frenklach, N. W. Moriarty, B. Eiteneer, M. Goldenberg, C. T. Bowman, R. K. Hanson, S. Song, W. C. Gardiner Jr., V. V. Lissianski, and Z. Qin. *GRI-Mech 3.0*. Accessed: 2011/08.

[2] Buncefield Major Incident Investigation Board. The final report of the major incident investigation board. Technical report, Buncefield Major Incident Investigation Board, 2008.

[3] M. Johnson. The potential for vapor cloud explosions - lessons from buncefield. Technical report, GL Noble Denton.

[4] W. Fickett and W. C. Davis. *Detonation Theory and Experiment*. General Publishing Company, Ltd., 2000.

[5] J. H. S. Lee. *The detonation phenomenon*, volume 1. 2008.

[6] A. Teodorczyk, J. H. S. Lee, and R. Knystautas. Propagation mechanism of quasi-detonations. In *Symposium (International) on Combustion*, volume 22, pages 1723–1731, 1989.

[7] A. Teodorczyk, J. H. S. Lee, and R. Knystautas. The structure of fast turbulent flames in very rough, obstacle-filled channels. In *Symposium (International) on Combustion*, volume 23, pages 735–741, 1991.

[8] A. Teodorczyk. Fast deflagrations and detonations in obstacle-filled channels. *Journal of Power Technologies*, 79, 1995.

[9] T. Obara, J. Sentanuhady, Y. Tsukada, and S. Ohyagi. Reinitiation process of detonation wave behind a slit-plate. *Shock Waves*, 18(2):117–127, June 2008.

[10] S. Ohyagi, T. Obara, S. Hoshi, P. Cai, and T. Yoshihashi. Diffraction and re-initiation of detonations behind a backward-facing step. *Shock Waves*, 12(3):221–226, November 2002.

[11] M. I. Radulescu and B. M. Maxwell. The mechanism of detonation attenuation by a porous medium and its subsequent re-initiation. *Journal of Fluid Mechanics*, 667:96–134, January 2011.

[12] T. Obara, T. Kobayashi, and S. Ohyagi. Mechanism of deflagration-to-detonation transitions above repeated obstacles. *Shock Waves*, 22(6):627–639, September 2012.

[13] S. V. Khomik, B. Veyssiere, S. P. Medvedev, V. Montassier, and H. Olivier. Limits and mechanism of detonation re-initiation behind a multi-orifice plate. *Shock Waves*, 22(3):199–205, March 2012.

[14] V. N. Gamezo, T Ogawa, and E. S. Oran. Numerical simulations of flame propagation and DDT in obstructed channels filled with hydrogenair mixture. *Proceedings of the Combustion Institute*, 31(2):2463–2471, January 2007.

[15] G. Ben-Dor. *Shock Wave Reflection Phenomena*. Springer, 2 edition, 2007.

[16] H. Hornung. Regular and mach reflection of shock waves. *Annual review of fluid mechanics*, 18:33–58, 1986.

[17] R. Sorin, R. Zitoun, B. Khasainov, and D. Desbordes. Detonation diffraction through different geometries. *Shock Waves*, 19(1):11–23, December 2008.

[18] V. A. Subbotin. Collision of transverse detonation waves in gases. *Combustion, Explosion, and Shock Waves*, 11(3):411–414, 1975.

[19] M. I. Radulescu and J. H. S. Lee. The failure mechanism of gaseous detonations: experiments in porous wall tubes. *Combustion and flame*, 131(1):29–46, 2002.

[20] S. Chandrasekhar. *Hydrodynamic and Hydromagnetic Stability*. The International Series of Monographs on Physics. Dover Publ., 1961.

[21] P. Mach and M.I. Radulescu. Mach reflection bifurcations as a mechanism of cell multiplication in gaseous detonations. *Proceedings of the Combustion Institute*, 33(2):2279–2285, January 2011.

[22] Y. Mahmoudi and K. Mazaheri. High resolution numerical simulation of the structure of 2-d gaseous detonations. *Proceedings of the Combustion Institute*, 33(2):2187–2194, January 2011.

[23] R. Bhattacharjee, S. SM. Lau-Chapdelaine, G. Maines, L. Maley, and M. I. Radulescu. Detonation wave attenuation by a cylinder and the subsequent re-initiation rgimes. In *Proceedings of the 23rd ICDERS, Irving, California, USA, 24-29 July*, 2011.

[24] R.R. Bhattacharjee. *Experimental Investigation of Detonation Re-Initiation Mechanisms following a Mach Reflection of a Quenched Detonation*. Master's thesis, University of Ottawa, 2013.

[25] M. Brouillette. The richtmyer-meshkov instability. *Annual Review of Fluid Mechanics*, 34(1):445–468, 2002.

[26] M. Short and G. Sharpe. Pulsating instability of detonations with a two-step chain-branching reaction model: theory and numerics. *Combustion Theory and Modelling*, 7(2):401–416, June 2003.

[27] D. J. Seery and C. T. Bowman. A shock tube study of methane oxidation.

[28] C. J. Goy, A. J. Moran, and G. O. Thomas. Autoignition characteristics of gaseous fuels at representative gas turbine conditions. *ASME Paper*, (2001-GT), 2001.

[29] R. K. Cheng and A. K. Oppenheim. Autoignition in methane-hydrogen mixtures. *Combustion and Flame*, 58:125–139, 1984.

[30] L. J. Spadaccini and M. B. Colket. Ignition delay characteristics of methane fuels. *Progress in energy and combustion science*, 20(5):431–460, 1994.

[31] N. Lamoureux, C. E. Paillard, and V. Vaslier. Low hydrocarbon mixtures ignition delay times investigation behind reflected shock waves. *Shock waves*, 11(4):309–322, 2002.

[32] A. Lifshitz, K. Scheller, A. Burcat, and G. B. Skinner. Shock-tube investigation of ignition in methane-oxygen-argon mixtures. *Combustion and Flame*, 16(3):311–321, 1971.

[33] A. Grillo and M. W. Slack. Shock tube study of ignition delay times in methane oxygen nitrogen argon mixtures. *Combustion and Flame*, 27:377–381, 1976.

[34] J. Huang, P. G. Hill, W. K. Bushe, and S. R. Munshi. Shock-tube study of methane ignition under engine-relevant conditions: experiments and modeling. *Combustion and Flame*, 136(1):25–42, 2004.

[35] W. M. Heffington, G. E. Parks, K. G. P. Sulzmann, and S. S. Penner. Studies of methane-oxidation kinetics. In *Symposium (International) on Combustion*, volume 16, pages 997–1011, 1977.

[36] A. E. Lutz. A numerical study of thermal ignition. Technical Report SAND-88-8228, Sandia National Labs., June 1988. Mechanism obtained from http://www2.galcit.caltech.edu/EDL/mechanisms/mechs/lutz88.

[37] K. Kailasanath, E. S. Oran, J. P. Boris, and T. R. Young. Determination of detonation cell size and the role of transverse waves in two-dimensional detonations. *Combustion and Flame*, 61(3):199–209, 1985.

[38] M. H. Lefebvre, E. S. Oran, K. Kailasanath, and P. J. Van Tiggelen. Simulation of cellular structure in a detonation wave. *Progress in Astronautics and Aeronautics*, 153:64–64, 1993.

[39] S. Ohyagi, T. Obara, F. Nakata, and S. Hoshi. A numerical simulation of reflection processes of a detonation wave on a wedge. *Shock Waves*, 10(3):185–190, 2000.

[40] B. Khasainov, C. Priault, H.N. Presles, and D. Desbordes. Influence d'un obstacle central sur la transmission d'une dtonation d'un tube dans un grand volume. *Comptes Rendus de l'Acadmie des Sciences-Series IIB-Mechanics*, 329(9):679–685, 2001.

[41] D. A. Jones, M. Sichel, and E. S. Oran. Reignition of detonations by reflected shocks. *Shock Waves*, 5(1):47–57, 1995.

[42] Charles K. Westbrook and Paul A. Urtiew. Chemical kinetic prediction of critical parameters in gaseous detonations. In *Symposium (International) on Combustion*, volume 19, pages 615–623, 1982.

[43] C. Gardner. *Experimental investigations of auto-ignition delay times and soot formation in gaseous fuel mixtures.* Ph.D. thesis, University of Wales, 2005.

[44] S. Gordon and B. J. McBride. *Computer Program for Calculation of Complex Chemical Equilibrium Compositions and Applications*, volume 1311. 1994.

[45] J. E. Shepherd. *'ZND'- ZND Detonation Struture Calculation.* Accessed: 2011/08 from http://www2.galcit.caltech.edu/EDL/public/old_tools.html.

[46] J. E. Shepherd. *'CV' Constant Volume explosion.* Accessed: 2011/08 from http://www2.galcit.caltech.edu/EDL/public/old_tools.html.

[47] PA Blythe, AK Kapila, and M Short. Homogeneous ignition for a three-step chain-branching reaction model. *Journal of engineering mathematics*, 56(2):105–128, 2006.

[48] Gary J Sharpe and Nabeil Maflahi. Homogeneous explosion and shock initiation for a three-step chain-branching reaction model. *Journal of Fluid Mechanics*, 566:163194, 2006.

[49] S. Kao and J. E. Shepherd. Numerical solution methods for control volume explosions and ZND detonation structure. Technical Report FM2006.007, 2008.

[50] F. Zhang. *Shock Waves Science and Technology Library: Detonation Dynamics*, volume 6. Springer, 2012.

[51] J. J. Quirk. AMRITA. In *VKI 29th CFD lecture series, Febuary*, 1998.

[52] P. L. Roe. Approximate riemann solvers, parameter vectors, and difference schemes. *Journal of Computational Physics*, 43:357–372, 1981.

[53] P. L. Roe and J. Pike. Efficient construction and utilisation of approximate riemann solutions, computing methods in applied sciences and engineering. In *Proceedings of the 6th International Symposium, Versailles, France; Netherlands*, pages 499–518, 1984.

[54] H. C. Yee, R. F. Warming, and A. Harten. Implicit total variation diminishing (TVD) schemes for steady-state calculations. *Journal of Computational Physics*, 57(3):327–360, 1985.

[55] C. B. Laney. *Computational gasdynamics.* Cambridge University Press, 1998.

[56] P. Mach. *Bifurcating Mach Shock Reflections with Application to Detonation Structure.* Master's thesis, University of Ottawa, 2011.

[57] M.S. Liou and C.J. Steffen. A new flux splitting scheme. *Journal of computational physics*, 107(1):23–39, 1993.

[58] D. I. Pullin. Direct simulation methods for compressible inviscid ideal-gas flow. *Journal of Computational Physics*, 34(2):231–244, 1980.

[59] J.J. Quirk. Godunov-type schemes applied to detonation flows. Technical report, DTIC Document, 1993.

[60] B. Einfeldt, C.D. Munz, P.L. Roe, and B. Sjgreen. On godunov-type methods near low densities. *Journal of Computational Physics*, 92(2):273–295, 1991.

[61] G. J. Sharpe and J. J. Quirk. Nonlinear cellular dynamics of the idealized detonation model: Regular cells. *Combustion Theory and Modelling*, 12(1):1–21, December 2007.

[62] S. Xu and T. Aslam. High resolution numerical simulation of ideal and non-ideal compressible reacting flows with embedded internal boundaries. *Combustion Theory and Modelling*, 1:113–142, 1997.

[63] J.J. Quirk. *An adaptive grid algorithm for computational shock hydrodynamics.* Ph.D. thesis, Cranfield Institute of Technology, 1991.

[64] J.J. Quirk. A parallel adaptive grid algorithm for computational shock hydrodynamics. *Applied numerical mathematics*, 20(4):427–453, 1996.

[65] M.J. Berger and J. Oliger. Adaptive mesh refinement for hyperbolic partial differential equations. *Journal of computational Physics*, 53(3):484–512, 1984.

[66] M.J. Berger and P. Colella. Local adaptive mesh refinement for shock hydrodynamics. *Journal of computational Physics*, 82(1):64–84, 1989.

[67] R. Courant, K. Friedrichs, and H. Lewy. On the partial difference equations of mathematical physics. *IBM Journal of Research and Development*, 11(2):215–234, 1967.

[68] M. Short, A.K. Kapila, and J.J. Quirk. The chemical-gas dynamic mechanisms of pulsating detonation wave instability. *Philosophical Transactions of the Royal Society of London. Series A: Mathematical, Physical and Engineering Sciences*, 357(1764):3621–3637, 1999.

[69] V. N. Gamezo, T. Ogawa, and E. S. Oran. Flame acceleration and DDT in channels with obstacles: Effect of obstacle spacing. *Combustion and Flame*, 155(1):302–315, 2008.

[70] T. Ogawa, E.S. Oran, and V.N. Gamezo. Numerical study on flame acceleration and DDT in an inclined array of cylinders using an AMR technique. *Computers & Fluids*, 2012.

[71] T. Ogawa, V. N. Gamezo, and E. S. Oran. Flame acceleration and transition to detonation in an array of square obstacles. *Journal of Loss Prevention in the Process Industries*, December 2011.

[72] E. S. Oran, J. P. Boris, D. A. Jones, and M. Sichel. Ignition in a complex mach structure. *Progress in Astronautics and Aeronautics*, 153:241–241, 1993.

[73] M. Arienti and J. E. Shepherd. A numerical study of detonation diffraction. *Journal of Fluid Mechanics*, 529:117–146, April 2005.

[74] C. Leung. *Examination of the Pulsating Detonation Instability in a Two-Step model using Characteristics*. Master's thesis, University of Ottawa, Ottawa, 2010.

[75] M. Short and J. J. Quirk. On the nonlinear stability and detonability limit of a detonation wave for a model three-step chain-branching reaction. *Journal of Fluid Mechanics*, 339(89-119):1, 1997.

[76] R. R. Bhattacharjee, S. SM. Lau-Chapdelaine, G. Maines, L. Maley, and M. I. Radulescu. Detonation re-initiation mechanism following the mach reflection of a quenched detonation. *Proceedings of the Combustion Institute*, August 2012.

[77] J. Tang and M.I. Radulescu. Dynamics of shock induced ignition in ficketts model: Influence of. *Proceedings of the Combustion Institute*, July 2012.

[78] S. SM. Lau-Chapdelaine and M. I. Radulescu. Non-uniqueness of solutions in asymptotically self-similar shock reflections. *Shock Waves*. Submitted 2011, reviewed 2012.

[79] D. J. Seery and C. T. Bowman. An experimental and analytical study of methane oxidation behind shock waves. *Combustion and Flame*, 14(1):37–47, 1970.

[80] D. G. Goodwin. An open-source, extensible software suite for CVD process simulation. In *The Electrochemical Society*, volume 14, pages 155–162, 2003.

Appendix A

Calibration

A.1 Sensitivity

In experiments, the sensitivity of the gas is adjusted by changing pressure. In simulations it is done by changing the half-reaction length scale (i.e. how fast the gas reacts). This requires matching the half-reaction length with the appropriate pressure.

A.1.1 Defining half-reaction length

The half-reaction length is defined as the distance behind the incident shock by which point half of the heat has been released. The half-reaction length was approximated to be equal to the distance between the shock and maximum temperature gradient location. Figure A.1 compares the induction and half-reaction lengths in a one-step ZND detonation with relevant activation energy and heat release. The half-reaction length is unambiguous for this chemical model. The maximum temperature gradient is shown to approximate the half-reaction length closely; this is likely also the case using real chemistry. Note that the induction zone is also approximated as the zone between the shock and maximum temperature gradient.

A.1.2 Effect of initial pressure on half-reaction length

The effect of initial pressure on the half-reaction length is shown in figure A.2. Power-law regression of the data gives a relation for the half-reaction length as a function of initial

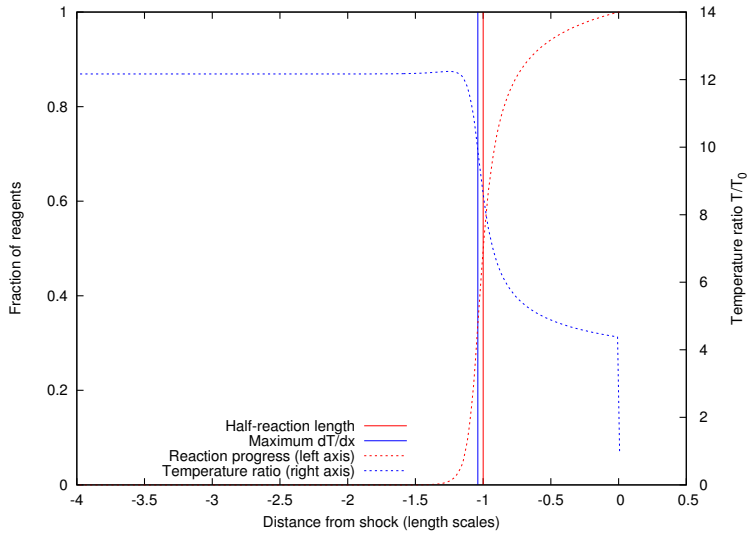

Figure A.1: Comparison of induction and half-reaction lengths for a one-step model with $Q/RT_0 = 60.5$ and $E_a/RT_0 = 43.3$

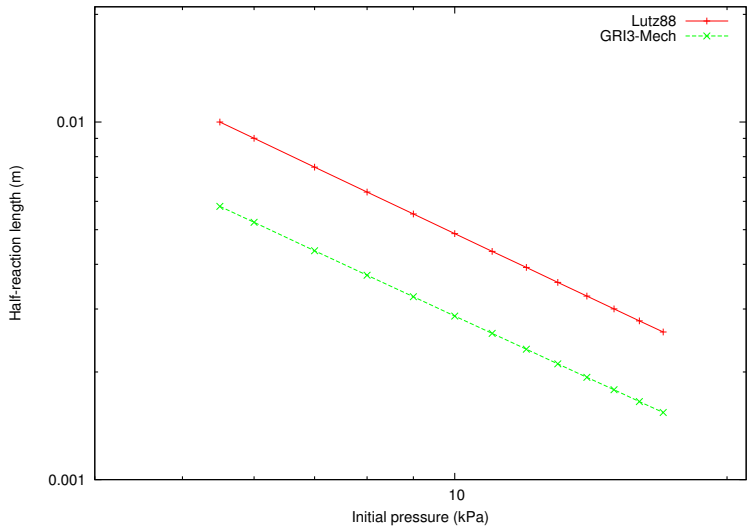

Figure A.2: Effect of initial pressure on half-reaction length using the Lutz88 [36] and GRI 3.0 [1] mechanisms

Table A.1: Length scale factors used to adjust gas sensitivity using the GRI 3.0 mechanism [1]

P_0	$\Delta_{\frac{1}{2}}$	l_{throat}	$\#\frac{grids}{pore}$	ls
5.5 kPa	0.00581 m	0.0507 m	6	1.45
10.3 kPa	0.00277 m	0.0507 m	6	3.05
11.9 kPa	0.00234 m	0.0507 m	6	3.62
12.5 kPa	0.00221 m	0.0507 m	6	3.83
17.6 kPa	0.00148 m	0.0507 m	6	5.72

pressure for the Lutz88 mechanism [36]

$$\Delta_{\frac{1}{2}} = 0.0769792183(P_0[kPa])^{-1.1980265347} \tag{A.1}$$

and GRI 3.0 mechanism [1]

$$\Delta_{\frac{1}{2}} = 0.0430500617(P_0[kPa])^{-1.1758936482}. \tag{A.2}$$

A.1.3 Length scale calculation

The half-reaction length is used as the characteristic length scale for non-dimensionalization. AMRITA CFD [51] scales its base grid size similarly. Six grid points were (arbitrarily) chosen to cover the throat, measuring $l_{throat} = 0.057$ m. A length scale factor ls is introduced

$$\Delta_{\frac{1}{2}} \times ls = \frac{l_{throat}}{\#\text{grid points covering throat}} \tag{A.3}$$

allowing the half-reaction length to change and the throat size to remain constant. The length scale factors used to adjust the gas sensitivity are shown in table A.1.

It has been suggested that a minimum of 32 grid points per half-reaction length are necessary to propery resolve detonations [11]. The space between each base grid point can be split into r number of smaller cells, where r is called the refinement ratio. The process is repeated on the refined grid to a total maximum number of refinement levels $lmax$. The refinement ratio was kept constant at $r = 2$ while $lmax$ was varied

$$\text{Resolution} = \frac{r^{lmax}}{ls} \tag{A.4}$$

Table A.2: Refinement ratio, maximum refinement levels and resolution used

P_0	ls	r	$lmax$	$\frac{\text{Resolution}}{\text{induction length}}$
5.5 kPa	1.45	2	6	44.14
10.3 kPa	3.05	2	7	41.97
11.9 kPa	3.62	2	7	35.36
12.5 kPa	3.83	2	7	33.46
17.6 kPa	5.72	2	8	44.76

to meet the minimum resolution requirement and is shown in table A.2.

Selection of the length scale factor and maximum refinement levels is done by following the algorithm shown in figure A.3:

1. Establish desired initial state (T_0, P_0, ρ_0) and chemistry (e.g. $CH_4 + 2O_2$, GRI 3.0 mechanism [1]);
2. Calculate detonation velocity using full chemistry model. This can be done using the code B.1;
3. Calculate ZND profile using full chemistry model. This can be done using the code B.4;
4. Determine half-reaction length by measuring the distance between the incident shock and maximum temperature gradient;
5. Solve for ls in the length scale factor equation A.3;
6. Solve for $lmax$ in the refinement equation A.4 (with a resolution of 32).

A.2 Isentropic exponent

The isentropic exponent γ was assumed constant simulations. The isentropic exponent behind the shock γ_{vN}, calculated using full chemistry, was used as a compromise between pre-shock, post-shock and post-reaction isentropic exponents because the ignition delay is sensitive to post-shock conditions and regions of interest lie behind the leading shock.

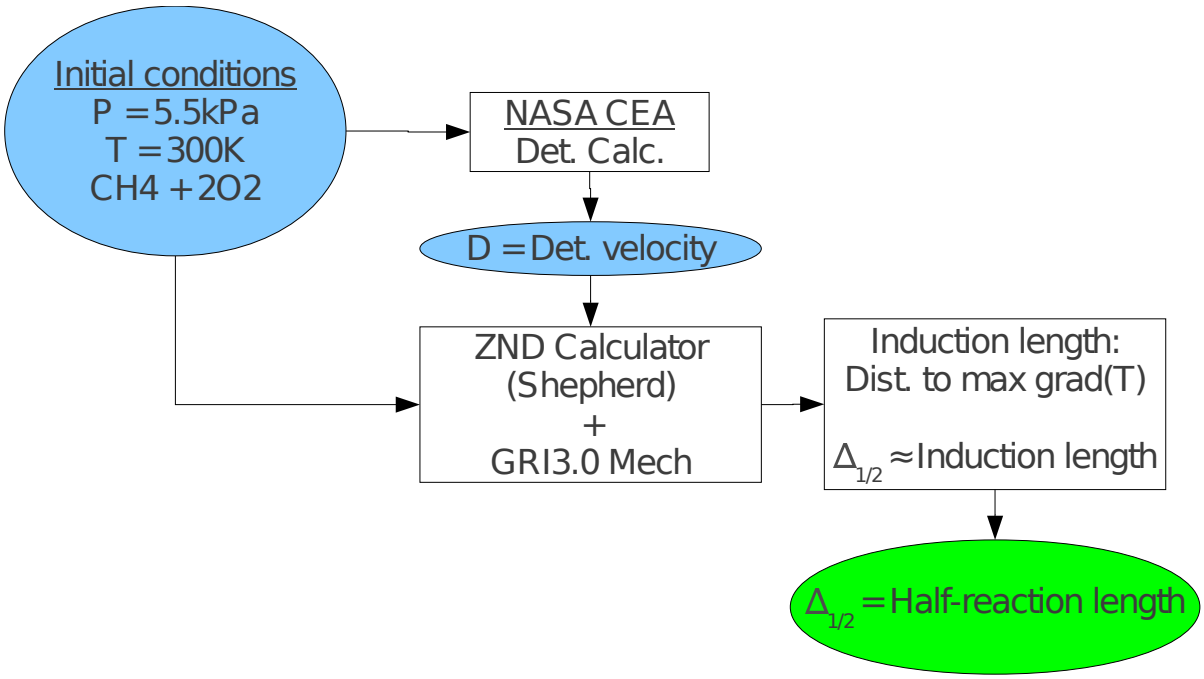

Figure A.3: Algorithm used to find half-reaction length

1. Establish desired initial state (T_0, P_0, ρ_0) and chemistry (e.g. $CH_4 + 2O_2$, GRI 3.0 mechanism [1]).

2. Determine detonation Mach number M_{CJ} and velocity D_{CJ}. This can be done with code B.1.

3. Compute von-Neumann (post-shock) state (T_{vN}, P_{vN},ρ_{vN}, γ_{vN}) using frozen chemistry and the shock velocity D_{CJ}. This can be done with code B.2.

A.3 Activation Energy

A.3.1 Ignition Delay

Reaction rates can be described by the irreversible one-step Arrhenius equation

$$\frac{D\lambda}{Dt} = ke^{\frac{-E_a}{RT}} \tag{A.5}$$

where λ is the reaction progress variable, E_a is the activation energy, R is the universal gas constant and T is the temperature. The rate $\frac{D\lambda}{Dt}$ can be expressed using a rate

equation

$$\frac{D\lambda}{Dt} = \frac{1}{\tau}[A]^a[B]^b...[Z]^z$$

with reaction time τ and molar concentrations of each species $[A]$ to $[Z]$ raised to their respective empirical rate exponents a to z and, using the Arrhenius rate equation A.3.1, rearranged to

$$\frac{\tau}{[A]^a[B]^b...[Z]^z} = ke^{\frac{-E_a}{RT}}. \tag{A.6}$$

The concentration of a species $[A]$ in a perfect gas is expressed as

$$[A] = \frac{n_A}{V}$$
$$[A] = \frac{P_A V/RT}{V}$$
$$[A] = \frac{P_A}{RT}$$

where the number of moles n_A of that species is contained in volume V, and P_A is the partial pressure exerted by that species. Concentrations in equation A.6 can therefore be replaced by partial pressures

$$\frac{\tau}{\left(\frac{P_A}{RT}\right)^a\left(\frac{P_B}{RT}\right)^b...\left(\frac{P_Z}{RT}\right)^z} = ke^{\frac{-E_a}{RT}}. \tag{A.7}$$

The natural logarithm

$$\ln\left(\frac{\tau}{\left(\frac{P_A}{RT}\right)^a\left(\frac{P_B}{RT}\right)^b...\left(\frac{P_Z}{RT}\right)^z}\right) = \ln(k) - \left(\frac{E_a}{R}\right)\frac{1}{T} \tag{A.8}$$

gives an linear equation of ignition time versus inverse temperature with activation energy as its slope. In a stoichiometric two-reactant mixture, concentration of both reactants together suffices because they decrease at an equal rate. For stoichiometric methane-oxygen, this can be written as

$$\ln\left(\frac{\tau}{\left(\frac{P_{CH_4}+P_{2O_2}}{RT}\right)^a}\right) = \ln(k) - \left(\frac{E_a}{R}\right)\frac{1}{T}$$

without inert species (e.g. noble gases) which serve only to dilute reactants. Their combined rate exponent is the sum of their individual rate exponents. An exponent

$a = -1.2$ found by Seery and Bowman [79] was used and other sources have found values in the vicinity for this reaction [30]. This method allows comparison of experiments with different temperatures, pressures and dilutions. Data from numerous such experiments are plotted in figure 3.3.

An example using experimental data is tabulated in table A.3.

Table A.3: Ignition delay for stoichiometric methane-oxygen diluted to 11% by mole, at $P_{vN} = 604$kPa, $T_{vN} = 1749$ K [31]

$\%CH_4 + 2O_2$	$P_{total}(kPa)$	T (K)	$\tau_{ig}(\mu s)$	$P_{[CH_4+2O_2]}$ (kPa)	$1/T(1/K)$	$\frac{\tau_{ig}}{\left(\frac{P_{CH_4+2O_2}}{RT_{vN}}\right)^{-1.2}}(\mu s)$
11%	604	1749	71	66.44	0.000572	0.000440

A.3.2 Ignition Delay Calculation

The ignition delay was found using the GRI 3.0 mechanism [1]. This mechanism was compared to experimental data and the Lutz88 mechanism [36] in figure 3.3 by calculating the ignition delay as a function of temperature. This was done using Shepherd's CV calculator [46] but can also be done using the newer Cantera software [80]. The combustion is approximated using a constant volume combustion. The algorithm to find ignition delay using a chemical mechanism follows:

1. Continue from post-shock calculation section A.2;
2. Perform a constant-volume combustion calculation using the von-Neumann state as the pre-reaction state to determine the ignition time τ_{ig}. This can be done using the code B.3.

A.3.3 Activation Energy Calculation

The activation energy E_a of a reaction is the amount of energy, per mole, required for the reaction to begin. The activation energy is found using the ignition delay equation A.8 or from the slope of its plot, shown in figure 3.3. The slope in this case is more-or-less constant over a large temperature range, suddenly changes and is once again approximately constant.

Performing combustion calculations with pre-combustion temperatures slightly above T_{vN+} and below T_{vN-} (e.g. $T_{vN} \pm 5\%$) the target temperature T_{vN} will give the corresponding ignition delay times τ_+ and τ_-. These temperatures and ignition delay times can be used to find the activation energy (the slope of the line equation A.8)

$$\frac{E_a}{R} \approx \frac{\ln\left(\frac{\tau_+}{\left(\frac{P_{CH_4+2O_2}}{RT_{vN+}}\right)^a}\right) - \ln\left(\frac{\tau_-}{\left(\frac{P_{CH_4+2O_2}}{RT_{vN-}}\right)^a}\right)}{1/T_{vN+} - 1/T_{vN-}}$$

which simplifies to

$$\frac{E_a}{R} \approx \frac{\ln\left(\frac{\tau_+}{\tau_-}\right) - a\ln\left(\frac{T_{vN+}}{T_{vN-}}\right)}{1/T_{vN+} - 1/T_{vN-}}$$

and if $\ln\left(\frac{\tau_+}{\tau_-}\right) >> |a| \ln\left(\frac{T_{vN+}}{T_{vN-}}\right)$, can be approximated to

$$\frac{E_a}{R} \approx \frac{\ln(\tau_+) - \ln(\tau_-)}{1/T_{vN+} - 1/T_{vN-}}. \tag{A.9}$$

The activation energy E_a/R is then non-dimensionalized by post-shock temperature T_{vN} for the two-step model. An extra step must be taken to non-dimensionalize for the one step model in order to account for constant isentropic exponent γ. The activation energy is divided by the post-shock temperature, as before, then multiplied by the Rankine-Hugoniot shock relation for temperature

$$\frac{T_{vN}}{T_0} = \frac{\left(1 + \frac{\gamma_{vN}-1}{2}M_{CJ}^2\right)\left(\frac{2\gamma_{vN}}{\gamma_{vN}-1}M_{CJ}^2 - 1\right)}{M_{CJ}^2\left(\frac{2\gamma_{vN}}{\gamma_{vN}-1} + \frac{\gamma_{vN}-1}{2}\right)} \tag{A.10}$$

with detonation Mach number M_{CJ} and post-shock isentropic exponent γ_{vN}, in order to non-dimensionalize by pre-shock conditions.

The algorithm for calculating activation energy, shown in figure A.4, follows:

1. Continue from ignition delay calculation section A.3.2;
2. Vary the pre-combustion temperature T_{vN} slightly (eg. $\pm 5\%$) and repeat the ignition delay calculation section A.3.2 with this new temperature;
3. Approximate activation energy with equation A.9;

4. Non-dimensionalize by dividing the result by post-shock temperature T_{vN};

5. One-step chemistry: Multiply the result by Rankine-Hugoniot temperature ratio equation A.10.
   Two-step chemistry: Finished.

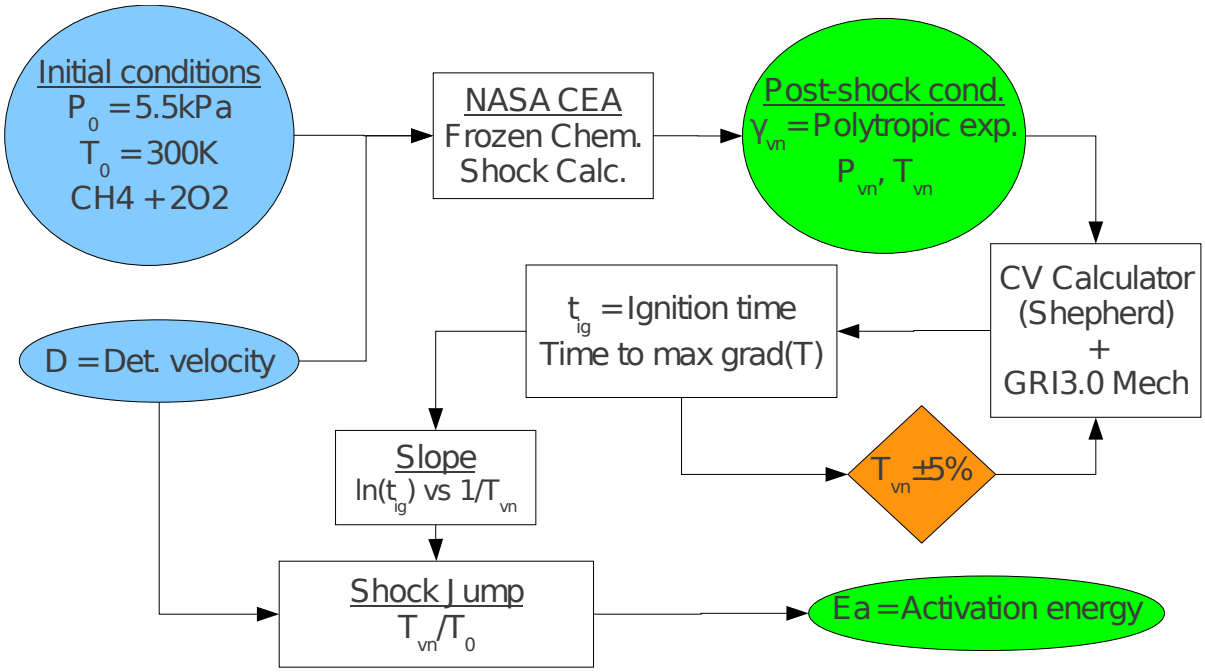

Figure A.4: Algorithm used to find activation energy

Activation energy was calculated once, for initial conditions at 5.5 kPa, and assumed constant. Results of these calculations are shown in tables A.5 and A.4

Table A.4: Stoichiometric methane-oxygen activation energy with Lutz88 [36] mechanism

P_0 (kPa)	T_0 (K)	c_0 (m/s) (CEA)	D_{CJ} (m/s) (CEA)	M_{CJ}	P_{vN} (kPa) (CEA)	T_{vN} (K) (CEA)	τ_{ig} (s) (CV)	$\frac{E_a}{RT_{vN}}$	$\frac{E_a}{RT_0}$	$\frac{E_a}{RT_0}$ $const.\gamma$
						1830.18	2.16×10^{-5}			
5.5	300	356.4	2262.2	6.3474	271.07	1743.03	3.51×10^{-5}	10.213	59.337	45.2
						1655.88	6.01×10^{-5}			

Table A.5: Stoichiometric methane-oxygen activation energy with GRI 3.0 [1] mechanism

P_0 (kPa)	T_0 (K)	c_0 (m/s) (CEA)	D_{CJ} (m/s) (CEA)	M_{CJ}	P_{vN} (kPa) (CEA)	T_{vN} (K) (CEA)	τ_{ig} (s) (CV)	$\frac{E_a}{RT_{vN}}$	$\frac{E_a}{RT_0}$	$\frac{E_a}{RT_0}$ $const.\gamma$
						1830.18	1.13×10^{-5}			
5.5	300	356.4	2262.2	6.3474	271.07	1743.03	2.88×10^{-5}	11.003	63.927	48.7
						1655.88	3.36×10^{-5}			

Table A.6: Heat release of stoichiometric methane-oxygen

P_0 (kPa)	T_0 (K)	c_0 (m/s) (CEA)	D_{CJ} (m/s) (CEA)	M_{CJ}	γ_{vN} (CEA)	Q/RT_{vN}	Q/RT_0
5.5	300	356.4	2262.2	6.3474	1.1709	13.72	60.4594

A.4 Heat Release

The heat release Q is the amount of energy added to the environment, per mole of reactants. For a detonation through prefect gas it is derived from Chapman-Jouget perfect gas combustion model [5]

$$\frac{Q}{RT_0} = \frac{\gamma}{2(\gamma^2 - 1)} \left(M_{CJ} - \frac{1}{M_{CJ}} \right)^2 \tag{A.11}$$

where M_{CJ} is the detonation Mach number (through pre-shocked gas), R is the universal gas constant, T_0 is the pre-shock temperature, and γ is the (constant) isentropic exponent. Once again the post-shock isentropic exponent γ_{vN} is used. The algorithm is shown in figure A.5 and results of a sample calculation are shown in table A.6.

To non-dimensionalize for the two-step model, the result of equation A.11 is divided by the Rankine-Hugoniot temperature equation A.10.

A.5 Reaction pre-exponential factor k_r

The pre-exponential factor k_r is calibrated by selecting the proper ratio $\frac{\Delta_i}{\Delta_r}$. The induction length Δ_i is calculated in the same manner as the half-reaction length in section A.1.1.

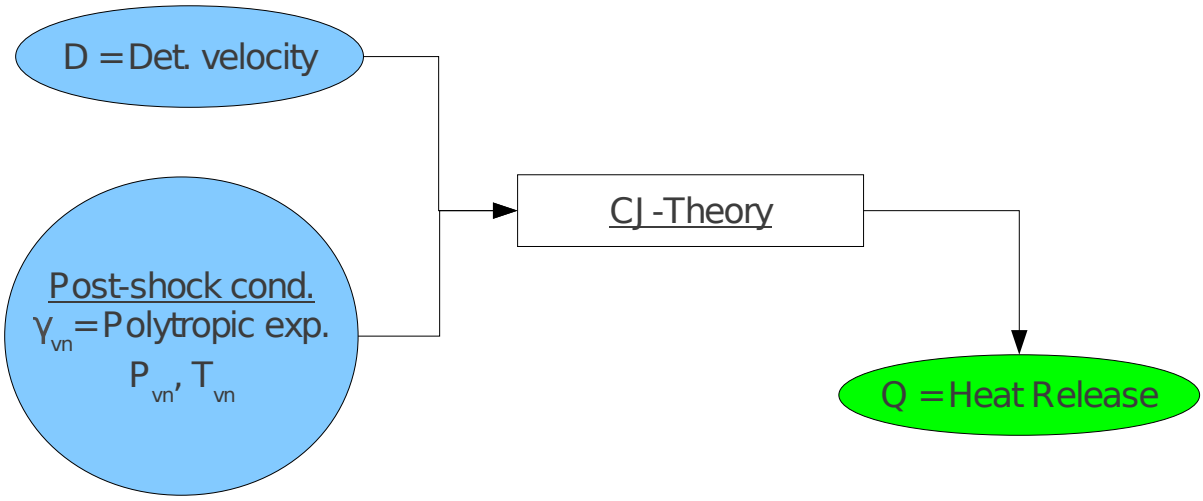

Figure A.5: Algorithm used to find heat release

The reaction length Δ_r is defined as the distance between the thermicity half-height points [49]. The locations of both half-of-maximum thermicity points are determined (interpolated for) from the ZND profile data.

A.6 Reaction order ν

Obtaining the reaction order exponent ν required in the two-step reaction equation 3.7 is discussed in the ignition delay section A.3.1. Note that $\nu = -a$ because section A.3.1 is concerned with ignition *times* while equation 3.7 deals with *rates*. A value of $\nu = 0.8$ was used instead of $\nu = -a = 1.2$ in order to better match the real chemistry ZND structure.

Appendix B

Code and Scripts

B.1 NASA CEA: Detonation Mach Number

Calculates the Chapman-Jouget Mach number M_{CJ} of a detonation travelling through stoichiometric oxygen-methane at an initial temperature $T_0 = 300$ K, pressure $P_0 = 0.0542807797$ atm.

B.1.1 Preparation

The input file must be prepared as detailed below.

B.1.2 Input

```
reac name O2 moles=1 t(k)=300.00
name CH4 moles=0.5 t(k)=300.00
prob detonation case=1 t=300.0, p(atm)=0.0542807797
output siunits
end
```

B.1.3 Commands

The NASA CEA program is run and the prompts followed.

B.1.4 Output

```
1
2  ****************************************************************************
3
4           NASA-GLENN CHEMICAL EQUILIBRIUM PROGRAM CEA2, MAY 21, 2004
5                     BY  BONNIE MCBRIDE AND SANFORD GORDON
6        REFS: NASA RP-1311, PART I, 1994 AND NASA RP-1311, PART II, 1996
7
8  ****************************************************************************
9
10
11
12 reac  name O2     moles=1       t(k)=300.00
13       name CH4    moles=0.5     t(k)=300.00
14
15 prob  detonation   case=1  t=300.0, p(atm)=0.0690846287
16
17 output  siunits
18 end
19
20 OPTIONS: TP=F  HP=F  SP=F  TV=F  UV=F  SV=F  DETN=T  SHOCK=F  REFL=F  INCD
       =F
21 RKT=F  FROZ=F  EQL=F  IONS=F  SIUNIT=T  DEBUGF=F  SHKDBG=F  DETDBG=F
       TRNSPT=F
22
23 T,K =    300.0000
24
25 TRACE= 0.00E+00  S/R= 0.000000E+00  H/R= 0.000000E+00  U/R= 0.000000E+00
26
27 P,BAR =      0.070000
28
29    REACTANT              MOLES      (ENERGY/R),K    TEMP,K  DENSITY
30         EXPLODED FORMULA
31 N: O2                  1.000000    0.653777E+01    300.00  0.0000
32           O  2.00000
33 N: CH4                 0.500000   -0.896432E+04    300.00  0.0000
34           C  1.00000  H  4.00000
35
36  SPECIES BEING CONSIDERED IN THIS SYSTEM
37 (CONDENSED PHASE MAY HAVE NAME LISTED SEVERAL TIMES)
```

```
 LAST thermo.inp UPDATE:     9/09/04

 g 7/97  *C                tpis79  *CH              g 4/02  CH2
 ...     ...               ...     ...             ...     ...
 n 4/83  C(gr)             g11/99  H2O(cr)         g 8/01  H2O(L)
 g 8/01  H2O(L)

O/F =    0.000000

                          EFFECTIVE FUEL      EFFECTIVE OXIDANT          MIXTURE
ENTHALPY                      h(2)/R              h(1)/R                   h0/R
(KG-MOL)(K)/KG          -0.11183452E+03     0.00000000E+00          -0.11183452E
    +03

KG-FORM.WT./KG                bi(2)               bi(1)                    b0i
 *O                       0.49974975E-01      0.00000000E+00          0.49974975E
    -01
 *C                       0.12493744E-01      0.00000000E+00          0.12493744E
    -01
 *H                       0.49974975E-01      0.00000000E+00          0.49974975E
    -01

POINT ITN       T             O             C             H
  1    25    3130.263      -16.432       -18.890       -11.738

POINT ITN       T             O             C             H
  1     3    3178.067      -16.212       -18.594       -11.528

POINT ITN       T             O             C             H
  1     4    3270.260      -16.228       -18.471       -11.504

POINT ITN       T             O             C             H
  1     3    3264.334      -16.227       -18.478       -11.505

POINT ITN       T             O             C             H
  1     2    3264.335      -16.227       -18.478       -11.505


                        DETONATION PROPERTIES OF AN IDEAL REACTING GAS
CASE = 1

              REACTANT                          MOLES          ENERGY        TEMP
```

```
76                                                                KJ/KG-MOL      K
77  NAME          O2                              1.0000000        54.358
        300.000
78  NAME          CH4                             0.5000000      -74533.907
        300.000
79
80  O/F=      0.00000   %FUEL=   0.000000   R,EQ.RATIO=  1.000000   PHI,EQ.RATIO=
        0.000000
81
82  UNBURNED GAS
83
84  P1, BAR                0.0700
85  T1, K                  300.00
86  H1, KJ/KG             -929.85
87  M1, (1/n)              26.680
88  GAMMA1                 1.3584
89  SON VEL1,M/SEC          356.4
90
91  BURNED GAS
92
93  P, BAR                 1.8599
94  T, K                  3264.33
95  RHO, KG/CU M       1.3940-1
96  H, KJ/KG               907.44
97  U, KJ/KG              -426.80
98  G, KJ/KG             -43881.5
99  S, KJ/(KG)(K)          13.7207
100
101 M, (1/n)               20.342
102 (dLV/dLP)t           -1.08503
103 (dLV/dLT)p             2.5973
104 Cp, KJ/(KG)(K)        14.5469
105 GAMMAs                 1.1167
106 SON VEL,M/SEC         1220.6
107
108 DETONATION PARAMETERS
109
110 P/P1                  26.570
111 T/T1                  10.881
112 M/M1                  0.7624
113 RHO/RHO1              1.8618
114 DET MACH NUMBER       6.3769
```

```
 DET VEL,M/SEC       2272.6

 MOLE FRACTIONS

 *CO                 0.16950
 *CO2                0.08464
 *H                  0.07071
 HO2                 0.00007
 *H2                 0.08347
 H2O                 0.32936
 *O                  0.05603
 *OH                 0.12014
 *O2                 0.08606

   * THERMODYNAMIC PROPERTIES FITTED TO 20000.K

     PRODUCTS WHICH WERE CONSIDERED BUT WHOSE MOLE FRACTIONS
     WERE LESS THAN 5.000000E-06 FOR ALL ASSIGNED CONDITIONS

 *C                  *CH                 CH2                 CH3                 CH2OH
...                  ...                 ...                 ...                 ...
```

B.2 NASA CEA: von-Neumann/Post-Shock/Pre-Reaction State

Calculates the von-Neumann state for a detonation travelling at $2262.2\frac{\mathrm{m}}{\mathrm{s}}$ through stoichiometric oxygen-methane at an initial temperature $T_0 = 300\,\mathrm{K}$, pressure $P_0 = 0.0542807797$ atm.

B.2.1 Preparation

The input file must be prepared as detailed below.

B.2.2 Input

```
1 reac name O2 moles=1 t(k)=300.00
2 name CH4 moles=0.5 t(k)=300.00
3 prob shock case=1 t=300.0, p(atm)=0.0542807797 u1=2262.2
```

```
4 incd froz
5 output siunits
6 end
```

B.2.3 Commands

The NASA CEA program is run and the prompts followed.

B.2.4 Output

Note that the portion of the output shown below only shows the equilibrium state. The frozen state which follows this is of interest.

```
1
2  ***************************************************************************

3
4           NASA-GLENN CHEMICAL EQUILIBRIUM PROGRAM CEA2, MAY 21, 2004
5                     BY  BONNIE MCBRIDE AND SANFORD GORDON
6        REFS: NASA RP-1311, PART I, 1994 AND NASA RP-1311, PART II, 1996
7
8  ***************************************************************************

9
10
11
12  reac  name O2     moles=1       t(k)=300.00
13        name CH4  moles=0.5       t(k)=300.00
14
15  prob  shock   case=1  t=300.0, p(atm)=0.0542807797 u1=2262.2
16    incd froz  eql
17
18  output  siunits
19  end
20
21  OPTIONS: TP=F  HP=F  SP=F  TV=F  UV=F  SV=F  DETN=F  SHOCK=T  REFL=F  INCD
        =T
22  RKT=F  FROZ=T  EQL=T  IONS=F  SIUNIT=T  DEBUGF=F  SHKDBG=F  DETDBG=F
        TRNSPT=F
23
24  T,K =    300.0000
```

```
25
26 TRACE= 0.00E+00  S/R= 0.000000E+00  H/R= 0.000000E+00  U/R= 0.000000E+00
27
28 P,BAR =       0.055000
29
30     REACTANT              MOLES      (ENERGY/R),K    TEMP,K  DENSITY
31          EXPLODED FORMULA
32  N: O2                  1.000000    0.653777E+01    300.00   0.0000
33            O  2.00000
34  N: CH4                 0.500000   -0.896432E+04    300.00   0.0000
35            C  1.00000   H  4.00000
36
37   SPECIES BEING CONSIDERED IN THIS SYSTEM
38  (CONDENSED PHASE MAY HAVE NAME LISTED SEVERAL TIMES)
39   LAST thermo.inp UPDATE:     9/09/04
40
41   g 7/97   *C                tpis79   *CH               g 4/02   CH2
42   ...      ...               ...      ...              ...      ...
43   n 4/83   C(gr)             g11/99   H2O(cr)          g 8/01   H2O(L)
44   g 8/01   H2O(L)
45
46     *** INPUT FOR SHOCK PROBLEMS ***
47
48  INCDEQ = T    REFLEQ = F    INCDFZ = T     REFLFZ = F
49
50  U1 =     2.262200E+03
51
52  MACH1 = 0.000000E+00
53
54  O/F =    0.000000
55
56                              EFFECTIVE FUEL      EFFECTIVE OXIDANT        MIXTURE
57  ENTHALPY                        h(2)/R              h(1)/R                h0/R
58  (KG-MOL)(K)/KG          -0.11183452E+03     0.00000000E+00      -0.11183452E
        +03
59
60  KG-FORM.WT./KG                  bi(2)               bi(1)                 b0i
61    *O                      0.49974975E-01      0.00000000E+00       0.49974975E
          -01
62    *C                      0.12493744E-01      0.00000000E+00       0.12493744E
          -01
63    *H                      0.49974975E-01      0.00000000E+00       0.49974975E
```

```
      −01
64
65
66
67
68                                SHOCK WAVE PARAMETERS ASSUMING
69
70                        EQUILIBRIUM COMPOSITION FOR INCIDENT SHOCKED CONDITIONS
71
72
73  CASE = 1
74
75                  REACTANT                              MOLES          ENERGY          TEMP
76                                                                      KJ/KG-MOL          K
77  NAME            O2                                 1.0000000          54.358
        300.000
78  NAME            CH4                                0.5000000      −74533.907
        300.000
79
80  O/F=      0.00000   %FUEL=   0.000000   R,EQ.RATIO= 1.000000   PHI,EQ.RATIO=
        0.000000
81
82  INITIAL GAS (1)
83  MACH NUMBER1        6.3479
84  U1, M/SEC          2262.20
85  P, BAR             0.05500
86  T, K                300.00
87  RHO, KG/CU M      5.8829−2
88  H, KJ/KG           −929.85
89  U, KJ/KG          −1023.34
90  G, KJ/KG          −3499.11
91  S, KJ/(KG)(K)       8.5642
92
93  M, (1/n)            26.680
94  Cp, KJ/(KG)(K)      1.1811
95  GAMMAs              1.3584
96  SON VEL,M/SEC        356.4
97
98  SHOCKED GAS (2)--INCIDENT--EQUILIBRIUM
99  U2, M/SEC          1213.11
100 P, BAR              1.4512
101 T, K               3227.29
```

```
102  RHO, KG/CU M      1.0970-1
103  H, KJ/KG            893.11
104  U, KJ/KG           -429.69
105  G, KJ/KG          -43701.2
106  S, KJ/(KG)(K)       13.8179
107
108  M, (1/n)            20.285
109  (dLV/dLP)t        -1.08629
110  (dLV/dLT)p          2.6379
111  Cp, KJ/(KG)(K)      15.0254
112  GAMMAs              1.1155
113  SON VEL,M/SEC       1214.7
114
115  P2/P1               26.385
116  T2/T1               10.758
117  M2/M1               0.7603
118  RHO2/RHO1           1.8648
119  V2, M/SEC           1049.09
120
121  MOLE FRACTIONS
122
123  *CO                 1.6939-1
124  ...                 ...
125  O3                  6.7382-8
126
127    * THERMODYNAMIC PROPERTIES FITTED TO 20000.K
128
129      PRODUCTS WHICH WERE CONSIDERED BUT WHOSE MOLE FRACTIONS
130      WERE LESS THAN 5.000000E-09 FOR ALL ASSIGNED CONDITIONS
131
132  *C                  *CH                 CH2                 CH3                 CH2OH
133  ...                 ...                 ...                 ...                 ...
```

B.3 CV: Constant-Volume Combustion

Calculates the constant-volume combustion for stoichiometric oxygen-methane pre-reaction temperature $T_{vN} = 1743.03$ K, pressure $P_{vN} = 2.6752528991$ atm.

B.3.1 Preparation

The programs can be downloaded from Explosion Dynamics Laboratory's website [46]. The chemical model in CHEMKIN format must be downloaded to the same folder.

B.3.2 Input

```
CASE
NOSHK !Do not shock
T1 1743.03 ! initial temperature (post-shock, K)
P1 2.6752528991 ! initial pressure (post-shock, atm)
REAC
CH4 0.3333 ! methane mol fraction
O2 0.6667 ! oxygen mol fraction
END
ATOL 1.E-11 ! absolute tolerance
RTOL 1.E-12 ! relative tolerance
TMAX 3.8E-01 ! Maximum time allowed (s)
END
```

B.3.3 Commands

1. Rename your CHEMKIN formatted chemical model to "chem.inp";
2. Run "ckinterp.exe";
3. Prepare the input file;
4. Run "cv.exe".

B.3.4 Output

The peak temperature occurs at $t = 1.8823 \times 10^{-5}$ s. Lines have been removed to save space and replaced with ellipses.

```
CASE #      7

INITIAL CONDITIONS
TEMPERATURE (K)                  1743.
PRESSURE (ATM)                   2.675
DENSITY (G/CC)                 4.9907E-04
```

```
SPECIES MOLE FRACTIONS:
O2              0.6667
CH4             0.3333

REACTION ZONE STRUCTURE:



ITER      TIME            TEMP            DT/dt       P
          (S)             (K)             (K/S)       (atm)
    0      0.00           1.743E+03      -3.296E+05   2.68
    1     2.691E-12       1.743E+03      -3.296E+05   2.68
    2     5.383E-12       1.743E+03      -3.296E+05   2.68
    3     7.425E-10       1.743E+03      -3.299E+05   2.68
  ...       ...             ...             ...         ...
 1590     4.256E-02       3.611E+03      -5.250E-06   7.52
 1591     0.234           3.611E+03      -5.221E-05   7.52
 1592     0.380           3.611E+03      -7.872E-06   7.52
TIME = TMAX, LAST POINT:
 1592     0.380           3.611E+03      -7.872E-06   7.52
NUMBER OF INTEGRATOR STEPS 1592

FINAL SPECIES MOLE FRACTIONS :
  0.9019E-01   0.8265E-01   0.6947E-01   0.8670E-01   0.1314
  0.2939       0.1567E-03   0.8924E-05   0.1315E-08   0.2089E-09
  0.9599E-10   0.1183E-10   0.4215E-10   0.3464E-11   0.1771
  0.6843E-01   0.5034E-05   0.5079E-07   0.1473E-10   0.4812E-12
  0.3371E-12   0.1866E-13   0.5783E-13   0.2147E-16   0.1799E-17
  0.5411E-21   0.8949E-23   0.8937E-12   0.1590E-12   0.2627E-14
  0.3413-101   0.5882-102   0.9814-103   0.2611-103   0.7533-116
  0.1615E-98   0.1165-101   0.2502-115   0.6125-102   0.9170-105

  0.6555-104   0.2668-108   0.1951-123   0.1035-107   0.2099-105
  0.9216-104   0.5048-104   0.3076-110   0.7368-100   0.4655E-32
  0.6702E-34   0.2216E-16   0.4256E-18

Time to peak  (s) :                    1.8823E-05

time to 10% of peak  (s) :             1.8600E-05

time to 90% of peak (s) :              1.8822E-05
```

B.4 ZND: Zel'dovich-von-Neumann-Döring Profile

Calculates the ZND for a stoichiometric oxygen-methane detonation with pre-reaction temperature $T_{vN} = 300$ K, pressure $P_0 = 5.5$ kPA.

B.4.1 Preparation

The programs can be downloaded from Explosion Dynamics Laboratory's website [45]. The chemical model in CHEMKIN format must be downloaded to the same folder.

B.4.2 Input

```
CASE 0
UDET  226220 ! CJ detonation velocity (cm/s)
T1 300.  ! initial temperature (preshock)
P1 0.0542807797   ! initial pressure (preshock) (atm)
REAC
CH4  0.3333    ! methane mol fraction
O2  .6667   ! oxygen mol fraction
END
ATOL  1.E-11  ! absolute tolerance (originally 1.E-07)
RTOL  1.E-12  ! relative tolerance (originally 1.E-08)
PLOT  1    !prints out plot output every nth solver step
END
```

B.4.3 Commands

1. Rename your CHEMKIN formatted chemical model to "chem.inp";
2. Run "ckinterp.exe";
3. Prepare the input file;
4. Run "znd.exe".

B.4.4 Output

The peak temperature occurs at $t = 1.8823 \times 10^{-5} s$. Lines have been removed to save space and replaced with ellipses.

```
 CKLIB:  Chemical Kinetics Library
         CHEMKIN-II Version 4.9, April 1994
         DOUBLE PRECISION


ZND: DETONATION STRUCTURE CALCULATION
VERSION 5.6D - LAST MOD ON 6/03/00
CALCULATION RUN ON 18- 8-2011 AT 12:51:35

SPECIES USED IN THIS PROBLEM
H           H2          O           O2          OH          H2O         HO2
H2O2        N2          AR          CH          CH2CO       C2H2        C3H2
C2H4        C           C2H5        C2H3        C2H         HCCOH       HCCO
C2H6        C5H3        C4H2        C5H2        C6H2        CH2         CH2(S)
CO          CO2         HCO         CH2O        CH3O        CH2OH       CH3OH
CH3         CH4         C3H3        C4H3


CASE #     1       1

 INITIAL CONDITIONS
TEMPERATURE (K)                  300.0
PRESSURE (ATM)                 5.9215E-02
DENSITY (G/CC)                 6.4183E-05
DETONATION VELOCITY (CM/S)     2.2659E+05

AREA SPATIAL DERIV (CM)          0.000

SPECIES MOLE FRACTIONS:
O2                0.6667
CH4               0.3333

REACTION ZONE STRUCTURE:

MACH      DIST       TIME       PRES       TEMP       DEN        VELOCITY   SOUND
          GAMMA      WEIGHT     SIGMA      AREA                  C^2-U^2
NUMBER    (CM)       (SEC)      (ATM)      (K)        (G/CC)     (CM/S)     (CM/S)
                     (G/G-MOL)  (1/S)       (CM^2)               (CM^2/S^2)
```

```
 0.336     0.00       0.00       2.92       1766.9   5.380E-04   27031.6
    80508.7     1.18     26.681      -140.           1.00         5.751E+09

 ...       ...        ...        ...        ...      ...         ...       ...
             ...      ...          ...              ...          ...

 0.977     4.40      6.163E-05  1.52       3227.0   1.165E-04  124797.8
    127722.4     1.23     20.297       558.           1.00         7.385E+08

Mach number very close to 1! Eigenvalue detonation?

 1.000     4.48      6.226E-05  1.48       3213.8   1.142E-04  127395.1
    127457.2     1.23     20.300      3.543E+03       1.00         1.583E+07

NUMBER OF INTEGRATOR STEPS 1307

FINAL SPECIES MOLE FRACTIONS :
  0.7359E-01   0.8515E-01   0.5763E-01   0.8826E-01   0.1130
  0.3287       0.6992E-04   0.3180E-05   0.7608-100   0.7608-100
  0.1244E-10   0.6365E-14   0.1581E-14   0.6598E-23   0.1856E-19
  0.9453E-10   0.3945E-23   0.1523E-18   0.8773E-16   0.7198E-16
  0.9095E-13   0.5139E-25   0.3591E-39   0.5435E-29   0.2913E-38
  0.1134E-43   0.6566E-11   0.6640E-12   0.1687       0.8490E-01

  0.1121E-05   0.1155E-07   0.2127E-13   0.1303E-11   0.7608-100
  0.3524E-11   0.1867E-12   0.1243E-24   0.1112E-31

REACTION ZONE LENGTHS (CM) :

MAXIMUM TEMPERATURE GRAD Z                0.9006
MACH .75 Z                                0.9167
MACH .90 Z                                 2.299
Z SIGMA                                   0.9006
T SIGMA                                   3.1297E-05

END OF DATA ON INPUT, ZND FINISHED
```

B.5 AMRITA: Detonation diffraction and reflection using one-step chemistry

Calculates the detonation diffraction and reflection over a cylindrical obstacle using the method described in chapter 3 and the one-step chemistry model. This specific example is for an initial pressure $P_0 = 5.5$ kPa.

B.5.1 Preparation

The AMRITA CFD [51] program was installed and can be found at `http://www.amrita-cfd.org/`. Values of interest can be modified as follows:

- Line 140 controls the isentropic exponent γ.
- Line 142 controls heat release $\tilde{Q}$.
- Line 143 controls activation energy $\tilde{E}_a$.
- Line 393 controls the length scale ls.
- Lines 399 and 400 control resolution.
- Output ranges can be changed by modifying the "min" and "max" values of the various plots between lines 281 and 385.

B.5.2 Input

File name: 1step_run_circle_detonation.amrita

```
1  fold::amrita { run simulation
2     fold::amrita { prelims
3        ReactiveEulerEquations {
4           space = 2D
5           add2W = VORT,E_RATE
6        }
7        fold::amrita { init resources
8           fold::amrita { assign sufficient resources
9              fold::amrita { define array sizes
10                ArraySizes {
11                   NL      = 10         # maximum number of grid levels
12                   NGD     = 28000       # maximum number of mesh patches
```

```
13                    NGIJ    = 700000      # maximum number of perimeter cells
14                    NGIxJ   = 20000000    # maximum number of grid cells
15                    NEX     = 200000      # length of external boundaries
                          table
16                    NBDYS   = 100000      # maximum number of scrunched
                          boundaries
17                    NGHOST = 2          # number of ghost cells
18                    #NGIxJ=2500000
19                    #NEX=40000
20                    #NGD=8000
21                    #NGIJ=100000
22                 }
23              }
24           }
25           fold::amrita { get 1step
26              if(!&amrso("code/1step")) then
27                 fold::amrita { build code
28                    fold::amrita { generate auxcode
29                       fold::print { soot_trace
30                          fold>file=code/soot_trace,recursion off,dollar off
31                          fold::amrita { daisy chain Ls2
32                             AddIntegrationStep {
33                                step = soot  (aka Ls2)  :record_vort(IM,JM,NG
                                      ,DX,DY,W)
34                             }
35                             set amrita:bcg::integration .= *Ls2
36                          }
37                          fold::print {  record_vort
38                             *
39                             *
40                             *      RECORD_VORT:
41                             *
42                             *
43                                    SUBROUTINE RECORD_VORT(IM,JM,NG,DX,DY,W)
44                             #include "$amrita:bcg::commonblk"
45                                    AMRINT IM,JM,NG
46                                    AMRDBL DX,DY
47                                    AMRDBL W(NW,amrCpatch(IM,JM,NG))
48                                    DO I=1,IM
49                                       DO J=1,JM
50                                          DUDY = (W(2,I,J+1)/W(1,I,J+1)
51                                     X                 -W(2,I,J-1)/W(1,I,J-1))/(2*DY
```

```
                                    )
52                                      DVDX = (W(3,I+1,J)/W(1,I+1,J)
53                                 X                -W(3,I-1,J)/W(1,I-1,J))/(2*DX
                                    )
54                                      VORT = DVDX-DUDY
55                                      IF(ABS(VORT).GE.ABS(W(6,I,J))) THEN
56                                         W(6,I,J) = ABS(VORT)
57                                      ENDIF
58                                   END DO
59                                END DO
60                                RETURN
61                                END
62                          }
63                       }
64                       fold::print { energy_release
65                          fold>file=code/energy_release,recursion off,dollar
                               off
66                          fold::amrita { daisy chain Ls3
67                             AddIntegrationStep {
68                                step = energy_release_rate  (aka Ls3)  :
                                      record_e_rate(IM,JM,NG,DX,DY,W)
69                             }
70                             set amrita:bcg::integration .= *Ls3
71                          }
72                          fold::print {  record_e_rate
73                             *
74                             *
75                             *      RECORD_E_RATE:
76                             *
77                             *
78                                    SUBROUTINE RECORD_E_RATE(IM,JM,NG,DX,DY,W)
79                                 #include "$amrita:bcg::commonblk"
80                                    AMRINT IM,JM,NG
81                                    AMRDBL DX,DY
82                                    AMRDBL W(NW,amrCpatch(IM,JM,NG))
83                                    CALL AMR::GET_CONST('amrita:EquationSet:
                                         expr::GAMMA',GMz)
84                                    CALL AMR::GET_CONST('amrita:EquationSet:
                                         expr::Q',Qz)
85                                    CALL AMR::GET_CONST('amrita:EquationSet:
                                         expr::E',Ez)
86                                    DO I=1,IM
```

```
87                                      DO J=1,JM
88                                          P = (GMz-1)*(W(4,I,J)-0.5*(W(2,I,J)
                                                **2+W(3,I,J)**2)/W(1,I,J)-W(5,I,
                                                J)*Qz)
89                                          RHO_DZDT = -W(1,I,J)*W(5,I,J)*EXP(-
                                                Ez*W(1,I,J)/P)
90                                          IF(ABS(RHO_DZDT).GE.ABS(W(7,I,J)))
                                                THEN
91                                             W(7,I,J) = ABS(RHO_DZDT)
92                                          ENDIF
93                                      END DO
94                                  END DO
95                                  RETURN
96                                  END
97                          }
98                      }
99                  }
100                 BasicCodeGenerator {
101                     solver = 1step
102                     scheme = roe'$znd::model
103                     auxcode= code/soot_trace,code/energy_release
104                 }
105                 fold::amrita { use minmod
106                     set solver::PHI = 1
107                     set solver::Pact= 1.1
108                     export solver::{PHI,Pact}
109                 }
110             }
111         endif
112     }
113     fold::amrita { define DrawObstacleBody
114         proc DrawObstacleBody {
115             }
116             plot amr_sol:axs::PSI[] contours L0.0 m<0>
117             red   ::= amr_sol:axs::PSI[]<0 ? -1 : 69
118             green ::= amr_sol:axs::PSI[]<0 ? -1 : 110
119             blue  ::= amr_sol:axs::PSI[]<0 ? -1 : 150
120             plot image {g0} RGB<red[],green[],blue[]>
121         end proc
122     }
123     fold::amrita { define DrawCylinderBody
124         proc DrawCylinderBody {
```

```
125                 fold::amrita { parameters
126                    ls = 1.0
127                    xo = 135
128                    yo = 0
129                    rad  = 45
130                    arc = 0 to 180
131                 }
132              }
133              AmritaBlue
134              filled circle $ls*($xo),$ls*($yo),$ls*$rad sector $arc
135           end proc
136        }
137        fold::amrita { define DetonationCylinderProblem
138           proc DetonationCylinderProblem {
139                fold::amrita { parameters
140                   gamma      =     1.17     # ratio of specific heats
141                   d  [0:?]   =     1.0      # overdrive
142                   Q  [0:?]   =     60.5     # heat release
143                   E  [0:70]  =      48.3      # activation energy
144                   lmax       =       1      # maximum number of grid
                         levels
145                   r          =       2      # refinement ratio
146                   Npts[0:?]  =      64      # mesh points in half-
                         reaction length
147                   Xd         =     33.0     # fix position of detonation
                         #was 33.0
148                   piston_face=   -1E10      # trick interp with -infinity
149                   Ztol       = 0.005
150                   io         = .
151                   profiles   "= $io/znd/Q=$Q/E=$E/d=$d
152                   im         =    200       # base grid points in x-
                         direction
153                   jm         =     24       # base grid points in y-
                         direction
154                   npatches   =      1
155                   rad        =     18       # radius of cylinder
156                   xo         =     54      # centre of
157                   yo         =      0       # cylinder
158                   xo2        =    159       # centre of second
159                   yo2        =    $jm       # cylinder
160                   X2         =     150   # some plane between the
                         cylinders
```

```
161                  ls          =    1.0       # scaling factor
162                  two_circles=      0        # 1 for true, 0 for false
163                  yplot1   =    0       # position along y-axis to print
                        results (bottom boundary)
164                  yplot2   =   23       # position along y-axis to print
                        results (top boundary)
165               }
166            } <-> ParamSet::
167            fold::amrita { define Domain
168               def Domain
169                  lscale $ls
170                  do n=1,$npatches
171                     patch <+,1,w$im,h$jm>
172                  end do
173               end def
174            }
175            fold::amrita{ def SolutionField
176               def SolutionField
177                  fold::amrita { fix problem specfic quantities
178                     specify GAMMA ::= $gamma
179                     specify Q     ::= $Q
180                     specify E     ::= $E
181                  }
182                  fold::amrita { get W'znd
183                     fold::amrita { get znd
184                        ComputeZndProfile {
185                           <- ParamSet::
186                           rtn      = znd
187                           profiles = $profiles
188                        }
189                     }
190                     Xd     ::= X[]-($ls*$Xd)
191                     RM       ::= interp($znd.RHO,Xd[])
192                     UM       ::= interp($znd.U  ,Xd[])
193                     PM       ::= interp($znd.P  ,Xd[])
194                     ZM       ::= interp($znd.Z  ,Xd[])
195                  }
196                  setfield <RHO=RM[],U=UM[],V=0,P=PM[],Z=ZM[]>
197               end def
198            }
199            fold::amrita { def BoundaryConditions
200               fold::amrita { get W'piston
```

```
201                     RB        ::= interp($znd.RHO,$piston_face)
202                     UB        ::= interp($znd.U  ,$piston_face)
203                     PB        ::= interp($znd.P  ,$piston_face)
204                     ZB        ::= interp($znd.Z  ,$piston_face)
205                     W'piston  ::= <RHO=RB[],U=UB[],V=0,P=PB[],Z=ZB[]>
206                  }
207                  def BoundaryConditions
208                     Nbdy  domain: reflect
209                     Ebdy  domain: extrapolate linearly
210                     Wbdy  domain: prescribe W'piston
211                     Sbdy  domain: reflect
212                     fold::amrita { define internal boundary
213                        cutoff ::= $ls*$X2
214                        wt12   ::= X[]-cutoff[]
215                        wt12   ::= wt12[]>0 ? 1 : 0
216                        if($two_circles) then
217                          Xc      ::= (1-wt12[])*$ls*$xo + wt12[]*$ls*$xo2
                                  # two circles
218                          Yc      ::= (1-wt12[])*$ls*$yo + wt12[]*$ls*$yo2
219                        else
220                          Xc      ::= $ls*$xo
                                                          # one circle
221                          Yc      ::= $ls*$yo
222                        endif
223                        AXS::InternalBoundary {
224                          PSI = (($ls*$rad)-sqrt((X[]-(Xc[]))**2+(Y[]-(Yc
                                []))**2))
225                        }
226                     }
227                  end def
228               }
229               fold::amrita { def Mesh Adaption
230                  def MeshAdaption
231                     adaption  on
232                     lmax      $lmax
233                     r         $r
234                  end def
235               }
236               fold::amrita { def RefinementCriteria
237                  def RefinementCriteria
238                     fold::amrita{ for density gradient
239                        setflags [ooo|oxx|ooo] abs(RHO[+i]-RHO[])>0.1
```

```
240                     setflags [oxo|oxo|ooo] abs(RHO[+j]-RHO[])>0.1
241                  }
242                  fold::amrita{ for reaction zone
243                     setflags [oxo|xxx|oxo] Z[]>0.05 && RHO[]>2.0
244                     setflags [ooo|oxx|ooo] abs(RHO[+i]-RHO[])>0.0001 &&
                            abs(Z[]>0.99)
245                     setflags [oxo|oxo|ooo] abs(RHO[+j]-RHO[])>0.0001 &&
                            abs(Z[]>0.99)
246                     setflags [ooo|oxx|ooo] abs(Z[+i]-Z[])>$Ztol
247                     setflags [oxo|oxo|ooo] abs(Z[+j]-Z[])>$Ztol
248                  }
249                  fold::amrita{ for the internal boundaries
250                     setflags [ooo|oxo|ooo] ON_BODY[]
251                  }
252               end def
253            }
254            fold::amrita { now run it!
255               makefield
256               do l=1,$lmax
257                  adapt
258                  makefield
259               end do
260            }
261         end proc
262      }
263      fold::amrita { diagnostics
264         fold::amrita { define SootTraceImage
265            proc SootTraceImage {
266                 fold::amrita { parameters
267                    SOOT              = W::VORT # what to plot
268                    exposure [0:1]    = 1       # darkness of image
269                    grid              = {G}     # select grid
270                    tol               = 0.2     # threshold for amp1
                          amp2
271                    amp1              = 0.5     # weak   features
272                    amp2              = 0.25    # strong features
273                 }
274               }
275               minmax $SOOT[] -> min, max
276               wt          ::= abs(($SOOT[]-$min)/($max-$min))
277               greyshading ::= wt[]<$tol? wt[]**$amp1 : wt[]**$amp2
278               plot image $grid m<$exposure*greyshading[]>
```

```
279             end proc
280         }
281         fold::amrita{ define DensityGradientPlot
282             proc DensityGradientPlot {
283                 exposure [0:1]      = 1.0  # darkness of image
284                 grid                = {G}  # select grid
285                 max                 = 2.
286                 min                 = 0.
287                 }
288                 DrhoDx       ::= (RHO[+i]-RHO[-i])/(X[+i]-X[-i])
289                 DrhoDy       ::= (RHO[+j]-RHO[-j])/(Y[+j]-Y[-j])
290                 schlieren    ::= sqrt(DrhoDx[]**2+DrhoDy[]**2)
291                 wt           ::= 1-((schlieren[]-$min)/($max-$min))
292                 wt           ::= wt[]>0 ? wt[] : 0
293                 greyshading ::= $exposure*wt[]
294                 plot image $grid m<greyshading[]>
295             end proc
296         }
297         fold::amrita{ define PressureGradientPlot
298             proc PressureGradientPlot {
299                 exposure [0:1]      = 0.8  # darkness of image
300                 amplification [0:?]=  15  # magnification of weak
                        features
301                 grid                = {G}  # select grid
302                 }
303                 DPDx       ::= (P[+i]-P[-i])/(X[+i]-X[-i])
304                 DPDy       ::= (P[+j]-P[-j])/(Y[+j]-Y[-j])
305                 Pgrad    ::= sqrt(DPDx[]**2+DPDy[]**2)
306                 minmax Pgrad[] -> min, max
307                 wt           ::= (Pgrad[]-$min)/($max-$min)
308                 greyshading ::= $exposure*exp(-$amplification*wt[])
309                 plot image $grid m<greyshading[]>
310             end proc
311         }
312         fold::amrita{ define DensityPlot
313             proc DensityPlot {
314                 exposure [0:1]      = 1.0  # darkness of image
315                 grid                = {G}  # select grid
316                 max                 = 10.0
317                 min                 = 0
318                 }
319                 wt           ::= 1-((RHO[]-$min)/($max-$min))
```

```
320                wt          ::= wt[]>0 ? wt[] : 0
321                greyshading ::= $exposure*wt[]
322                plot image $grid m<greyshading[]>
323             end proc
324          }
325          fold::amrita{ define PPlot
326             proc PPlot {
327                exposure [0:1]     = 1.0  # darkness of image
328                grid               = {G}  # select grid
329                max                = 100
330                min                = 0
331                }
332                wt          ::= 1-((P[]-$min)/($max-$min))
333                wt          ::= wt[]>0 ? wt[] : 0
334                greyshading ::= $exposure*wt[]
335                plot image $grid m<greyshading[]>
336             end proc
337          }
338          fold::amrita{ define TemperaturePlot
339             proc TemperaturePlot {
340                exposure [0:1]     = 1.0  # darkness of image
341                grid               = {G}  # select grid
342                max                = 20
343                min                = 0
344                }
345                RT ::= P[] / RHO[]
346                wt          ::= 1-((RT[]-$min)/($max-$min))
347                wt          ::= wt[]>0 ? wt[] : 0
348                greyshading ::= $exposure*wt[]
349                plot image $grid m<greyshading[]>
350           end proc
351          }
352          fold::amrita{ define Z Plot
353             proc ZPlot {
354                exposure [0:1]     = 1.0  # darkness of image
355                amplification [0:?]=  15  # magnification of weak
                      features
356                grid               = {G}  # select grid
357                max                = 1.0
358                min                = 0
359                }
360                wt          ::= (Z[]-$min)/($max-$min)
```

```
361                     greyshading ::= $exposure*wt[]
362                     plot image $grid m<greyshading[]>
363                  end proc
364              }
365              fold::amrita{ define DzdtPlot
366                 proc DzdtPlot {
367                     DZDT                = W::E_RATE # what to plot
368                     exposure [0:1]      = 1         # darkness of image
369                     grid                = {G}       # select grid
370                     tol                 = 0.75       # threshold for amp1 amp2
371                     #amp1                = 0.2       # weak   features
372                     #amp2                = 0.25      # strong features
373                     amp1                = 1.0       # weak   features
374                     amp2                = 1.0      # strong features
375                     Ea                  = 28
376                     }
377                     minmax $DZDT[] -> min, max
378                     wt           ::= 1-abs(($DZDT[]-$min)/($max/50-$min))
379                     #greyshading ::= wt[]<$tol? wt[]**$amp1 : wt[]**$amp2
380                     greyshading ::= wt[]>0 ? wt[] : 0
381                     plot image $grid m<$exposure*greyshading[]>
382                     end proc
383              }
384           }
385        }
386        plugin amr_sol
387        fold::amrita { init plotting
388           autoscale
389           postscript on
390        }
391     }
392
393  do lsMult = 1.45,1.45, 1
394  echo lsMult: $lsMult
395    set throatsize #=6        #Throat will be poresize/2
396        DetonationCylinderProblem {
397           <- ParamSet::
398           fold::amrita { parameters
399              lmax = 6
400              r    = 2
401    ls    = $lsMult*1.0      #Reaction length scale changed with multiplier!
402           }
```

```
403       }
404    logfile logs/1step
405    solver  code/1step
406    set IO=io
407    #flowin io/model47 #restart option at given model
408    do phase=1,95 #WAS 100
409       time -> t
410       do counter=1,10 #used to be up to 20
411          echo phase: $phase counter: $counter
412          march 1 steps with cfl=0.5
413       end do
414       fold::amrita{ plot output
415          fold::print {
416             fold> file.=throatsize$throatsize/ls$lsMult/lmax$ParamSet::lmax
                     /time.txt
417             $phase $t
418          }
419    fold::amrita { print Temperature Profile
420      printfile throatsize$throatsize/ls$lsMult/lmax$ParamSet::lmax/profiles/
          RT_bottom$phase.dat
421      along y=0 print X[],P[]/RHO[]
422      printfile throatsize$throatsize/ls$lsMult/lmax$ParamSet::lmax/profiles/
          RT_top$phase.dat
423      along y=24*$lsMult print X[],P[]/RHO[]
424    }
425          fold::amrita { schlieren
426             plotfile throatsize$throatsize/ls$lsMult/lmax$ParamSet::lmax/
                    sch/sch$phase.ps
427                PlotDomain
428                DensityGradientPlot
429                #DrawObstacleBody
430                DrawCylinderBody <- ParamSet::
431             plotfile
432          }
433          fold::amrita { density
434             plotfile throatsize$throatsize/ls$lsMult/lmax$ParamSet::lmax/
                    dens/dens$phase.ps
435                PlotDomain
436                DensityPlot
437                #DrawObstacleBody
438                DrawCylinderBody <- ParamSet::
439             plotfile
```

```
440         }
441         fold::amrita { pressure
442            plotfile throatsize$throatsize/ls$lsMult/lmax$ParamSet::lmax/p/
                  p$phase.ps
443               PlotDomain
444               PPlot
445               #DrawObstacleBody
446               DrawCylinderBody <- ParamSet::
447            plotfile
448         }
449         fold::amrita { grids
450            plotfile throatsize$throatsize/ls$lsMult/lmax$ParamSet::lmax/
                  grid/grid$phase.ps
451               plot grids
452            plotfile
453         }
454         fold::amrita { pgrad
455            plotfile throatsize$throatsize/ls$lsMult/lmax$ParamSet::lmax/
                  pgrad/pgrad$phase.ps
456               PlotDomain
457               PressureGradientPlot
458               DrawCylinderBody <- ParamSet::
459            plotfile
460         }
461         fold::amrita { Temperature
462            plotfile throatsize$throatsize/ls$lsMult/lmax$ParamSet::lmax/T/
                  T$phase.ps
463               PlotDomain
464               TemperaturePlot
465               DrawCylinderBody <- ParamSet::
466            plotfile
467         }
468         fold::amrita { reaction progress variable
469            plotfile throatsize$throatsize/ls$lsMult/lmax$ParamSet::lmax/Z/
                  Z$phase.ps
470               PlotDomain
471               ZPlot
472               DrawCylinderBody <- ParamSet::
473            plotfile
474         }
475         fold::amrita { plot soot foil
476            plotfile throatsize$throatsize/ls$lsMult/lmax$ParamSet::lmax/
```

```
                soot/soot$phase.ps
477             PlotDomain
478             SootTraceImage
479             DrawCylinderBody <- ParamSet::
480         plotfile
481       }
482       fold::amrita { openshutter
483         plotfile throatsize$throatsize/ls$lsMult/lmax$ParamSet::lmax/
                dzdt/dzdt$phase.ps
484             PlotDomain
485             DzdtPlot
486             DrawCylinderBody <- ParamSet::
487         plotfile
488       }
489     }
490     flowout $IO/model$phase
491   end do
492 end do
493 }
```

B.5.3 Commands

The code can be run with the command

```
amrita 1step_run_circle_detonation.amrita
```

B.5.4 Output

A portion of the output is shown in the results chapter 4.

B.6 AMRITA: Detonation diffraction and reflection using two-step chemistry

Calculates the detonation diffraction and reflection over a cylindrical obstacle using the method described in chapter 3 and the two-step chemistry model. This specific example is for an initial pressure $P_0 = 5.5$ kPa.

B.6.1 Preparation

The AMRITA CFD [51] program was installed and can be found at `http://www.amrita-cfd.org/`. The two-step library and script were located in the same directory. Values of interest can be modified as follows:

- Line 18 controls the isentropic exponent γ.
- Line 20 controls heat release $\tilde{Q}$.
- Line 21 controls activation energy $\tilde{E}_a$.
- Line 22 controls the reaction pre-exponential factor K_r and adopts the value of the induction to reaction length ratio $\frac{\Delta_i}{\Delta_r}$.
- Line 24 controls the reaction order ν.
- Line 356 controls the length scale ls.
- Lines 355 and 36 control resolution.
- Output ranges can be changed by modifying the "min" and "max" values of the various plots between lines 233 and 347.

B.6.2 Input

File name: 2step_run_circle_detonation.amrita

```
1  fold::amrita { 2step model 1D detonation dynamics
2     fold::amrita { preliminaries
3       ArraySizes {
4          NL      = 10          # maximum number of grid levels
5          NGD     = 28000        # maximum number of mesh patches
6          NGIJ    = 700000       # maximum number of perimeter cells
7          NGIxJ   = 30000000     # maximum number of grid cells
8          NEX     = 200000       # length of external boundaries table
9          NBDYS   = 100000       # maximum number of scrunched boundaries
10         NGHOST = 2           # number of ghost cells
11         }
12    }
13    fold::amrita { define procedures
14       fold::amrita { DetonationCylinderProblem
15        proc DetonationCylinderProblem {
```

```
16              fold::amrita { parameters
17                 fold::amrita { Physical detonation parameters
18                    gamma      =     1.17     # ratio of specific heats
19                    d  [0:?]   =     1.0     # overdrive
20                    Q  [0:?]   =      13.7     # exothermic overall heat
                         release
21                    E [0:?]  =     11.0      # initiation activation
                         energy
22                    Ke         =     19.1       # Reaction constant
23
24                    ETA        =   1.2       # Reaction order
25                    ls         =    1.0       # scaling factor
26                 }
27              fold::amrita { Internal boundary parameters
28                    rad        =     18       # radius of cylinder
29                    xo         =     54      # centre of
30                    yo         =      0       # cylinder
31              }
32                 fold::amrita { Grid and refinement parameters
33                    im         =     200     # width of domain in terms of
                         number of induction lengths (base grid points)
34                    jm         =     24     # height of domain in terms of
                         number of induction lengths (base grid points)
35                    lmax       =      1     # maximum number of grid
                         levels
36                    rI         =      2     # refinement ratio
37                    ptol       =     0.5    # packing tolerance
38                 }
39                 fold::amrita { Misc.
40                    cfl        = 0.8
41                    Npts[0:?]  =     256      # mesh points in half-
                         reaction length  !!!??? Is this activated !!!???
42                    dx         =     1.0     # fix half-reaction length
43                    Xd         =    33.0    # fix position of detonation
44                    piston_face=   -1E10     # trick interp with -infinity
45                    profiles  "= znd     # directory for output of znd
                         profiles
46                    chan       = 40          # fortran channel for output
                         of znd files
47                  #  xc         =    105        # position of disturbance
                          band
48                  #  b1         =    0.2       # amplitude of Ze
```

```
                    disturbance
49                  #  b2          =    4          # width of disturbance in x-
                        direction
50                  }
51               }
52            } <-> ParamSet::
53            fold::amrita { body of procedure
54               fold::amr_sol'Domain {
55                 lscale $ls
56                 patch <1,+,w$im,h$jm>
57               }
58               fold::amr_sol'SolutionField {
59                  fold::amrita { fix problem specific quantities
60                     specify Q     ::= $Q
61                     specify E     ::= $E
62                     specify GAMMA ::= $gamma
63                     specify ETA   ::= $ETA
64                     specify Ke    ::= $Ke
65                  }
66                  fold::amrita { get W'znd
67 #                    fold::amrita { get znd
68 #                       ComputeZndProfileworking {
69 #                          <- ParamSet::
70 #                          Npts     = $Npts
71 #                          rtn      = znd
72 #                          profiles = $profiles
73 #                          model    = 2ie
74 #                          Xc       = 4
75 #                          Zc       = 0.01
76 #                       }
77 #                    }
78                     Xd     ::= X[]-$Xd*$ls
79                     set znd "=znd/znd
80                     set zndfile = $amrita::cwd/$znd
81                     W'znd  ::= <RHO= interp($zndfile.RHO,Xd[]),\
82                                  U  = interp($zndfile.U  ,Xd[]),\
83                                  V  = 0,\
84                                  P  = interp($zndfile.P  ,Xd[]),\
85                                  Zi = interp($zndfile.Zi ,Xd[]),\
86                                  Ze = interp($zndfile.Ze ,Xd[])>
87                     fold::amrita { get initial density and pressure
88                        Dens ::= interp($zndfile.RHO,Xd[])
```

```
89                      Pres ::= interp($zndfile.P,Xd[])
90                      minmax Dens[] -> rho0, rhoshk
91                      minmax Pres[] -> P0, Pshk
92                      set Study::rho0 = $rho0
93                      set Study::P0   = $P0
94                   }
95                }
96                setfield W'znd
97 #               W'disturbance  ::= <RHO= interp($zndfile.RHO,Xd[]),\
98 #                                  U  = interp($zndfile.U  ,Xd[]),\
99 #                                  V  = 0,\
100 #                                 P  = interp($zndfile.P  ,Xd[]),\
101 #                                 Zi = 1-($b1*rand(1)),\
102 #                                 Ze = interp($zndfile.Ze ,Xd[])>
103 #                zone ::= (abs(X[]-$xc)<$b2/2)
104 #                setfield W'disturbance zone[]
105             }
106             fold::amr_sol'BoundaryConditions {
107                fold::amrita { get W'piston
108                   W'piston ::= <RHO= interp($znd.RHO,$piston_face),\
109                                U  = interp($znd.U  ,$piston_face),\
110                                V  = 0,\
111                                P  = interp($znd.P  ,$piston_face),\
112                                Zi = interp($znd.Zi ,$piston_face),\
113                                Ze = interp($znd.Ze ,$piston_face)>
114                }
115                Ebdy domain: extrapolate
116                Wbdy domain: prescribe W'piston
117                Nbdy domain: reflect
118                Sbdy domain: reflect
119                fold::amrita { define internal boundary
120                      Xc     ::= $ls*$xo                                  #
                            one circle
121                      Yc     ::= $ls*$yo
122                      AXS::InternalBoundary {
123                        PSI = (($ls*$rad)-sqrt((X[]-(Xc[]))**2+(Y[]-(Yc
                              []))**2))
124                      }
125                } # End internal boundary
126             }
127             fold::amr_sol'RefinementCriteria {
128                   fold::amrita{ for density gradient
```

```
129                         setflags [ooo|oxx|ooo] abs(RHO[+i]-RHO[])>0.06
130                         setflags [oxo|oxo|ooo] abs(RHO[+j]-RHO[])>0.06
131                      }
132                      fold::amrita{ for reaction zone
133                         setflags [oxo|xxx|oxo] abs(Zi[])<1.0 &&  abs(Ze[])
                               <0.95 && (RHO[]>1.1*$rho0)
134                         setflags [ooo|oxx|ooo] abs(RHO[+i]-RHO[])>0.06 &&
                               abs(Zi[]<1.0) && abs(Ze[]<0.95)
135                         setflags [oxo|oxo|ooo] abs(RHO[+j]-RHO[])>0.06 &&
                               abs(Zi[]<1.0) && abs(Ze[]<0.95)
136                         setflags [ooo|oxx|ooo] abs(RHO[+i]-RHO[])>0.06 &&
                               abs(Ze[]<0.95) && abs(Zi[]<1.0)
137                         setflags [oxo|oxo|ooo] abs(RHO[+j]-RHO[])>0.06 &&
                               abs(Ze[]<0.95) && abs(Zi[]<1.0)
138                         setflags [ooo|oxx|ooo] abs(Zi[+i]-Zi[])>0.01
139                         setflags [oxo|oxo|ooo] abs(Zi[+j]-Zi[])>0.01
140                         setflags [ooo|oxx|ooo] abs(Ze[+i]-Ze[])>0.01
141                         setflags [oxo|oxo|ooo] abs(Ze[+j]-Ze[])>0.01
142                      }
143                      fold::amrita{ for the internal boundaries
144                         setflags [ooo|oxo|ooo] ON_BODY[]
145                      }
146                }
147                fold::amr_sol'MeshAdaption {
148                   adaption  on
149                   lmax      $lmax
150                   rI        $rI
151                   ptol      $ptol
152                }
153                makefield {G$lmax}
154             }
155          end proc
156       }
157    }
158    utilize 2steplib
159    plugin amr_sol
160    ReactiveEulerEquations {
161       model = 2ie
162       space = 2D
163       add2W = VORT
164    }
165    fold::amrita { load solver
```

```
166       fold::amrita { build solver
167          fold::amrita { generate auxcode
168                       fold::print { soot_trace
169                          fold>file=code/soot_trace,recursion off,dollar off
170                          fold::amrita { daisy chain Ls2
171                             AddIntegrationStep {
172                                step = soot  (aka Ls2)  :record_vort(IM,JM,NG
                                      ,DX,DY,W)
173                             }
174                             set amrita:bcg::integration .= *Ls2
175                          }
176                          fold::print {  record_vort
177                             *
178                             *
179                             *      RECORD_VORT:
180                             *
181                             *
182                                    SUBROUTINE RECORD_VORT(IM,JM,NG,DX,DY,W)
183                             #include "$amrita:bcg::commonblk"
184                                    AMRINT IM,JM,NG
185                                    AMRDBL DX,DY
186                                    AMRDBL W(NW,amrCpatch(IM,JM,NG))
187                                    DO I=1,IM
188                                       DO J=1,JM
189                                          DUDY = (W(2,I,J+1)/W(1,I,J+1)
190                                    X                -W(2,I,J-1)/W(1,I,J-1))/(2*DY
                                          )
191                                          DVDX = (W(3,I+1,J)/W(1,I+1,J)
192                                    X                -W(3,I-1,J)/W(1,I-1,J))/(2*DX
                                          )
193                                          VORT = DVDX-DUDY
194                                          IF(ABS(VORT).GE.ABS(W(7,I,J))) THEN
195                                             W(7,I,J) = ABS(VORT)
196                                          ENDIF
197                                       END DO
198                                    END DO
199                                    RETURN
200                                    END
201                          }
202                       }
203          }
204          BasicCodeGenerator {
```

```
205                  scheme  = roe'3cb
206                  solver  = 2step
207                  auxcode= code/soot_trace
208          }
209       }
210       fold::amrita { set solver parameters
211          set solver::PHI  = 1
212          set solver::Pact = 0.3
213          export solver::{PHI,Pact}
214       }
215       solver code/2step
216    }
217    fold::amrita { generate characteristics
218       fold::amrita { diagnostics
219         fold::amrita { define DrawCylinderBody
220             proc DrawCylinderBody {
221                 fold::amrita { parameters
222                     ls = 1.0
223                     xo = 135
224                     yo = 0
225                     rad  = 45
226                     arc = 0 to 180
227                 }
228             }
229             AmritaBlue
230             filled circle $ls*($xo),$ls*($yo),$ls*$rad sector $arc
231             end proc
232          }
233         fold::amrita{ define DensityGradientPlot
234                    proc DensityGradientPlot {
235                     exposure [0:1]      = 1.0  # darkness of image
236                     grid                = {G}  # select grid
237                     max                 = 2.
238                     min                 = 0.
239                     }
240                     DrhoDx       ::= (RHO[+i]-RHO[-i])/(X[+i]-X[-i])
241                     DrhoDy       ::= (RHO[+j]-RHO[-j])/(Y[+j]-Y[-j])
242                     schlieren    ::= sqrt(DrhoDx[]**2+DrhoDy[]**2)
243                 minmax schlieren[] -> min, max
244                     wt           ::= 1-((schlieren[]-$min)/($max-$min))
245                     wt           ::= wt[]>0 ? wt[] : 0
246                     greyshading ::= $exposure*wt[]
```

```
247                plot image $grid m<greyshading[]>
248             end proc
249          } #End of DensityGradientPlot
250          fold::amrita{ define PressureGradientPlot
251             proc PressureGradientPlot {
252                exposure [0:1]      = 0.8  # darkness of image
253                amplification [0:?]=  15  # magnification of weak
                      features
254                grid                = {G}  # select grid
255                }
256                DPDx       ::= (P[+i]-P[-i])/(X[+i]-X[-i])
257                DPDy       ::= (P[+j]-P[-j])/(Y[+j]-Y[-j])
258                Pgrad    ::= sqrt(DPDx[]**2+DPDy[]**2)
259                minmax Pgrad[] -> min, max
260                wt           ::= (Pgrad[]-$min)/($max-$min)
261                greyshading ::= $exposure*exp(-$amplification*wt[])
262                plot image $grid m<greyshading[]>
263             end proc
264          }
265          fold::amrita{ define DensityPlot
266             proc DensityPlot {
267                exposure [0:1]      = 1.0  # darkness of image
268                grid                = {G}  # select grid
269                max                 = 1.0
270                min                 = 0
271                }
272                wt           ::= 1-((RHO[]-$min)/($max-$min))
273                wt           ::= wt[]>0 ? wt[] : 0
274                greyshading ::= $exposure*wt[]
275                plot image $grid m<greyshading[]>
276             end proc
277          }
278          fold::amrita{ define PressurePlot
279             proc PressurePlot {
280                exposure [0:1]      = 1.0  # darkness of image
281                grid                = {G}  # select grid
282                max                 = 1
283                min                 = 0
284                }
285                wt           ::= 1-((P[]-$min)/($max-$min))
286                wt           ::= wt[]>0 ? wt[] : 0
287                greyshading ::= $exposure*wt[]
```

```
288                plot image $grid m<greyshading[]>
289             end proc
290          }
291          fold::amrita{ define RT_Plot
292             proc RT_Plot {
293                exposure [0:1]     = 1.0  # darkness of image
294                grid               = {G}  # select grid
295                max                = 2.5
296                min                = 0
297                }
298                RT ::= P[] / RHO[]
299                wt          ::= 1-((RT[]-$min)/($max-$min))
300                wt          ::= wt[]>0 ? wt[] : 0
301                greyshading ::= $exposure*wt[]
302                plot image $grid m<greyshading[]>
303           end proc
304          }
305          fold::amrita{ define Ze Plot
306             proc ZePlot {
307                exposure [0:1]     = 1.0  # darkness of image
308                amplification [0:?]=  15  # magnification of weak
                      features
309                grid               = {G}  # select grid
310                max                = 1.0
311                min                = 0
312                }
313                wt          ::= (Ze[]-$min)/($max-$min)
314                greyshading ::= $exposure*wt[]
315                plot image $grid m<greyshading[]>
316             end proc
317          }
318          fold::amrita{ define Zi Plot
319             proc ZiPlot {
320                exposure [0:1]     = 1.0  # darkness of image
321                amplification [0:?]=  15  # magnification of weak
                      features
322                grid               = {G}  # select grid
323                max                = 1.0
324                min                = 0
325                }
326                wt          ::= (Zi[]-$min)/($max-$min)
327                greyshading ::= $exposure*wt[]
```

```
328                 plot image $grid m<greyshading[]>
329              end proc
330           }
331           fold::amrita{ define Soot Trace
332              proc SootTraceImage {
333                fold::amrita { parameters
334                   SOOT              = W::VORT # what to plot
335                   exposure [0:1]    = 1       # darkness of image
336                   grid              = {G}     # select grid
337                   tol               = 0.2     # threshold for amp1 amp2
338                   amp1              = 0.5     # weak   features
339                   amp2              = 0.25    # strong features
340                }
341                }
342                minmax $SOOT[] -> min, max
343                wt          ::= abs(($SOOT[]-$min)/($max-$min))
344                greyshading ::= wt[]<$tol? wt[]**$amp1 : wt[]**$amp2
345                plot image $grid m<$exposure*greyshading[]>
346              end proc
347           }
348     }
349
350
351     do loopCounter = 1,1, 1
352        DetonationCylinderProblem {
353           <- ParamSet::
354           fold::amrita { parameters
355              lmax = 6
356              ls   = 1.45            #Reaction length scale changed with
                    lsMult
357           }
358        }
359        echo Detonation Cylinder Problem: Q/RTvn=$ParamSet::Q Ea/RTvn=
              $ParamSet::E Kr=$ParamSet::Ke ls=$ParamSet::ls lmax=$ParamSet::
              lmax
360        fold::amrita { setup logfile
361           logfile logs/log
362        }
363        autoscale
364        postscript on
365        do phase=1,200
366           #flowin io/model$phase #restart option at given model
```

```
367            march 5 steps with cfl= $ParamSet::cfl
368            time -> t
369            echo t=$t
370            fold::amrita { output
371               fold::print {
372                  fold> file.=results/ls$ParamSet::ls/lmax$ParamSet::lmax/
                        time.txt
373                  $phase $t
374               }
375            }
376            fold::amrita { print Temperature profile
377               printfile results/ls$ParamSet::ls/lmax$ParamSet::lmax/profiles
                     /RT_bottom=$phase.dat
378               along y=0 print X[],P[]/RHO[]
379               printfile results/ls$ParamSet::ls/lmax$ParamSet::lmax/profiles
                     /RT_top=$phase.dat
380               along y=24 print X[],P[]/RHO[]
381            }
382            fold::amrita { density
383               plotfile results/ls$ParamSet::ls/lmax$ParamSet::lmax/dens/
                     dens_$phase.ps
384               PlotDomain
385               DensityPlot
386               #DrawObstacleBody
387               DrawCylinderBody <- ParamSet::
388               plotfile
389            }
390            fold::amrita { grids
391               plotfile results/ls$ParamSet::ls/lmax$ParamSet::lmax/grid/
                     grid_$phase.ps
392               plot grids
393               plotfile
394            }
395            flowout io/model$phase
396         end do
397      end do
398     }
399 }
```

B.6.3 Commands

The code can be run with the command

```
amrita 2step_run_circle_detonation.amrita
```

B.6.4 Output

A portion of the output is shown in the results chapter 4.